

# Bayesian Clustering via Fusing of Localized Densities

Alexander Dombowsky<sup>1</sup> and David B. Dunson<sup>1,2</sup>

<sup>1</sup>Department of Statistical Science, Duke University, Durham, NC, USA

<sup>2</sup>Department of Mathematics, Duke University, Durham, NC, USA

## Abstract

Bayesian clustering typically relies on mixture models, with each component interpreted as a different cluster. After defining a prior for the component parameters and weights, Markov chain Monte Carlo (MCMC) algorithms are commonly used to produce samples from the posterior distribution of the component labels. The data are then clustered by minimizing the expectation of a clustering loss function that favors similarity to the component labels. Unfortunately, although these approaches are routinely implemented, clustering results are highly sensitive to kernel misspecification. For example, if Gaussian kernels are used but the true density of data within a cluster is even slightly non-Gaussian, then clusters will be broken into multiple Gaussian components. To address this problem, we develop Fusing of Localized Densities (FOLD), a novel clustering method that melds components together using the posterior of the kernels. FOLD has a fully Bayesian decision theoretic justification, naturally leads to uncertainty quantification, can be easily implemented as an add-on to MCMC algorithms for mixtures, and favors a small number of distinct clusters. We provide theoretical support for FOLD including clustering optimality under kernel misspecification. In simulated experiments and real data, FOLD outperforms competitors by minimizing the number of clusters while inferring meaningful group structure.

*Keywords: Mixture model; Loss function; Decision theory; Kernel misspecification; Statistical distance*

# 1 INTRODUCTION

Clustering data into groups of relatively similar observations is a canonical task in exploratory data analysis. Algorithmic clustering methods, such as k-means, k-medoids, and hierarchical clustering, rely on dissimilarity metrics, an approach which is often heuristic but may perform well in practice; see [Hastie et al. \(2009\)](#), [Jain \(2010\)](#), and [Kiselev et al. \(2019\)](#) for an overview. In comparison, model-based clustering methods utilize mixtures of probability kernels to cluster data, ordinarily by inferring the component labels ([Fraley and Raftery, 2002](#)). Choices of kernel depend on the type of data being considered, with the Gaussian mixture model (GMM) particularly popular for continuous data. A conceptual advantage of model-based methods is the ability to express uncertainty in clustering. For example, the expectation-maximization (EM) algorithm uses maximum likelihood estimates of the component-specific parameters and weights to calculate each observations' posterior component allocation probabilities, which are interpreted as a measure of clustering uncertainty ([Bensmail et al., 1997](#)). As estimation of the weights and component-specific parameters is crucial for model-based clustering, there is a rich literature on quantifying rates of convergence for various mixture models, which is usually expressed in terms of the mixing measure (see [Guha et al., 2021](#) and references therein).

Bayesian mixture models have received increased attention as a clustering method in recent years. The Bayesian framework can account for uncertainty in the number of components and incorporate prior information on the component-specific parameters, with Markov chain Monte Carlo (MCMC) algorithms employed to generate posterior samples for the mixture weights, kernel parameters, and component labels for each data point. Based on posterior samples of the component labels, one can obtain Monte Carlo approximations to Bayes clustering estimators. For  $p$ -dimensional data  $\mathbf{X} = (X_1, \dots, X_n)$ , a Bayes estimator  $\mathbf{c}^*$  is the minimizer of an expected loss function conditional on  $\mathbf{X}$  over all possible clusterings  $\mathbf{c} = (c_1, \dots, c_n)$ . There are several popular choices of loss, including Binder's ([Binder, 1978](#)) and the Variation of Information (VI) ([Meilă, 2007](#)), which are distance metrics over the space of partitions and favor clusterings that are similar to the component labels. Further details on set partitions and their role in Bayesian clustering can be found in [Meilă \(2007\)](#), [Wade and Ghahramani \(2018\)](#), and [Paganin et al. \(2021\)](#). Several measures of uncertainty in clustering with Bayesian mixtures exist, including the posterior similarity matrix and credible balls of partitions ([Wade and Ghahramani, 2018](#)).

However, model-based clustering approaches, including Bayesian implementations, can be brittle in applications due to unavoidable impacts of model misspecification. While the data are assumed to come from a model  $X_i \sim f = \sum_{k=1}^K a_k g(\cdot; \tilde{\theta}_k)$ , in reality, data are generated via a true process  $f^0$ , which may or may not be in the support of the prior for  $f$ . A specific example is *kernel misspecification*, which occurs when  $f^0$  is in fact a mixture model whose components are not contained in the kernel family mixed over by the fitted model. Mixtures will often induce over-clustering in this setting by

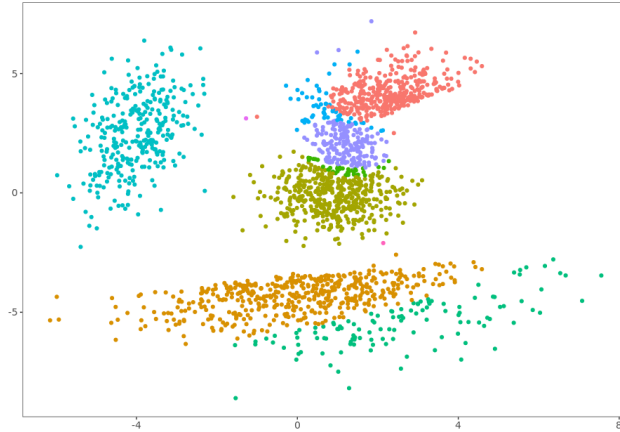


Figure 1: A Bayesian GMM with 10 components and Dirichlet prior concentration parameter equal to  $1/10$  is fit to data generated from a mixture of skew Gaussian distributions.

approximating a single component in  $f^0$  with many components from  $f$ . An example of this phenomena is shown in Figure 1, where a 10 component Bayesian GMM is fit to data generated from a mixture of bivariate skew Gaussian distributions. Despite using a concentration parameter of  $1/10$  in the symmetric Dirichlet prior to induce a small number of clusters (Rousseau and Mengersen, 2011), the GMM allocates the data into 10 poorly defined groups. A group of observations in the bottom third of the sample space is split into two, while several observations are placed into their own groups despite being near dense collections of data.

Several approaches have been proposed to address the issue of over-clustering due to kernel misspecification. A natural solution is to define a flexible class of kernels, exemplified by the mixtures in Karlis and Santourian (2009), O’Hagan et al. (2016), and Dang et al. (2023). To increase flexibility further, Rodríguez and Walker (2014) propose a mixture of nonparametric unimodal kernels. Similarly, Bartolucci (2005), Li (2005), Di Zio et al. (2007), and Malsiner-Walli et al. (2017) use carefully chosen mixtures of Gaussians to characterize the data within each cluster. However, there is an unfortunate pitfall with the general strategy of using flexible families of kernels. In particular, as the flexibility of the kernel increases, identifiability and optimal estimation rates for inferring the mixing measure tend to weaken, especially when the true number of mixture components is unknown (Nguyen, 2013; Ho and Nguyen, 2016a; Heinrich and Kahn, 2018). Even the transition from location Gaussian kernels with known covariance to location-scale Gaussian kernels can have substantial consequences on the convergence rate of the component means (Manole and Ho, 2022). Such problems motivated Ho et al. (2020) to propose an alternative estimator of the mixing measure that is more robust than maximum likelihood and Bayesian approaches and can achieve optimal convergence rates.

Alternatively, one can develop generalized Bayesian methods of clustering that avoid defining a fully generative probabilistic model for the data. For example, Duan and Dunson (2021) propose to conduct model-based clustering based on a pairwise distance matrix instead of the data directly to reduce

sensitivity to kernel misspecification. [Rigon et al. \(2023\)](#) instead define a Gibbs posterior for clustering, incorporating a clustering loss function in place of a likelihood function, completely bypassing modeling of the data. An alternative that maintains a fully generative model while robustifying inferences to misspecification is to use a coarsened posterior ([Miller and Dunson, 2019](#); [Gorsky et al., 2024](#)). This coarsening approach often has good practical performance in reducing over-clustering due to kernel misspecification.

Unfortunately, these approaches for accommodating kernel misspecification have various drawbacks. Along with slower convergence rates, flexible kernels typically require a large number of parameters, worsening the already burdensome computational cost of Bayesian clustering. The generalized Bayes approaches can perform well in certain settings. However, both Gibbs posteriors and coarsened posteriors are highly sensitive to key tuning parameters, which can be difficult to choose objectively in practice.

A key theoretical advance is given in [Aragam et al. \(2020\)](#), which attempts to solve the problem of clustering based on a mixture model by merging components in a Gaussian mixture. They rely on a two-stage procedure that lacks partition uncertainty quantification and assumes that the true number of kernels is known. However, the approach of viewing clusters as arising from merging closely overlapping kernels is promising. Related merging ideas have been implemented in both frequentist and Bayesian approaches in a variety of settings, and several algorithms exist for deciding how and when to combine components together ([Chan et al., 2008](#); [Baudry et al., 2010](#); [Hennig, 2010](#); [Melnykov, 2016](#); [Guha et al., 2021](#); [Manole and Khalili, 2021](#)).

In this paper, we propose a novel decision theoretic method for Bayesian clustering that mitigates the effects of model misspecification. Suppose we model the data with a Bayesian mixture model, with  $K$  components, component labels  $\mathbf{s} = (s_1, \dots, s_n)$ , component-specific atoms  $\tilde{\theta}_1, \dots, \tilde{\theta}_K$ , and kernels  $g(\cdot; \tilde{\theta}_1), \dots, g(\cdot; \tilde{\theta}_K)$ . Rather than focusing on  $\mathbf{s}$ , we compute clusters with the localized densities  $\{g(\cdot; \theta_i)\}_{i=1}^n$ , defined by  $\theta_i = \tilde{\theta}_{s_i}$ . We define a loss function for any clustering  $\hat{c}$  that favors allocating  $i$  and  $j$  to the same cluster when the statistical distance between  $g(\cdot; \theta_i)$  and  $g(\cdot; \theta_j)$  is small, encouraging grouping observations with overlapping component kernels. We cluster the data with a Bayes estimator, interpreted as a Fusing of Localized Densities (FOLD). Our method has a fully decision theoretic justification, leads to interpretable uncertainty quantification, and can be readily implemented using the output of existing MCMC algorithms for mixtures.

Though previous methods have utilized merging kernels to account for kernel misspecification, to our knowledge none have a formal Bayesian decision theoretic justification. Although FOLD requires combinatorial optimization when obtaining the point estimate, we suggest two reasonable approximations: one in which we reduce the optimization space to a smaller set of candidate clusterings, and another in which we use existing greedy algorithms to compute a locally-optimal solution. We also

provide concrete theoretical guarantees for our procedure, including the result that as the sample size grows, the clustering point estimate converges to an oracle clustering rule. In addition, we list intuitive examples of oracle rules and empirically validate our asymptotic theory using a simple example.

In Section 2, we explain our clustering method from a Bayesian decision theoretic perspective, provide a framework for uncertainty quantification, and demonstrate how to implement FOLD in practice. In Section 3, we show asymptotic concentration of FOLD for misspecified and well-specified regimes. We apply FOLD to a cell line data set in Section 4, showing excellent performance. Finally, we provide concluding remarks and some extensions in Section 5. The Supplementary Material contains additional simulations and real-data examples, as well as proofs for all theoretical results.

## 2 CLUSTERING WITH LOCALIZED DENSITIES

### 2.1 NOTATION AND SETUP

Let  $X_i^0 = (X_{i1}^0, \dots, X_{ip}^0) \in \mathbb{R}^p$  be multivariate observations, collected into  $\mathbf{X}^0 = (X_1^0, \dots, X_n^0)$ . Assume that  $X_1^0, \dots, X_n^0$  are random and generated from an unknown mixture model:  $X_i^0 \sim f^0$ , where  $f^0 = \sum_{m=1}^{M^0} a_m^0 g_m^0(\cdot)$ ,  $a_m^0 > 0$  for  $m = 1, \dots, M^0$ ,  $\sum_{m=1}^{M^0} a_m^0 = 1$ , and  $M^0 < \infty$ . Since  $f^0$  is a mixture, the data-generating process can be equivalently stated with the addition of latent variables  $s_i^0 \in \{1, \dots, M^0\}$ , so that  $(X_i^0 | s_i^0 = m) \sim g_m^0(\cdot)$  for all  $i = 1, \dots, n$ .  $\mathbb{P}^0$  refers to probability and convergence statements with respect to the true data generating process, with  $\mathbb{P}^0(A) = \int_A f^0(x) dx$  for any set  $A$ .

Throughout this article, we will focus on the setting in which  $\mathbf{X}^0$  is modeled with a mixture. Let  $X_i = (X_{i1}, \dots, X_{ip}) \in \mathbb{R}^p$ , where  $\mathbf{X} = (X_1, \dots, X_n)$ . A Bayesian mixture model assumes that  $\mathbf{X}$  are generated via

$$\lambda \sim \pi_\Lambda, \quad \theta_i | \lambda \sim \lambda, \quad X_i | \theta_i \sim g(X_i; \theta_i); \quad (1)$$

for all  $i = 1, \dots, n$ . Here,  $\lambda$  is a probability distribution over a parameter space  $\Theta$  and known as the *mixing measure*, whereas  $\mathcal{G} = \{g(\cdot; \theta) : \theta \in \Theta\}$  denotes a family of probability densities with support on  $\mathbb{R}^p$ . We will impose more conditions on both  $\Theta$  and  $\mathcal{G}$  when we develop our theoretical results in Section 3.  $\pi_\Lambda$  is the prior distribution for the mixing measure with support  $\Lambda$ , and examples of such priors are implemented in Bayesian finite mixture models, mixtures of finite mixtures (MFMs) (Miller and Harrison, 2018), Dirichlet process mixtures (DPMs) (Ferguson, 1973; Antoniak, 1974), and Pitman-Yor process mixtures (Ishwaran and James, 2001, 2003). Generally, realizations from  $\pi_\Lambda$  are almost-surely discrete (e.g., as in Sethuraman (1994)) and can be represented as  $\lambda = \sum_{k=1}^K a_k \delta_{\tilde{\theta}_k}$ , where  $1 \leq K \leq \infty$ ,  $\tilde{\theta}_k \in \Theta$ ,  $0 < a_k < 1$ , and  $\sum_{k=1}^K a_k = 1$ . Hence, sampling  $\theta_i$  from (1) results in ties amongst the *atoms*  $\boldsymbol{\theta} = (\theta_1, \dots, \theta_n)$ , which are represented by unique values  $\tilde{\boldsymbol{\theta}} = (\tilde{\theta}_1, \dots, \tilde{\theta}_{K_n})$  for some

$1 \leq K_n \leq n$ . From these ties we can construct a latent partition  $S = (S_1, \dots, S_{K_n})$  of the integers  $[n] = \{1, \dots, n\}$ , where  $S_k = \{i \in [n] : \theta_i = \tilde{\theta}_k\}$ . The latent partition may also be represented with labels  $\mathbf{s} = (s_1, \dots, s_n)$ , where  $s_i = k \iff i \in S_k$ . We will assume that the prior for  $\tilde{\boldsymbol{\theta}}$  is non-atomic, so the allocation of two observations to the same component is equivalent to equality in their atoms, i.e.  $s_i = s_j \iff \theta_i = \theta_j$ .

Ultimately, our goal is to cluster the data  $\mathbf{X}^0$  using the mixture model outlined in (1). The typical approach is to infer the conditional distribution of  $S$  after observing the data. More formally, by assuming that  $\lambda \sim \pi_\Lambda$ , we have induced a prior distribution for  $S$ ,  $\Pi(S)$ . We then cluster the data by inferring  $\Pi(S | \mathbf{X} = \mathbf{X}^0)$ , which we will refer to for the remainder of this article as  $\Pi(S | \mathbf{X}^0)$ . To construct a point estimate of  $S$ , we minimize the posterior expectation of a clustering loss function that favors similarity to  $S$ . The decision theoretic approach to Bayesian clustering was first proposed in Binder (1978), and was advocated for more recently in Wade and Ghahramani (2018) and Dahl et al. (2022). However, Bayesian methods can lead to homogenous, tiny, and often uninterpretable clusters in practice. These issues often arise in the presence of kernel misspecification. Even well-separated true clusters in  $\mathbf{X}^0$  will be broken into multiple components from  $\mathcal{G}$  under a minor degree of kernel misspecification. To address this issue, we propose a loss function focused on simplifying the overfitted kernels via merging rather than estimating the component labels.

## 2.2 DECISION THEORY FORMULATION

We aim to estimate a clustering  $\hat{C} = \{\hat{C}_1, \dots, \hat{C}_{\hat{K}_n}\}$  of  $\mathbf{X}^0$ , or labels  $\hat{\mathbf{c}} = (\hat{c}_1, \dots, \hat{c}_n)$ , based on merging components from the joint posterior that have similar kernels  $g(\cdot; \tilde{\theta}_k)$ . The motivation here is to remedy the cluster splitting that occurs in using multiple parametric kernels  $g(\cdot; \tilde{\theta}_k)$  to represent each "true" kernel  $g_m^0(\cdot)$ . We define the *localized density* of observation  $i$  to be  $g(\cdot; \theta_i)$ , a random probability density that takes values  $g(x; \theta_i)$  for all  $x \in \mathbb{R}^p$ , where  $\theta_i$  is the atom of observation  $i$  as defined in (1). Observe that the localized density is the distribution for  $X_i$  under the fitted mixture model given  $\theta_i$ , i.e.  $(X_i | \theta_i = \tilde{\theta}_k) \sim g(\cdot; \tilde{\theta}_k)$ . Prior variation in the localized densities is modeled by sampling  $\lambda \sim \pi_\lambda$ , and then sampling  $\theta_i \sim \lambda$ , for  $i = 1, \dots, n$ .

To counteract cluster splitting, we define the loss of assigning two observations into the same or different clusters as a function of the statistical distance between their localized densities. Figure 2 shows the behavior of the posterior distributions of the localized densities when the model  $f(x) = \sum_{k=1}^{30} a_k \mathcal{N}_2(x; \tilde{\theta}_k, 0.02I)$  is fit to a version of the moons data. The red points plot  $\mathbb{E}_\Pi(\theta_i | \mathbf{X}^0)$  for each  $i = 1, \dots, n$ , with gray circles representing the 95% high density regions of a  $\mathcal{N}_2(\mathbb{E}_\Pi(\theta_i | \mathbf{X}^0), 0.02I)$  distribution. The crescent clusters are split into multiple overlapping Gaussian kernels, but are recovered by fusing these kernels together.

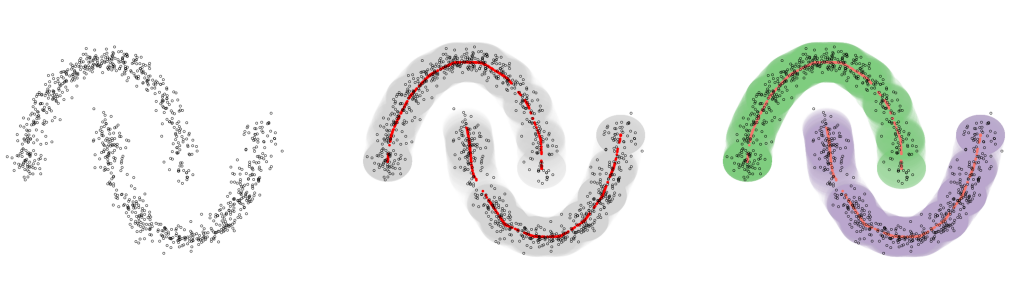


Figure 2: A Bayesian location Gaussian mixture is fit to a version of the moons data set. The localized densities are inferred, then merged together to recover the crescents.

We define the loss of any clustering  $\hat{\mathbf{c}}$  resulting from the model in (1) to be

$$\mathcal{L}(\hat{\mathbf{c}}, \boldsymbol{\theta}) = \sum_{i < j} \{ \mathbf{1}_{\hat{c}_i = \hat{c}_j} \mathcal{D}_{ij} + \omega \mathbf{1}_{\hat{c}_i \neq \hat{c}_j} (1 - \mathcal{D}_{ij}) \}, \quad (2)$$

where  $\omega > 0$ ,  $\mathcal{D}_{ij} = d\{g(\cdot; \theta_i), g(\cdot; \theta_j)\}$ , and  $d$  is any distance between probability distributions assumed to be bounded in the unit interval, i.e.  $0 \leq d\{P(\cdot), Q(\cdot)\} \leq 1$  for all measures  $P$  and  $Q$ , and with the property that  $d\{P(\cdot), Q(\cdot)\} = 1$  if and only if  $\text{supp}(P) \cap \text{supp}(Q) = \emptyset$ . A key example is when  $d$  is chosen to be the Hellinger distance, but this need not be the case in general. Observe that  $\mathcal{L}(\hat{\mathbf{c}}, \boldsymbol{\theta})$  is non-negative for any  $\hat{\mathbf{c}}$ . The loss of assigning  $\hat{c}_i = \hat{c}_j$  is  $\mathcal{D}_{ij}$ . If  $s_i = s_j$ , then  $\theta_i = \theta_j$  and hence there is no loss incurred. When  $s_i \neq s_j$ , then  $\theta_i \neq \theta_j$  but the loss will remain small when the kernels  $g(\cdot; \theta_i), g(\cdot; \theta_j)$  are similar under  $d$ . Conversely, allocating  $i$  and  $j$  to different clusters results in a loss of  $\omega(1 - \mathcal{D}_{ij})$ . If  $\mathcal{D}_{ij} = 1$ , i.e. if the supports of  $g(\cdot; \theta_i)$  and  $g(\cdot; \theta_j)$  are disjoint, then setting  $\hat{c}_i \neq \hat{c}_j$  accumulates zero loss. Otherwise, the loss depends on the separation in  $d$  between the localized densities and the loss parameter  $\omega$ .

Our loss  $\mathcal{L}(\hat{\mathbf{c}}, \boldsymbol{\theta})$  is invariant to permutations of the data indices and of the labels in either  $\hat{\mathbf{c}}$  or  $\mathbf{s}$ , which is desirable for clustering losses (Binder, 1978). In addition,  $\mathcal{L}(\hat{\mathbf{c}}, \boldsymbol{\theta})$  is a continuous relaxation of Binder’s loss function (Binder, 1978; Lau and Green, 2007),

$$\mathcal{L}_B(\hat{\mathbf{c}}, \mathbf{s}) = \sum_{i < j} \{ \mathbf{1}_{\hat{c}_i = \hat{c}_j} \mathbf{1}_{s_i \neq s_j} + \omega \mathbf{1}_{\hat{c}_i \neq \hat{c}_j} \mathbf{1}_{s_i = s_j} \}. \quad (3)$$

A key property of Binder’s loss is that it is a quasimetric over the space of partitions (Wade and Ghahramani, 2018; Dahl et al., 2022).  $\mathcal{L}(\hat{\mathbf{c}}, \boldsymbol{\theta})$  is not a quasimetric, but instead aims to mitigate the problem of cluster splitting arising under kernel misspecification. Note the difference in notation in the arguments of (3) and (2): we omit  $\mathbf{s}$  from the notion for  $\mathcal{L}(\hat{\mathbf{c}}, \boldsymbol{\theta})$  to reflect that we will incorporate information from the atoms in clustering  $\mathbf{X}^0$ , not just the latent partition. However, we can also state (3) in terms of  $\boldsymbol{\theta}$  by recalling that  $s_i = s_j \iff \theta_i = \theta_j$ . One can show that  $\mathcal{L}(\hat{\mathbf{c}}, \boldsymbol{\theta})$  can be rewritten

as the sum of  $\mathcal{L}_B(\hat{\mathbf{c}}, \mathbf{s})$  and a remainder term  $\mathcal{B}(\hat{\mathbf{c}}, \tilde{\boldsymbol{\theta}})$  that depends on the unique values  $\tilde{\boldsymbol{\theta}}$ , and that  $\mathcal{L}(\mathbf{s}, \boldsymbol{\theta}) = 0$  only when the components of  $f$  are completely separated under  $d$ . The closed form of the remainder  $\mathcal{B}(\hat{\mathbf{c}}, \tilde{\boldsymbol{\theta}})$  is given in the Supplement, and is interpreted as an added cost to Binder’s loss that encourages merging components.

**Proposition 1.**  $\mathcal{L}(\hat{\mathbf{c}}, \boldsymbol{\theta}) = \mathcal{L}_B(\hat{\mathbf{c}}, \mathbf{s}) + \mathcal{B}(\hat{\mathbf{c}}, \tilde{\boldsymbol{\theta}})$ , where  $\mathcal{B}(\mathbf{s}, \tilde{\boldsymbol{\theta}}) = 0$  if and only if  $d\{g(\cdot; \tilde{\theta}_k), g(\cdot; \tilde{\theta}_{k'})\} = 1$  for all component pairs  $k \neq k' = 1, \dots, K$ .

The parameter  $\omega$  calibrates separation of the clusters. For example, suppose we compare the clustering  $\hat{\mathbf{c}}_1$ , which includes clusters  $\hat{C}_h$  and  $\hat{C}_{h'}$ , with the clustering  $\hat{\mathbf{c}}_2$ , which is equivalent to  $\hat{\mathbf{c}}_1$  but now contains the merged cluster  $\hat{C}_h \cup \hat{C}_{h'}$ . The difference in their losses is  $\mathcal{L}(\hat{\mathbf{c}}_1, \boldsymbol{\theta}) - \mathcal{L}(\hat{\mathbf{c}}_2, \boldsymbol{\theta}) = \omega \sum_{i \in \hat{C}_h, j \in \hat{C}_{h'}} (1 - \mathcal{D}_{ij}) - \sum_{i \in \hat{C}_h, j \in \hat{C}_{h'}} \mathcal{D}_{ij}$ . The loss of  $\hat{\mathbf{c}}_2$  is less than that of  $\hat{\mathbf{c}}_1$  when

$$\frac{1}{|\hat{C}_h| |\hat{C}_{h'}|} \sum_{i \in \hat{C}_h, j \in \hat{C}_{h'}} \mathcal{D}_{ij} < \gamma := \frac{\omega}{1 + \omega}. \quad (4)$$

This implies that large values of  $\omega$  promote fusing clusters, while smaller values lead to more clusters having less between-cluster heterogeneity. When  $\hat{\mathbf{c}}_1 = \mathbf{s}$ , it is clear that a smaller loss can be attained by merging components with average pairwise statistical distance less than  $\gamma$ . Trivial clusterings are favored when  $\omega$  is taken to its lower and upper limits, similar to both Binder’s loss and the VI loss (Wade and Ghahramani, 2018; Dahl et al., 2022). As  $\omega \rightarrow 0$ , our loss is minimized by placing each observation in its own cluster, and, as  $\omega \rightarrow \infty$ , all observations are placed in a single cluster. Binder’s loss exhibits a similar interpretation, and one can show that, under the same settings outlined above,  $\mathcal{L}_B(\hat{\mathbf{c}}_2, \mathbf{s}) < \mathcal{L}_B(\hat{\mathbf{c}}_1, \mathbf{s})$  when  $|\hat{C}_h|^{-1} |\hat{C}_{h'}|^{-1} \sum_{i \in \hat{C}_h, j \in \hat{C}_{h'}} \mathbf{1}_{s_i \neq s_j} = |\hat{C}_h|^{-1} |\hat{C}_{h'}|^{-1} m_{hh'} < \gamma$ , where  $m_{hh'}$  counts the number of pairs across clusters  $h$  and  $h'$  that are allocated to different mixture components. However, the loss is always minimized when  $\hat{\mathbf{c}} = \mathbf{s}$ .

The risk of any clustering  $\hat{\mathbf{c}}$  is the posterior expectation of its loss, which integrates over the uncertainty in  $\boldsymbol{\theta}$  after observing the data;

$$\mathcal{R}(\hat{\mathbf{c}}) = \mathbb{E}_\Pi \{ \mathcal{L}(\hat{\mathbf{c}}, \boldsymbol{\theta}) \mid \mathbf{X}^0 \} = \sum_{i < j} \{ \mathbf{1}_{\hat{c}_i = \hat{c}_j} \Delta_{ij} + \omega \mathbf{1}_{\hat{c}_i \neq \hat{c}_j} (1 - \Delta_{ij}) \}, \quad (5)$$

where  $\Delta_{ij} = \mathbb{E}_\Pi(\mathcal{D}_{ij} \mid \mathbf{X}^0)$  is the posterior expected distance between the localized densities  $g(\cdot; \theta_i)$  and  $g(\cdot; \theta_j)$  for observations  $i$  and  $j$ , respectively. The point estimator of the clustering of  $\mathbf{X}^0$  is given by a Bayes estimator, denoted  $\mathbf{c}_{\text{FOLD}}$ , which is the minimizer of (5) over the space of all possible cluster allocations, i.e.  $\mathbf{c}_{\text{FOLD}} = \underset{\hat{\mathbf{c}}}{\operatorname{argmin}} \mathcal{R}(\hat{\mathbf{c}})$ . The expected statistical distance terms in the risk (5) exhibit several bounded and metric properties.

**Proposition 2.** Let  $\Delta = (\Delta_{ij})_{i,j}$ , where  $\Delta_{ij} = \mathbb{E}_{\Pi}(\mathcal{D}_{ij} \mid \mathbf{X}^0)$ . Then  $\Delta$  satisfies the following with  $\mathbb{P}^0$ -probability equal to 1 for all  $i, j, l = 1, \dots, n$ : (a)  $0 \leq \Delta_{ij} \leq 1$ ; (b)  $\Delta_{ii} = 0$ ,  $\Delta_{ji} = \Delta_{ij}$ , and  $\Delta_{il} \leq \Delta_{ij} + \Delta_{jl}$ ; and (c)  $\Delta_{ij} \leq \Pi(s_i \neq s_j \mid \mathbf{X}^0)$ .

Properties (a) and (b) follow naturally from the assumptions we have made regarding the statistical distance  $d$ . To show (c), recall that, conditional on  $\lambda = \sum_{k=1}^K a_k \delta_{\tilde{\theta}_k}$ , variation in  $\theta_i$  and  $\theta_j$  is explained by sampling from  $\lambda$  in (1). This implies that  $\mathbb{E}_{\Pi}(\mathcal{D}_{ij} \mid \mathbf{X}^0, \lambda) = \sum_{k \neq k'} d\{g(\cdot; \tilde{\theta}_k), g(\cdot; \tilde{\theta}_{k'})\} \Pi(s_i = k, s_j = k' \mid \mathbf{X}^0, \lambda)$ . Since  $0 \leq d(\cdot, \cdot) \leq 1$ , we have that  $\mathbb{E}_{\Pi}(\mathcal{D}_{ij} \mid \mathbf{X}^0, \lambda) \leq \sum_{k \neq k'} \Pi(s_i = k, s_j = k' \mid \mathbf{X}^0, \lambda) = \Pi(s_i \neq s_j \mid \mathbf{X}^0, \lambda)$ . Taking the expectation with respect to the posterior of  $\lambda$  on both sides of the inequality results in (c). Properties (a) and (b) imply that  $\mathcal{R}(\hat{\mathbf{c}})$  is non-negative for any clustering and that the sum in (5) may be taken over the indices  $i < j$ . Property (c) states that FOLD will generally favor a fewer number of clusters than Binder’s loss. One can show that Binder’s loss prefers assigning  $i$  and  $j$  to the same cluster when  $\Pi(s_i \neq s_j \mid \mathbf{X}^0) < \gamma$ . If  $\Delta_{ij} < \gamma < \Pi(s_i \neq s_j \mid \mathbf{X}^0)$ , FOLD will disagree with Binder’s loss, with FOLD preferring to merge  $i$  and  $j$  into the same cluster, implying that  $\mathbf{c}_{\text{FOLD}}$  is often more coarse than  $\mathbf{c}_{\text{B}} = \underset{\hat{\mathbf{c}}}{\operatorname{argmin}} \mathbb{E}_{\Pi} \{ \mathcal{L}_{\text{B}}(\hat{\mathbf{c}}, \mathbf{s}) \mid \mathbf{X}^0 \}$ .

Recently, the Variation of Information (VI) (Meilă, 2007) has attracted attention in the literature for use as a clustering loss function (Wade and Ghahramani, 2018; De Iorio et al., 2023; Denti et al., 2023), and we compare FOLD to the VI from a methodological point of view in the Supplement. The VI is primarily motivated from an information theoretic perspective, but it, like Binder’s loss, is a metric on the partition space (Meilă, 2007; Dahl et al., 2022) and encourages similarity to the component labels when used in Bayesian clustering. While the VI has been observed to yield fewer clusters than Binder’s loss empirically on synthetic and real data (Wade and Ghahramani, 2018), we show in a simulation study in the Supplementary and an application in Section 4 that  $\mathbf{c}_{\text{VI}}$  is still vulnerable to the over-clustering problem, albeit usually to a lesser degree than  $\mathbf{c}_{\text{B}}$ , whereas  $\mathbf{c}_{\text{FOLD}}$  is more robust.

### 2.3 UNCERTAINTY QUANTIFICATION

In applications of Bayesian clustering to real data, we often find that there is substantial uncertainty in the component labels a posteriori. To avoid overstating the significance of  $\mathbf{c}_{\text{FOLD}}$ , it is thus important to express this uncertainty in a clear and interpretable manner. We focus on the clustering that minimizes (2), i.e.  $\mathbf{c}_{\boldsymbol{\theta}} = \underset{\hat{\mathbf{c}}}{\operatorname{argmin}} \mathcal{L}(\hat{\mathbf{c}}, \boldsymbol{\theta})$ . Observe that  $\mathbf{c}_{\boldsymbol{\theta}}$  depends on  $\omega$  and may not be equal to  $\mathbf{s}$ . To see this, we recall (4), which shows that we can acquire a clustering with loss smaller than  $\mathbf{s}$  by merging any two components with statistical distance below  $\gamma$ . Thus, we formulate our measures of uncertainty with respect to the FOLD posterior  $\Pi(\mathbf{c}_{\boldsymbol{\theta}} \mid \mathbf{X}^0)$ , instead of  $\Pi(\mathbf{s} \mid \mathbf{X}^0)$ .

Accordingly, we adapt the notion of a credible ball for Bayesian clustering estimators (Wade and Ghahramani, 2018) to our procedure. The 95% credible ball around  $\mathbf{c}_{\text{FOLD}}$  is defined as  $B(\mathbf{c}_{\text{FOLD}}) =$

$\{\mathbf{c} : \mathbb{D}(\mathbf{c}_{\text{FOLD}}, \mathbf{c}) \leq \epsilon_{\text{FOLD}}\}$ , where  $\epsilon_{\text{FOLD}} \geq 0$  is the smallest radius such that

$$\Pi \{\mathbb{D}(\mathbf{c}_{\text{FOLD}}, \mathbf{c}_{\theta}) \leq \epsilon_{\text{FOLD}} \mid \mathbf{X}^0\} \geq 0.95.$$

We interpret  $B(\mathbf{c}_{\text{FOLD}})$  as a neighborhood of clusterings centered at  $\mathbf{c}_{\text{FOLD}}$  with posterior probability mass of at least 0.95. Larger  $\epsilon_{\text{FOLD}}$  means that the FOLD posterior distributes its mass across a larger set around  $\mathbf{c}_{\text{FOLD}}$ , implying that we are more uncertain about the cluster allocations of the point estimator. In practice, we characterize the credible ball with bounds that give a sense of the clusterings contained within it (Wade and Ghahramani, 2018), much like we would for an interval on the real line. The horizontal bounds of the credible ball consist of the clusterings  $\mathbf{c} \in B(\mathbf{c}_{\text{FOLD}})$  for which  $\mathbb{D}(\cdot, \mathbf{c}_{\text{FOLD}})$  attains its maximum value. We can also impose further restrictions on our bounds, such as requiring that they contain the minimum or maximum number of clusters over  $B(\mathbf{c}_{\text{FOLD}})$  while also maximizing  $\mathbb{D}(\cdot, \mathbf{c}_{\text{FOLD}})$  amongst groupings with the same number of clusters, giving rise to the notions of vertical upper and vertical lower bounds, respectively. Alternatively, one can display the posterior similarity matrix (PSM) for  $\mathbf{c}_{\theta}$ ,  $\mathcal{P}_{\text{FOLD}} = (\Pi \{c_{i\theta} = c_{j\theta} \mid \mathbf{X}^0\})_{i,j}$ , as a heatmap, with the entries ordered by  $\mathbf{c}_{\text{FOLD}}$ , as is common practice for both Binder’s loss and the VI.

## 2.4 IMPLEMENTATION WITH MCMC OUTPUT

Our methodology relies on Markov chain Monte Carlo (MCMC) samples from  $\Pi(\boldsymbol{\theta} \mid \mathbf{X}^0)$ , which are used to estimate pairwise distances between the localized densities,  $\Delta_{ij} \approx (1/T) \sum_{t=1}^T \mathcal{D}_{ij}^{(t)}$ , where  $\mathcal{D}_{ij}^{(t)} = d \left\{ g(\cdot; \theta_i^{(t)}), g(\cdot; \theta_j^{(t)}) \right\}$ , and  $\theta_i^{(t)}, \theta_j^{(t)}$  can be computed directly from samples of the components  $\mathbf{s}^{(t)}$  and unique values  $\tilde{\boldsymbol{\theta}}^{(t)}$  via  $\theta_i^{(t)} = \tilde{\theta}_k^{(t)} \iff s_i^{(t)} = k$ . When  $d$  is chosen to be the Hellinger distance, many families of kernels, such as the Gaussian family, admit a closed form of  $\mathcal{D}_{ij}$ . The label-switching problem, which results from the inherent non-identifiability of mixture models with any permutation of the labels yielding the same likelihood (Redner and Walker, 1984), has no impact on FOLD, as  $\Delta_{ij}$  is invariant to labeling. FOLD can be easily applied to virtually any mixture model for which samples from  $\Pi(\boldsymbol{\theta} \mid \mathbf{X}^0)$  can be obtained and pairwise statistical distances can be estimated.

In practice, the minimization of (5) must be approximated due to the enormous size of the partition space for even modest  $n$ . We discuss two methods for obtaining an approximate minimizer. The first is to simply reduce the set of partitions over which we minimize by only considering a tree of clusterings produced by hierarchical clustering on  $\Delta$ . We suggest generating candidates using average linkage due to the appearance of the average linkage dissimilarity metric as a criterion for merging clusters in (4). Figure 3 displays candidate clusterings of the moons data resulting from average linkage clustering on  $\Delta$ . The true grouping of the data is present amongst the candidates. Since these groupings are hierarchical, Figure 3 can be interpreted as an enumeration of clusterings favored by  $\mathcal{R}(\hat{\mathbf{c}})$ , arranged by increasing values of  $\omega$ . A similar method with single-linkage is defined in Aragam et al. (2020), and

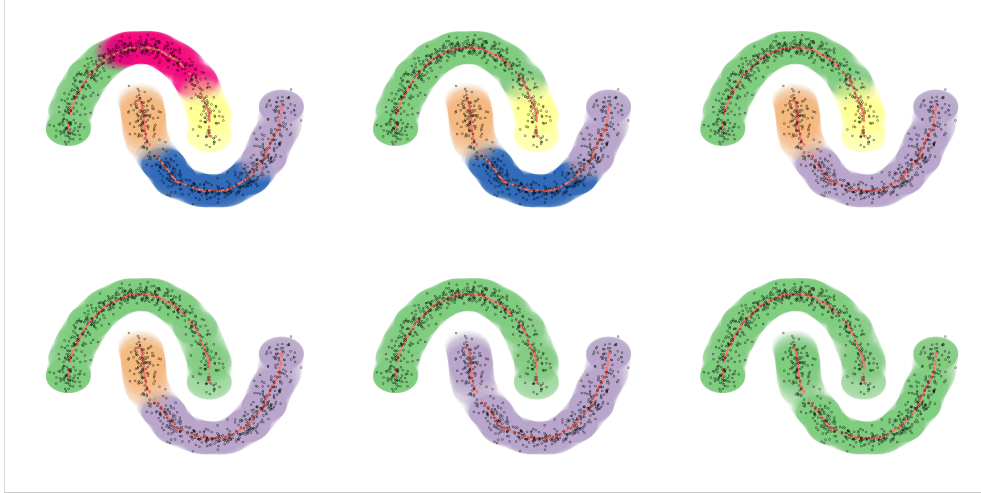


Figure 3: Candidate clusterings of the moons data under a location Gaussian mixture model, generated from average linkage hierarchical clustering on  $\Delta$ .

Medvedovic and Sivaganesan (2002) and Fritsch and Ickstadt (2009) have previously used hierarchical clustering on  $\mathbf{1}_n \mathbf{1}_n^T - \mathcal{P}$  to compute clustering point estimators, where  $\mathcal{P} = (\Pi \{s_i = s_j \mid \mathbf{X}^0\})_{i,j}$ .

Recent developments for minimizing risk functions have focused on greedy algorithms that take an existing candidate partition and make minor, but locally-optimal updates, typically by reallocation of objects to clusters. Examples include a method motivated by the Hasse diagram in Wade and Ghahramani (2018), the greedy algorithm in Rastelli and Friel (2018), and the SALS0 algorithm of Dahl et al. (2022). SALS0 provides a point estimate by first initializing a clustering, then reallocating observations to clusters and, finally, breaking existing clusters and then reallocating observations again over several parallel runs. The final point estimate is the partition that exhibits the smallest risk across all the runs. In our simulations and application, we implement FOLD with both the hierarchical clustering heuristic and SALS0, and find that they generally agree on the optimal clustering.

To express uncertainty in  $\mathbf{c}_{\text{FOLD}}$ , we rely on samples from  $\Pi(\mathbf{c}_\theta \mid \mathbf{X}^0)$ , defined by

$$\mathbf{c}_\theta^{(t)} = \underset{\hat{\mathbf{c}}}{\operatorname{argmin}} \sum_{i < j} \left\{ \mathbf{1}_{\hat{c}_i = \hat{c}_j} \mathcal{D}_{ij}^{(t)} + \omega \mathbf{1}_{\hat{c}_i \neq \hat{c}_j} (1 - \mathcal{D}_{ij}^{(t)}) \right\}. \quad (6)$$

As in the point estimation case,  $\mathbf{c}_\theta^{(t)}$  cannot be computed exactly and so we approximate the minimization in (6) either using a set of candidates generated from hierarchical clusterings of  $\mathcal{D}^{(t)} = (\mathcal{D}_{ij}^{(t)})_{i,j}$  or via a greedy algorithm such as SALS0. The posterior probability of a credible ball is approximated by  $\Pi \{ \mathbb{D}(\mathbf{c}_\theta, \mathbf{c}_{\text{FOLD}}) \leq \epsilon \mid \mathbf{X}^0 \} \approx (1/T) \sum_{t=1}^T \mathbf{1}_{\mathbb{D}(\mathbf{c}_\theta^{(t)}, \mathbf{c}_{\text{FOLD}}) \leq \epsilon}$  and FOLD computes  $\epsilon_{\text{FOLD}}$  by incrementally increasing the value of  $\epsilon$  over a grid. The entries of  $\mathcal{P}_{\text{FOLD}}$  are estimated via  $\Pi(c_{i\theta} = c_{j\theta} \mid \mathbf{X}^0) \approx (1/T) \sum_{t=1}^T \mathbf{1}_{c_{i\theta}^{(t)} = c_{j\theta}^{(t)}}$ .

## 2.5 SELECTION OF $\omega$

The loss parameter  $\omega$  controls the separation among the inferred clusters in  $\mathbf{c}_{\text{FOLD}}$ . This parameter is also influential in  $\mathbf{c}_{\text{VI}}$  and  $\mathbf{c}_{\text{B}}$  (Dahl et al., 2022), though there has been little discussion in the literature on how to select an appropriate  $\omega$  for these loss functions. The formulation of (2) in terms of statistical distances leads to two sensible methods for determining the loss parameter. First, similarly to common practice in choosing key tuning parameters in algorithmic clustering methods such as k-means and DBSCAN, we propose an elbow plot diagnostic to select  $\omega$ . At a grid of possible  $\omega$  values, we calculate  $r_\omega = (\sum_{h=1}^{K_\omega^*} r_{\omega h}) / \sum_{i < j} \Delta_{ij}$ , where  $r_{\omega h} = \sum_{i,j \in C_{\omega h}^*} \Delta_{ij}$ ,  $\mathbf{c}_\omega^*$  is the FOLD point estimator for that specific  $\omega$ , and  $C_\omega^* = \{C_{\omega 1}^*, \dots, C_{\omega K_\omega^*}^*\}$  is the partition associated with  $\mathbf{c}_\omega^*$ . The numerator in  $r_\omega$  sums over  $r_{\omega h} = \mathbb{E}_\Pi \left\{ \sum_{i,j \in C_{\omega h}^*} \mathcal{D}_{ij} \mid \mathbf{X}^0 \right\}$ , or the expected statistical distance between all localized densities associated with the  $h$ th cluster in  $\mathbf{c}_\omega^*$ , and the denominator normalizes so that  $r_\omega \in [0, 1]$  for all  $\omega$ .

To build some intuition about the utility of the elbow plot, recall that as  $\omega \rightarrow \infty$ , (5) is minimized by placing all observations in a single cluster, i.e.  $C_\infty^* = \{[n]\}$  and  $r_\infty = 1$ . In many cases, such as the data in Figure 3, decreasing  $\omega$  (and subsequently adding more clusters in  $C_\omega^*$ ) will decrease  $r_\omega$ , e.g. because  $\Delta_{ij} \approx 1$  for any  $i, j$  pairs in different crescents. Of course, at the other extreme, if we set  $\omega$  to be very small, we place all objects in their own cluster, making  $C_0^* = \{\{1\}, \dots, \{n\}\}$  and  $r_0 = 0$ . We construct the elbow plot to quantify the amount of improvement each time we increment  $\omega$  across this grid. At some point, the improvement in  $r_\omega$  becomes negligible as we decrease  $\omega$  because we begin to cut dense clusters into smaller and smaller sub-clusters. On an elbow plot, this causes the curve of  $r_\omega$  to bend, creating the so-called ‘‘elbow’’. It is at this threshold that we fix  $\omega$ . The threshold is easier to identify when the elbow plot is monotonic, and we verify this is the case if one uses hierarchical clustering to generate candidates.

**Proposition 3.** If candidate clusterings are selected using average linkage hierarchical clustering on  $\Delta$ , then there is a positive relationship between  $\omega$  and  $r_\omega$ .

A corollary of Proposition 3 is that any jump in the elbow plot corresponds to decreasing the number of clusters by one, meaning that there is a negative relationship between  $K_\omega^*$  and  $r_\omega$ . Therefore, one can relabel the x-axis of the elbow plot in terms of the number of clusters rather than  $\omega$ , leading to a more interpretable figure. An example of using an elbow plot to select  $\omega$  is given in Section 4.

Alternatively, one can use the default value  $\omega^{\text{AVG}} = \gamma^{\text{AVG}} / (1 - \gamma^{\text{AVG}})$ , with  $\gamma^{\text{AVG}} = \binom{n}{2}^{-1} \sum_{i < j} \Delta_{ij}$ . Under this choice of  $\omega$ , candidate clusters are combined when the average of  $\Delta_{ij}$  between the clusters is smaller than the average of  $\Delta_{ij}$  across the entire sample.  $\gamma^{\text{AVG}}$  estimates  $\bar{\mathcal{D}} = \binom{n}{2}^{-1} \sum_{i < j} \mathcal{D}_{ij} = \sum_{k < k'} (|S_k| |S_{k'}| / \binom{n}{2}) d \left\{ g(\cdot; \tilde{\theta}_k), g(\cdot; \tilde{\theta}_{k'}) \right\}$ , a weighted pairwise sum across the components. If we use  $\bar{\mathcal{D}} / (1 - \bar{\mathcal{D}})$  in place of  $\omega$  in (2), (4) implies that FOLD will favor merging mixture components when

$d\{g(\cdot; \tilde{\theta}_k), g(\cdot; \tilde{\theta}_{k'})\} < \bar{D}$ . Importantly, the decision to merge components will depend on how separated they are from the others and their sizes. To see this, consider the following example, in which we fit a mixture with  $K = 3$  components, where  $d\{g(\cdot; \tilde{\theta}_1), g(\cdot; \tilde{\theta}_2)\} = \epsilon > 0$ ,  $d\{g(\cdot; \tilde{\theta}_1), g(\cdot; \tilde{\theta}_3)\} = d\{g(\cdot; \tilde{\theta}_2), g(\cdot; \tilde{\theta}_3)\} = \delta > 0$ , and  $|S_1| = |S_2| = |S_3| = n/3$ . Then, as  $n$  grows large,  $\bar{D} \rightarrow (2/9)\epsilon + (4/9)\delta$ , and so FOLD will favor merging  $S_1$  and  $S_2$  into one cluster when  $\epsilon < (4/7)\delta$ . The smaller  $\delta$  is, the smaller  $\epsilon$  must be in order to merge  $S_1$  and  $S_2$ . Hence,  $\omega^{\text{AVG}}$  excels at problems in which  $f^0$  is composed of well-separated kernels that are approximated by multiple components in  $f$ . We provide simulation studies in the Supplement that show that  $\omega^{\text{AVG}}$  performs very well in this setting.

### 3 ASYMPTOTIC ANALYSIS

Though there is a rich literature on asymptotic properties of Bayesian mixture models for estimating the density (Ghosal et al., 1999; Ghosal and van der Vaart, 2007), number of components (Rousseau and Mengersen, 2011; Miller and Harrison, 2014; Cai et al., 2021; Ascolani et al., 2023), and the mixing measure (Nguyen, 2013; Ho and Nguyen, 2016a,b; Guha et al., 2021), little attention has been given to the large sample behavior of clustering estimators. Rajkowski (2019) focused on the maximum a posteriori (MAP) estimator for  $\mathbf{s}$  when data are generated from a DPM with Gaussian components and the kernels are correctly specified. They show multiple properties of the MAP estimator, including the key result that the intersection between the convex hulls of two clusters is at most a single observation. In this section, we show convergence of FOLD towards the *oracle clustering procedure* in which the objects are partitioned into groups using knowledge of the true data generating process. We take a different approach than Rajkowski (2019) by focusing on posterior contraction of the mixing measure  $\lambda$ , which allows us to consider misspecified models, either in the kernels or number of components.

#### 3.1 ASSUMPTIONS

We first require that the parameter space  $\Theta \subset \mathbb{R}^p$  is compact and  $f$ , defined formally as  $f(x) = \int g(x; \theta) \lambda(d\theta)$ , is identifiable with respect to the mixing measure, that is,  $\int g(x; \theta) \lambda_1(d\theta) = \int g(x; \theta) \lambda_2(d\theta)$  for all  $x \in \chi$  if and only if  $\lambda_1 = \lambda_2$  (Teicher, 1961). Identifiability of the mixing measure is satisfied by location and location-scale GMMs, as well as various exponential family mixtures (Barndorff-Nielsen, 1965) and location family mixtures (Teicher, 1961). More specifically, our results rely on contraction of the mixing measure  $\lambda$  to some oracle measure  $\lambda^*$ , which implies convergence of  $f$  to an oracle model  $f^* = \int g(\cdot; \theta) \lambda^*(d\theta)$ . An oracle measure is defined as any Kullback-Liebler (KL) divergence minimizer between our class of models and the true data generating process, i.e.  $\lambda^* \in \underset{\lambda \in \Lambda}{\operatorname{argmin}} \operatorname{KL}(f^0, f)$ , where recall  $\Lambda = \operatorname{supp}(\pi_\Lambda)$ . We now present the general assumptions required for our results.

**Assumption 1.** Suppose that the following conditions hold.

(A1) There exists an  $L > 0$  such that  $|\text{supp}(\lambda)| \leq L$  for all  $\lambda \in \Lambda$ .

(A2) The KL minimizer  $\lambda^* = \sum_{m=1}^{M^*} a_m^* \delta_{\theta_m^*}$  exists and is unique.

(A3)  $f^*$  and  $f^0$  are such that  $\text{supp}(f^0) \subseteq \text{supp}(f^*)$ .

(A4):  $\mathcal{G} = \{\tilde{g}(x - \theta) : \theta \in \Theta\}$  for some bounded probability density function  $\tilde{g}(\cdot)$ ,  $\tilde{g}(\cdot)$  is  $\zeta$ -Hölder continuous for some  $\zeta > 0$ , and for any fixed  $\theta'$ ,  $D_g(\theta, \theta') = d\{g(\cdot; \theta), g(\cdot; \theta')\}$  is continuous in  $\theta$ .

(A5) There exists a non-negative sequence  $\epsilon_n$  so that  $\epsilon_n \rightarrow 0$  and

$$\rho_n(\mathbf{X}^0) = \Pi \left\{ \lambda \in \Lambda : W_2(\lambda, \lambda^*) \gtrsim \epsilon_n \mid \mathbf{X}^0 \right\} \xrightarrow{\mathbb{P}^0} 0. \quad (7)$$

(A1) is satisfied by any mixture model in which the number of components is bounded, and examples include a finite mixture model, a truncated MFM, or truncated DPM. Assumption (A2) ensures that the limiting values of the clustering procedure are well-defined and exist. A simple example of when (A2) holds is when the kernels are correctly specified and  $\Pi(K = M^0) > 0$ , in which case  $\lambda^* = \lambda^0$  and  $f^* = f^0$ . We refer to the case in which  $\Pi(K = M^0) = 1$  as the exact-fitted and well-specified regime, which is permitted under assumptions (A1)-(A2). Under any misspecification, (A2) holds when  $\min_{\lambda \in \Lambda} \text{KL}(f^0, f) = \min_{\lambda \in \Omega} \text{KL}(f^0, f)$ , where  $\Omega$  is the space of all probability measures over  $\Theta$  (Guha et al., 2021). That is, assumption (A2) is satisfied in the misspecified regime when the minimum KL divergence is attained over  $\Lambda$ . This still allows for an exact-fitted and misspecified regime, in which  $\Pi(K = M^*) = 1$ . (A3) is a technical assumption to ensure there are no regions in the sample space under which  $f^0$  gives positive probability but  $f^*$  does not. Assumption (A4) restricts our results to location families, and the continuity conditions are satisfied by a variety of models including the location GMM with fixed covariance. Assumption (A5) is a crucial statement on the estimation of parameters in a mixture model. (A5) will hold under various Lipschitz and strong identifiability conditions on  $\mathcal{G}$  (Nguyen, 2013; Ho and Nguyen, 2016a; Guha et al., 2021) that are satisfied by the location GMM (Manole and Ho, 2022), and we discuss these conditions in detail in the Supplementary Material. (A5) will hold with  $\epsilon_n = (\log n/n)^{1/4}$  for second-order identifiable families, and first-order identifiable families with  $\epsilon_n = (\log n/n)^{1/2}$  if the kernels are correctly specified and  $\Pi(K = M^0) = 1$  (Guha et al., 2021); see Ho and Nguyen (2016a,b) for a characterization of first and second-order identifiable kernels.

### 3.2 CONVERGENCE TO THE ORACLE RULE

Synonymous with the oracle mixing measure is the oracle clustering procedure or rule. We define the oracle clustering procedure to be the minimizer of the oracle risk function  $\mathcal{R}^*(\hat{\mathbf{c}}) = \mathbb{E}_\Pi[\mathcal{L}(\hat{\mathbf{c}}, \boldsymbol{\theta}) \mid$

$\lambda^*, \mathbf{X}^0]$ ,

$$\mathbf{c}_{\text{FOLD}}^* = \underset{\hat{\mathbf{c}}}{\operatorname{argmin}} \mathcal{R}^*(\hat{\mathbf{c}}) = \underset{\hat{\mathbf{c}}}{\operatorname{argmin}} \sum_{i < j} \{ \mathbf{1}_{\hat{c}_i = \hat{c}_j} \Delta_{ij}^* + \omega \mathbf{1}_{\hat{c}_i \neq \hat{c}_j} (1 - \Delta_{ij}^*) \}, \quad (8)$$

where  $\Delta_{ij}^* = \mathbb{E}_{\Pi}(\mathcal{D}_{ij} \mid \lambda^*, \mathbf{X}^0) = \sum_{m < m'} d\{g(\cdot; \theta_m^*), g(\cdot; \theta_{m'}^*)\} q_{ij}^{mm'^*}$ , with  $q_{ij}^{mm'^*} = \Pi(s_i = m, s_j = m' \mid \mathbf{X}^0, \lambda^*) + \Pi(s_i = m', s_j = m \mid \mathbf{X}^0, \lambda^*)$ , and

$$\Pi(s_i = m, s_j = m' \mid \mathbf{X}^0, \lambda^*) = \frac{a_m^* a_{m'}^* g(X_i^0; \theta_m^*) g(X_j^0; \theta_{m'}^*)}{f^*(X_i^0) f^*(X_j^0)}.$$

Observe that  $\Delta_{ij}^*$  is a weighted sum of the total statistical distance between the oracle components, where the weight of each component pair is given by the conditional probability that  $s_i = m$  and  $s_j = m'$  (or vice versa) given  $\mathbf{X} = \mathbf{X}^0$  and  $\lambda = \lambda^*$ . We interpret the oracle clustering procedure as a rule for grouping the observations in  $\mathbf{X}^0$  based on the knowledge of the optimal parameter values in the mixture model. We can construct two simple examples of oracle rules which follow from the definition in (8).

**Proposition 4.** Instances of the oracle clustering procedure include:

- (a) If  $d\{g(\cdot; \theta_m^*), g(\cdot; \theta_{m'}^*)\} = 1$  for all  $m, m'$ , then  $\mathbf{c}_{\text{FOLD}}^* = \mathbf{s}^*$ , where  $s_i^* = s_j^*$  if and only if there exists a unique  $m \in [M^*]$  such that  $g(X_i^0; \theta_m^*) g(X_j^0; \theta_m^*) > 0$ .
- (b) If  $M^* = 2$  and  $d\{g(\cdot; \theta_1^*), g(\cdot; \theta_2^*)\} < \gamma$ , then  $\mathbf{c}_{\text{FOLD}}^* = \mathbf{c}_0$ , where  $c_{0i} = c_{0j}$  for all  $i, j$ .

We refer to the procedure on Proposition 4(a) as the ‘‘match rule’’ in that it allocates each observation to a mixture component with compatible support, and call the procedure in Proposition 4(b) the ‘‘merge rule’’, i.e., as the statistical distance between oracle components becomes smaller, we are more likely to combine them and subsequently place all observations in one cluster. A similar quantity exists for Binder’s loss function, denoted  $\mathbf{c}_{\text{B}}^* = \underset{\hat{\mathbf{c}}}{\operatorname{argmin}} \mathbb{E}_{\Pi}[\mathcal{L}_{\text{B}}(\hat{\mathbf{c}}, \mathbf{s}) \mid \lambda^*, \mathbf{X}^0]$ . Under the settings of Proposition 4(a),  $\mathbf{c}_{\text{B}}^* = \mathbf{c}_{\text{FOLD}}^* = \mathbf{s}^*$ , meaning that the match rule is the optimal clustering procedure under both FOLD and Binder’s loss when the oracle components are perfectly separated. Intuitively, this is because these settings reflect an ideal scenario in which all mixture components are perfectly separated and no merging is required. Otherwise, say in the setting of Proposition 4(b), the two methods can differ. A sufficient condition for  $\mathbf{c}_{\text{B}}^* = \mathbf{c}_0$  is  $q_{ij}^{12} < \omega(1 - q_{ij}^{12})$  for all pairs  $i, j$ . Any observations in the tails of the two oracle components will blow up the value of  $q_{ij}^{12}$ , hence, it is possible that  $\mathbf{c}_{\text{B}}^* \neq \mathbf{c}_0$  even for relatively large  $\omega$ . This implies that a concrete advantage of our approach is robustness to outliers when the oracle components are not well separated. We now state our primary theoretical result on the relationship between  $\mathbf{c}_{\text{FOLD}}$  and  $\mathbf{c}_{\text{FOLD}}^*$ .

**Theorem 1.** Fix  $0 < \delta < 1$ . Then under assumptions (A1)-(A5), with  $\mathbb{P}^0$ -probability tending to 1,

$$\binom{n}{2}^{-1} |\mathcal{R}(\mathbf{c}_{\text{FOLD}}) - \mathcal{R}^*(\mathbf{c}_{\text{FOLD}}^*)| \lesssim \max(\omega, 1) \{ \rho_n(\mathbf{X}^0) \bar{\Delta}^* + \mathcal{Q}(\mathbf{X}^0) \}, \quad (9)$$

where  $\bar{\Delta}^* = \binom{n}{2}^{-1} \sum_{i < j} \Delta_{ij}^*$ ,  $\mathcal{Q}(\mathbf{X}^0) = \binom{n}{2}^{-1} \sum_{i < j} \tau_n^*(X_i^0, X_j^0)$ , and  $\tau_n^*(X_i^0, X_j^0)$  is a function of  $(X_i^0, X_j^0, \epsilon_n, \rho_n(\mathbf{X}^0), \lambda^*, \zeta, \delta)$  so that  $\tau_n^*(X_i, X_j) \xrightarrow{\mathbb{P}^0} 0$ .

To prove Theorem 1, we first note that we can write  $\Delta_{ij}$  as the posterior expectation of a quantity that only depends on  $\lambda = \sum_{k=1}^K a_k \delta_{\tilde{\theta}_k}$ ,

$$\Delta_{ij} = \int_{\lambda \in \Lambda} \Pi(d\lambda | \mathbf{X}^0) \sum_{k < k'} D_g(\tilde{\theta}_k, \tilde{\theta}_{k'}) a_k a_{k'} \frac{g(X_i^0; \tilde{\theta}_k) g(X_j^0; \tilde{\theta}_{k'}) + g(X_i^0; \tilde{\theta}_{k'}) g(X_j^0; \tilde{\theta}_k)}{f(X_i^0) f(X_j^0)}. \quad (10)$$

Next, we decompose  $\Lambda = B_{\epsilon_n}(\lambda^*) \cup (\Lambda \setminus B_{\epsilon_n}(\lambda^*))$ , where  $B_{\epsilon_n}(\lambda^*) = \{ \lambda \in \Lambda : W_2(\lambda, \lambda^*) \leq \epsilon_n \}$ , and split (10) into a sum of integrals over these domains. Since  $0 \leq D_g(\theta, \theta') \leq 1$ , the integral over  $\Lambda \setminus B_{\epsilon_n}(\lambda^*)$  is bounded above by  $\rho_n(\mathbf{X}^0)$ , which goes to 0 in probability by (A5). Then, using a similar proof technique given in [Nguyen \(2013\)](#), we show that there exists a finite  $N$  so that for all  $n \geq N$  and  $\lambda \in B_{\epsilon_n}(\lambda^*)$ ,  $\lambda$  has at least  $M^*$  support points and for any  $m \in [M^*]$  there exists a set of indices  $\mathcal{I}_m^{(\lambda)} \subset [K]$  so that  $\max_{k \in \mathcal{I}_m^{(\lambda)}} \|\tilde{\theta}_k - \theta_m^*\| \leq \epsilon_n$  and  $\left| \sum_{k \in \mathcal{I}_m^{(\lambda)}} a_k - a_m^* \right| \leq \max(\epsilon_n, \epsilon_n^{2\delta})$ . Furthermore, if we denote  $\mathcal{I}^{(\lambda)} = \bigcup_{m=1}^{M^*} \mathcal{I}_m^{(\lambda)}$ , (A5) also implies that  $\sum_{k \notin \mathcal{I}^{(\lambda)}} a_k \leq \epsilon_n^{2\delta}$ . By (A4), these bounds translate into similar upper and lower bounds for  $\Delta_{ij}$ . We then sum over all  $i, j$  pairs and show that  $\binom{n}{2}^{-1} |\mathcal{R}(\hat{\mathbf{c}}) - \mathcal{R}^*(\hat{\mathbf{c}})|$  is uniformly bounded by the right hand side of (9) for all  $\hat{\mathbf{c}}$ . That is, the rate of convergence of  $\mathcal{R}(\hat{\mathbf{c}})$  to  $\mathcal{R}^*(\hat{\mathbf{c}})$  does not depend on the clustering estimator itself. Finally, we show that this implies convergence of the minimizers at the same rate.

The bound in (9) is split into two remainder terms. It follows from (A5) that  $\rho_n(\mathbf{X}^0) \bar{\Delta}^* \xrightarrow{\mathbb{P}^0} 0$  since  $0 \leq \bar{\Delta}^* \leq 1$ . Therefore, smaller values of  $\bar{\Delta}^*$  will cause this term to diminish faster. This can arise when  $f^*$  is comprised of many closely overlapping components. Hence, convergence to the oracle rule will actually benefit from overfitting.  $\mathcal{Q}(\mathbf{X}^0)$  is a more general remainder term that results from translating the posterior contraction of  $\tilde{\theta}_k$  and  $a_k$  to the sum in (10). In particular, this remainder term will depend on  $\delta$ , which controls the rate at which the irrelevant mixture components are emptied, the Hölder constant  $\zeta$ , which controls convergence of  $g(X_i^0; \tilde{\theta}_k)$  to  $g(X_i^0; \theta_m^*)$ , and  $L - M^*$ , or the degree to which the number of components is misspecified, with larger  $L$  implying a slower rate of convergence.

In the Supplementary Material we empirically validate Theorem 1 on a simple simulated example. We simulate data from  $M^0 = 4$  Gaussian components with covariance equal to  $0.25I$ , then fit a 4-component Bayesian mixture model, meaning that  $f^0(x) = f^*(x) = \sum_{m=1}^4 a_m^0 \mathcal{N}(x; \mu_m^0, 0.25I)$ . We compute  $\mathbf{c}_{\text{FOLD}}$ ,  $\mathbf{c}_{\text{FOLD}}^*$ ,  $\mathbf{c}_{\text{B}}$ , and  $\mathbf{c}_{\text{B}}^*$ , the latter of which denotes the oracle clusters corresponding to Binder's loss, for increasing sample size. We show that both  $\mathcal{R}(\hat{\mathbf{c}}) \rightarrow \mathcal{R}^*(\hat{\mathbf{c}})$  and  $\mathbf{c}_{\text{FOLD}} \rightarrow \mathbf{c}_{\text{FOLD}}^*$

as  $n \rightarrow \infty$ . Additionally, there are substantial differences between  $\mathbf{c}_{\text{FOLD}}^*$  and  $\mathbf{c}_{\text{B}}^*$  because oracle FOLD corresponds to the merge rule for some of the Gaussian components, while oracle Binder prefers estimation of each individual component.

## 4 EXAMPLE: GSE81861 CELL LINE DATASET

We apply FOLD to the GSE81861 cell line dataset (Li et al., 2017), which measures single cell counts in 57,241 genes from 630 single-cell transcriptomes. There are 7 distinct cell lines present in the dataset, so we compare FOLD and other model-based clustering methods to the true cell line labels as a performance benchmark. First, we apply routine pre-processing steps for RNA sequence analysis (as in Chandra et al. (2023)). We discard cells with low read counts, giving  $n = 519$  total cells. We then normalize the data using SCRAN (Lun et al., 2016) and select informative genes with M3Drop (Andrews and Hemberg, 2019). We use principal component analysis (PCA) for dimension reduction by taking  $\mathbf{X}^0$  to be the projection of the normalized cell counts onto the first  $p = 5$  principal components, then scale the projections to have zero mean and unit variance.

We fit a  $p$ -dimensional Bayesian Gaussian finite mixture to  $\mathbf{X}^0$  with  $K = 50$  components, and simulate 25,000 posterior samples after a burn-in of 1,000. Every fourth iteration is discarded, leaving 6,000 samples remaining. Along with  $\mathbf{c}_{\text{FOLD}}$ , we calculate model-based clusterings with the VI loss, Binder’s loss, and `mclust` (Scrucca et al., 2016), the latter of which implements the EM algorithm and chooses the number of clusters via the Bayesian information criterion (BIC). We also compare to algorithmic clustering methods, including average linkage hierarchical clustering (HCA), k-means, DBSCAN, and spectral clustering. Details on hyperparameter choices for all methods are given in the Supplement. For FOLD, we create candidate clusterings by average-linkage clustering on  $\Delta$ , then choose  $\omega$  by consulting the elbow plot in Figure 4. The plot suggests 6 clusters, which corresponds to  $\omega = 25$ . We also implement SALSO over 150 independent runs to minimize (5). However, over repeated replications we find that the SALSO estimate is either equal to or has a higher risk than the point estimate given by hierarchical clustering on  $\Delta$ . Binder’s loss and the VI loss are implemented with  $\omega = 1$  (the default value in `mcclust` (Fritsch, 2022)), which results in  $\mathbf{c}_{\text{VI}} = \mathbf{c}_{\text{B}}$ .

Figure 5 shows the UMAP plots (McInnes et al., 2018) of the original normalized count data along with colors indicating the true cell types and the clusterings from the three model-based methods. The adjusted Rand index (ARI) (Hubert and Arabie, 1985) with the true cell types and number of clusters ( $\hat{K}_n$ ) for  $\mathbf{c}_{\text{FOLD}}$  and all other clusterings are given in Table 1. First, observe that the Bayesian clustering methods outperform the competitors in the ARI, indicating that the overfitted Gaussian components are accurately approximating the distribution within each type. However, FOLD notably excels over the other Bayesian methods with an ARI of 0.995, only misclassifying six observations. Note that the VI, Binder’s loss, and `mclust` split the GM12878 and H1 cell types into two clusters

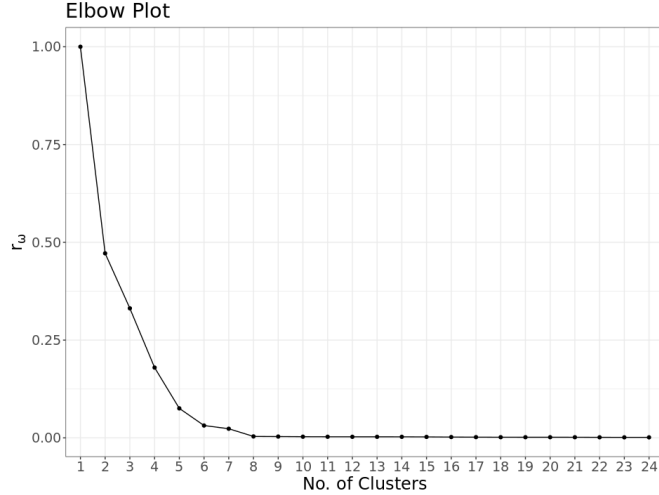


Figure 4: Elbow plot for choosing the number of clusters in  $\mathbf{c}_{\text{FOLD}}$  with the cell line dataset.

each, while FOLD correctly identifies both types, keeping each as single clusters. The splitting of types is not unexpected in this application since the GM12878 and H1 types were each sequenced in two separate batches (Li et al., 2017), indicating that FOLD is more robust to the batch effect than other Bayesian methods. However,  $\mathbf{c}_{\text{FOLD}}$  underestimates the number of groups by combining the H1437 and IMR90 cell types. The other model-based methods merge these types as well, with the VI and Binder’s loss producing 9 clusters and `mclust` giving 7 clusters. Of the algorithmic methods, k-means performs the best, estimating the correct number of types while achieving an ARI of 0.904. However, k-means splits the GM12878 and A549 types into two clusters each, the latter of which is always kept as one cluster by the model-based methods.

	FOLD	VI	Binder	Mclust	HCA	K-Means	DBSCAN	Spectral
ARI	0.995	0.915	0.915	0.854	0.622	0.904	0.679	0.620
$\hat{K}_n$	6	9	9	7	7	7	5	5

Table 1: Adjusted Rand index (ARI) with the true cell lines and the number of clusters ( $\hat{K}_n$ ) for FOLD and competitors on the cell line dataset.

The 95% credible ball around  $\mathbf{c}_{\text{FOLD}}$  is displayed in Figure 6. The credible ball communicates that there is substantial uncertainty in cell types where batch effects occur. The horizontal and vertical upper bounds effectively merge the GM12878 type with the H1437 cell type, which is likely due to the proximity of these two types in the sample space. Conversely, the vertical lower bound splits the GM12878 cell type into two clusters. We are also uncertain in our classification of the H1 cell type, which is similarly split into multiple clusters by the vertical lower bound because of separate batching. Interestingly, in all bounds, the H1437 and IMR90 cell types are allocated to the same cluster. This type merging could be explained by the fact that IMR90 consists of a small number of cells or that

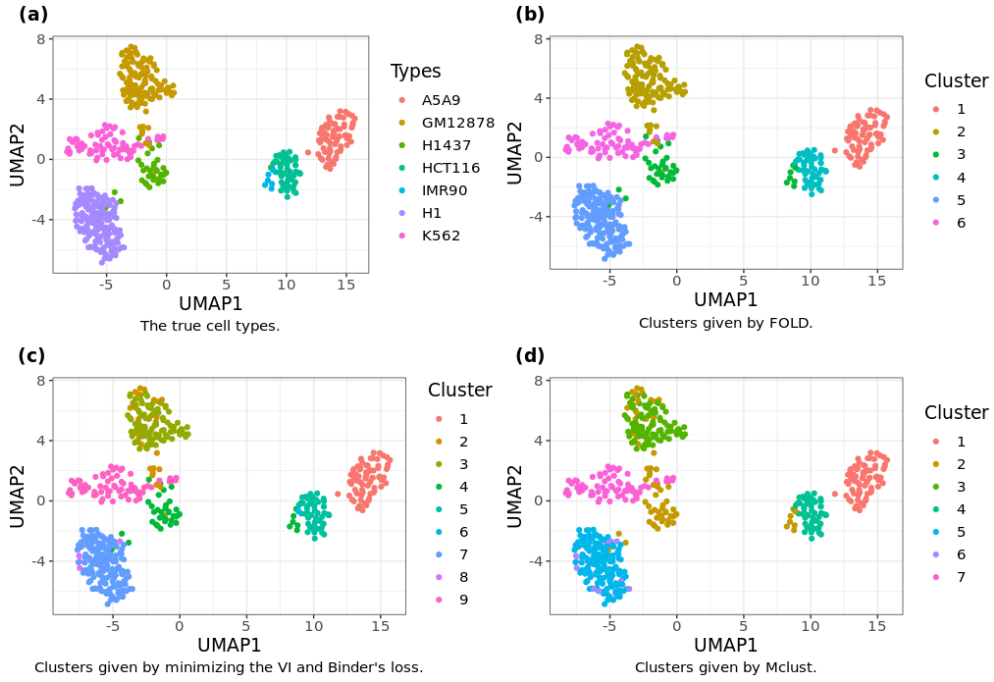


Figure 5: UMAP plots of the cell line dataset with colors corresponding to the true cell types,  $\mathcal{C}_{\text{FOLD}}$ , VI/Binder, and `mclust`, respectively.

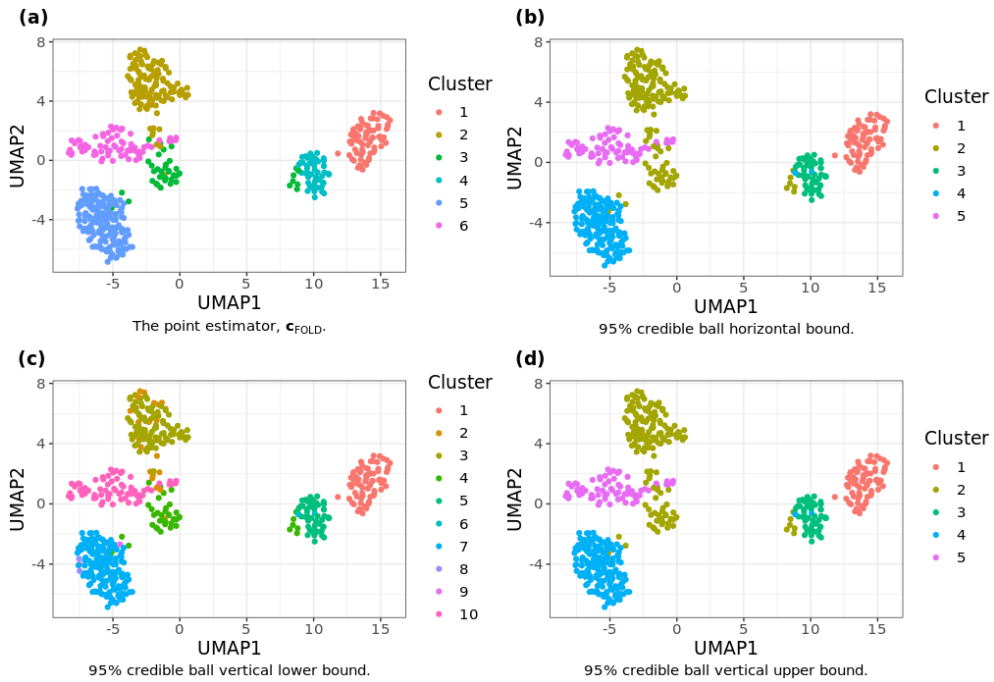


Figure 6: The clustering  $\mathcal{C}_{\text{FOLD}}$  along with the horizontal, vertical lower, and vertical upper bounds for the cell line dataset. Here,  $\mathbb{D}(\cdot, \cdot)$  is the VI and the bounds are unique.

both types are isolated from the lung (Li et al., 2017). In the Supplementary Material, we further evaluate our methodology by applying FOLD and competitors to six clustering datasets.

## 5 DISCUSSION

Fusing of Localized Densities (FOLD) is a Bayesian method for cluster analysis that characterizes clusters as possibly containing multiple mixture components. We first detailed the decision theoretic justification behind our approach, in which we obtain a point estimate of the clustering by minimizing a novel loss function. Our loss function has several appealing properties, such as favoring the merging of overlapping kernels, simplification to Binder’s loss when all the mixture components are well separated, and invariance to permutations of the labels. Uncertainty in cluster allocations is expressed with a credible ball and posterior similarity matrix. We have given concrete guidance on tuning the loss parameter, including an elbow plot method and default value that performs excellently on simulated examples.

Throughout the article, we have primarily focused on the Gaussian mixture model because of its ubiquity in the literature and useful theoretical properties. However, FOLD can be applied to any parametric mixture in which a bounded statistical distance between kernels is simple to compute. For the Hellinger distance, this includes the beta, exponential, gamma, and Weibull families. A near identical approach can be applied to discrete families, where localized mass functions would replace the role of the localized densities.

We have shown that under regularity conditions, our clustering point estimator converges to the oracle clustering procedure as  $n \rightarrow \infty$  for both misspecified and well-specified kernel regimes. The oracle rule categorizes observations into clusters using knowledge about the KL-minimizer. We gave two concrete examples of oracle rules, including the match rule and the merge rule. Our findings imply similar behavior for Binder’s loss, meaning that analogous rules could be potentially derived for other methods such as the VI. These results would provide valuable insight into the overall asymptotic performance of Bayesian clustering. In addition, our results could be extended by focusing on contraction of the mixing measure in terms of the Voronoi loss function (Manole and Ho, 2022), a loss specifically intended for strongly identifiable families that has been shown to contract at a faster rate.

Though we implemented FOLD with the Hellinger distance in our simulations and application, other distribution metrics could be used instead. For a general statistical distance  $d$ , one could set  $\mathcal{D}_{ij} = 1 - \exp\{-d(g(\cdot; \theta_i), g(\cdot; \theta_j))\}$ . The loss of co-clustering  $i$  and  $j$  is  $1 - \exp\{-d(g(\cdot; \theta_i), g(\cdot; \theta_j))\}$ . This implies that we would favor co-clustering  $i$  and  $j$  when  $d(g(\cdot; \theta_i), g(\cdot; \theta_j)) < -\log(1 - \gamma)$ . For  $\theta_i \in \mathbb{R}^p$ , an even simpler variant is to choose  $\mathcal{D}_{ij} = 1 - \exp\{-\rho \|\theta_i - \theta_j\|^2\}$ , where  $\rho > 0$  is some fixed bandwidth, which would promote merging components with similar atoms. Alternatively, one can view  $\Delta$  as a stochastic distance matrix and employ k-medoids, hierarchical clustering, or spectral clustering

to cluster the data. Finally, the general notion of specifying loss functions for Bayesian clustering using  $\theta$  and not just  $s$  provides a promising direction for future research.

## ACKNOWLEDGEMENTS

This work was supported by the National Institutes of Health (NIH) under Grants 1R01AI155733, 1R01ES035625, and 5R01ES027498; the United States Office of Naval Research (ONR) Grant N00014-21-1-2510; and the European Research Council (ERC) under Grant 856506.

## REFERENCES

- Aeberhard, S. and Forina, M. (1991). Wine. UCI Machine Learning Repository. DOI: <https://doi.org/10.24432/C5PC7J>.
- Andrews, T. S. and Hemberg, M. (2019). M3Drop: dropout-based feature selection for scRNAseq. *Bioinformatics*, 35(16):2865–2867.
- Antoniak, C. E. (1974). Mixtures of Dirichlet processes with applications to Bayesian nonparametric problems. *The Annals of Statistics*, 2(6):1152–1174.
- Aragam, B., Dan, C., Xing, E. P., and Ravikumar, P. (2020). Identifiability of nonparametric mixture models and Bayes optimal clustering. *The Annals of Statistics*, 48(4):2277–2302.
- Ascolani, F., Lijoi, A., Rebaudo, G., and Zanella, G. (2023). Clustering consistency with Dirichlet process mixtures. *Biometrika*, 110(2):551–558.
- Azzalini, A. and Capitanio, A. (1999). Statistical applications of the multivariate skew normal distribution. *Journal of the Royal Statistical Society: Series B (Statistical Methodology)*, 61(3):579–602.
- Azzalini, A. and Valle, A. D. (1996). The multivariate skew-normal distribution. *Biometrika*, 83(4):715–726.
- Barndorff-Nielsen, O. (1965). Identifiability of mixtures of exponential families. *Journal of Mathematical Analysis and Applications*, 12(1):115–121.
- Bartolucci, F. (2005). Clustering univariate observations via mixtures of unimodal normal mixtures. *Journal of Classification*, 22(2):203–219.
- Baudry, J.-P., Raftery, A. E., Celeux, G., Lo, K., and Gottardo, R. (2010). Combining mixture components for clustering. *Journal of Computational and Graphical Statistics*, 19(2):332–353.

- Bechtel, Y. C., Bonaiti-Pellie, C., Poisson, N., Magnette, J., and Bechtel, P. R. (1993). A population and family study N-acetyltransferase using caffeine urinary metabolites. *Clinical Pharmacology & Therapeutics*, 54(2):134–141.
- Bensmail, H., Celeux, G., Raftery, A. E., and Robert, C. P. (1997). Inference in model-based cluster analysis. *Statistics and Computing*, 7(1):1–10.
- Berenfeld, C., Rosa, P., and Rousseau, J. (2022). Estimating a density near an unknown manifold: a Bayesian nonparametric approach. *arXiv preprint arXiv:2205.15717*.
- Binder, D. A. (1978). Bayesian cluster analysis. *Biometrika*, 65(1):31–38.
- Cacciatore, S. and Tenori, L. (2022). *KODAMA: Knowledge discovery by accuracy maximization*. R package version 1.9.
- Cai, D., Campbell, T., and Broderick, T. (2021). Finite mixture models do not reliably learn the number of components. In Meila, M. and Zhang, T., editors, *Proceedings of the 38th International Conference on Machine Learning*, volume 139 of *Proceedings of Machine Learning Research*, pages 1158–1169. PMLR.
- Chan, C., Feng, F., Ottinger, J., Foster, D., West, M., and Kepler, T. B. (2008). Statistical mixture modeling for cell subtype identification in flow cytometry. *Cytometry Part A: The Journal of the International Society for Analytical Cytology*, 73(8):693–701.
- Chandra, N. K., Canale, A., and Dunson, D. B. (2023). Escaping the curse of dimensionality in Bayesian model-based clustering. *Journal of Machine Learning Research*, 24(144):1–42.
- Chen, J. (1995). Optimal rate of convergence for finite mixture models. *The Annals of Statistics*, 23(1):221–233.
- Crawford, S. L. (1994). An application of the Laplace method to finite mixture distributions. *Journal of the American Statistical Association*, 89(425):259–267.
- Crawford, S. L., DeGroot, M. H., Kadane, J. B., and Small, M. J. (1992). Modeling lake-chemistry distributions: Approximate Bayesian methods for estimating a finite-mixture model. *Technometrics*, 34(4):441–453.
- Dahl, D. B., Johnson, D. J., and Müller, P. (2022). Search algorithms and loss functions for Bayesian clustering. *Journal of Computational and Graphical Statistics*, 31(4):1189–1201.
- Dang, U. J., Gallagher, M. P., Browne, R. P., and McNicholas, P. D. (2023). Model-based clustering and classification using mixtures of multivariate skewed power exponential distributions. *Journal of Classification*, pages 1–23.

- De Iorio, M., Favaro, S., Guglielmi, A., and Ye, L. (2023). Bayesian nonparametric mixture modeling for temporal dynamics of gender stereotypes. *The Annals of Applied Statistics*, 17(3):2256–2278.
- Denti, F., Camerlenghi, F., Guindani, M., and Mira, A. (2023). A common atoms model for the Bayesian nonparametric analysis of nested data. *Journal of the American Statistical Association*, 118(541):405–416.
- Di Zio, M., Guarnera, U., and Rocci, R. (2007). A mixture of mixture models for a classification problem: The unity measure error. *Computational Statistics & Data Analysis*, 51(5):2573–2585.
- Duan, L. L. and Dunson, D. B. (2021). Bayesian distance clustering. *Journal of Machine Learning Research*, 22(224):1–27.
- Ferguson, T. S. (1973). A Bayesian analysis of some nonparametric problems. *The Annals of Statistics*, 1(2):209–230.
- Fraley, C. and Raftery, A. E. (2002). Model-based clustering, discriminant analysis, and density estimation. *Journal of the American Statistical Association*, 97(458):611–631.
- Fritsch, A. (2022). *Mclust: Process an MCMC sample of clusterings*. R package version 1.0.1.
- Fritsch, A. and Ickstadt, K. (2009). Improved criteria for clustering based on the posterior similarity matrix. *Bayesian Analysis*, 4(2):367–391.
- Ghosal, S., Ghosh, J. K., and Ramamoorthi, R. (1999). Posterior consistency of Dirichlet mixtures in density estimation. *The Annals of Statistics*, 27(1):143–158.
- Ghosal, S. and van der Vaart, A. (2007). Posterior convergence rates of Dirichlet mixtures at smooth densities. *The Annals of Statistics*, 35(2):697–723.
- Gorsky, S., Chan, C., and Ma, L. (2024). Coarsened mixtures of hierarchical skew normal kernels for flow cytometry analyses. *Bayesian Analysis*, Forthcoming.
- Guha, A., Ho, N., and Nguyen, X. (2021). On posterior contraction of parameters and interpretability in Bayesian mixture modeling. *Bernoulli*, 27(4):2159–2188.
- Hahsler, M., Piekenbrock, M., and Doran, D. (2019). dbscan: Fast density-based clustering with R. *Journal of Statistical Software*, 91:1–30.
- Hastie, T., Tibshirani, R., and Friedman, J. H. (2009). *The Elements of Statistical Learning: Data Mining, Inference, and Prediction*, volume 2. Springer.
- Heinrich, P. and Kahn, J. (2018). Strong identifiability and optimal minimax rates for finite mixture estimation. *The Annals of Statistics*, 46(6A):2844–2870.

- Hennig, C. (2010). Methods for merging Gaussian mixture components. *Advances in Data Analysis and Classification*, 4(1):3–34.
- Ho, N. and Nguyen, X. (2016a). Convergence rates of parameter estimation for some weakly identifiable finite mixtures. *The Annals of Statistics*, 44(6):2726–2755.
- Ho, N. and Nguyen, X. (2016b). On strong identifiability and convergence rates of parameter estimation in finite mixtures. *Electronic Journal of Statistics*, 10(1):271–307.
- Ho, N., Nguyen, X., and Ritov, Y. (2020). Robust estimation of mixing measures in finite mixture models. *Bernoulli*, 26(2):828–857.
- Hubert, L. and Arabie, P. (1985). Comparing partitions. *Journal of Classification*, 2(1):193–218.
- Ishwaran, H. and James, L. F. (2001). Gibbs sampling methods for stick-breaking priors. *Journal of the American Statistical Association*, 96(453):161–173.
- Ishwaran, H. and James, L. F. (2003). Some further developments for stick-breaking priors: Finite and infinite clustering and classification. *Sankhyā: The Indian Journal of Statistics (2003-2007)*, 65(3):577–592.
- Jain, A. K. (2010). Data clustering: 50 years beyond K-means. *Pattern Recognition Letters*, 31(8):651–666.
- Karlis, D. and Santourian, A. (2009). Model-based clustering with non-elliptically contoured distributions. *Statistics and Computing*, 19(1):73–83.
- Kiselev, V. Y., Andrews, T. S., and Hemberg, M. (2019). Challenges in unsupervised clustering of single-cell RNA-seq data. *Nature Reviews Genetics*, 20(5):273–282.
- Krijthe, J. H. (2016). RSSL: R package for semi-supervised learning. In *Reproducible Research in Pattern Recognition. RRPR 2016. Lecture Notes in Computer Science, vol 10214*, pages 104–115.
- Krijthe, J. H. and Loog, M. (2015). Implicitly constrained semi-supervised least squares classification. In *14th International Symposium on Advances in Intelligent Data Analysis XIV (Lecture Notes in Computer Science Volume 9385)*, pages 158–169.
- Lau, J. W. and Green, P. J. (2007). Bayesian model-based clustering procedures. *Journal of Computational and Graphical Statistics*, 16(3):526–558.
- Li, H., Courtois, E. T., Sengupta, D., Tan, Y., Chen, K. H., Goh, J. J. L., Kong, S. L., Chua, C., Hon, L. K., Tan, W. S., et al. (2017). Reference component analysis of single-cell transcriptomes

- elucidates cellular heterogeneity in human colorectal tumors. *Nature Genetics*, 49(5):708–718. PMID: 28319088.
- Li, J. (2005). Clustering based on a multilayer mixture model. *Journal of Computational and Graphical Statistics*, 14(3):547–568.
- Lubischew, A. A. (1962). On the use of discriminant functions in taxonomy. *Biometrics*, 18(4):455–477.
- Lun, A. T., Bach, K., and Marioni, J. C. (2016). Pooling across cells to normalize single-cell RNA sequencing data with many zero counts. *Genome Biology*, 17(1):1–14.
- Malsiner-Walli, G., Frühwirth-Schnatter, S., and Grün, B. (2017). Identifying mixtures of mixtures using Bayesian estimation. *Journal of Computational and Graphical Statistics*, 26(2):285–295.
- Manole, T. and Ho, N. (2022). Refined convergence rates for maximum likelihood estimation under finite mixture models. In Chaudhuri, K., Jegelka, S., Song, L., Szepesvari, C., Niu, G., and Sabato, S., editors, *Proceedings of the 39th International Conference on Machine Learning*, volume 162 of *Proceedings of Machine Learning Research*, pages 14979–15006. PMLR.
- Manole, T. and Khalili, A. (2021). Estimating the number of components in finite mixture models via the group-sort-fuse procedure. *The Annals of Statistics*, 49(6):3043–3069.
- McInnes, L., Healy, J., Saul, N., and Großberger, L. (2018). UMAP: Uniform manifold approximation and projection. *Journal of Open Source Software*, 3(29):861.
- Medvedovic, M. and Sivaganesan, S. (2002). Bayesian infinite mixture model based clustering of gene expression profiles. *Bioinformatics*, 18(9):1194–1206.
- Meilă, M. (2007). Comparing clusterings—an information based distance. *Journal of Multivariate Analysis*, 98(5):873–895.
- Melnykov, V. (2016). Merging mixture components for clustering through pairwise overlap. *Journal of Computational and Graphical Statistics*, 25(1):66–90.
- Miller, J. W. and Dunson, D. B. (2019). Robust Bayesian inference via coarsening. *Journal of the American Statistical Association*, 114(527):1113–1125.
- Miller, J. W. and Harrison, M. T. (2014). Inconsistency of Pitman-Yor process mixtures for the number of components. *The Journal of Machine Learning Research*, 15(1):3333–3370.
- Miller, J. W. and Harrison, M. T. (2018). Mixture models with a prior on the number of components. *Journal of the American Statistical Association*, 113(521):340–356.

- Nguyen, X. (2011). Wasserstein distances for discrete measures and convergence in nonparametric mixture models. Technical report, Univ. of Michigan Dept. of Statistics.
- Nguyen, X. (2013). Convergence of latent mixing measures in finite and infinite mixture models. *The Annals of Statistics*, 41(1):370–400.
- O’Hagan, A., Murphy, T. B., Gormley, I. C., McNicholas, P. D., and Karlis, D. (2016). Clustering with the multivariate normal inverse Gaussian distribution. *Computational Statistics & Data Analysis*, 93:18–30.
- Paganin, S., Herring, A. H., Olshan, A. F., and Dunson, D. B. (2021). Centered partition processes: Informative priors for clustering (with discussion). *Bayesian Analysis*, 16(1):301 – 670.
- Rajkowski, Ł. (2019). Analysis of the maximal a posteriori partition in the Gaussian Dirichlet process mixture model. *Bayesian Analysis*, 14(2):477–494.
- Rand, W. M. (1971). Objective criteria for the evaluation of clustering methods. *Journal of the American Statistical Association*, 66(336):846–850.
- Rastelli, R. and Friel, N. (2018). Optimal Bayesian estimators for latent variable cluster models. *Statistics and Computing*, 28(6):1169–1186.
- Redner, R. A. and Walker, H. F. (1984). Mixture densities, maximum likelihood and the EM algorithm. *SIAM Review*, 26(2):195–239.
- Rigon, T., Herring, A. H., and Dunson, D. B. (2023). A generalized Bayes framework for probabilistic clustering. *Biometrika*, 110(3):559–578.
- Rodríguez, C. E. and Walker, S. G. (2014). Univariate Bayesian nonparametric mixture modeling with unimodal kernels. *Statistics and Computing*, 24(1):35–49.
- Roeder, K. (1990). Density estimation with confidence sets exemplified by superclusters and voids in the galaxies. *Journal of the American Statistical Association*, 85(411):617–624.
- Rousseau, J. and Mengersen, K. (2011). Asymptotic behaviour of the posterior distribution in over-fitted mixture models. *Journal of the Royal Statistical Society: Series B (Statistical Methodology)*, 73(5):689–710.
- Scrucca, L., Fop, M., Murphy, T. B., and Raftery, A. E. (2016). Mclust 5: Clustering, classification and density estimation using Gaussian finite mixture models. *The R Journal*, 8(1):289–317.
- Sethuraman, J. (1994). A constructive definition of Dirichlet priors. *Statistica Sinica*, 4(2):639–650.

- Teicher, H. (1961). Identifiability of mixtures. *The Annals of Mathematical Statistics*, 32(1):244–248.
- Wade, S. (2015). *Mclust.ext: Point estimation and credible balls for Bayesian cluster analysis*. R package version 1.0.
- Wade, S. (2023). Bayesian cluster analysis. *Philosophical Transactions of the Royal Society A*, 381(2247):20220149.
- Wade, S. and Ghahramani, Z. (2018). Bayesian cluster analysis: Point estimation and credible balls (with discussion). *Bayesian Analysis*, 13(2):559–626.

## SUPPLEMENTARY MATERIAL

The Supplementary Material contains additional simulation studies, proofs for all results, and technical details. Our methodology is implemented in the package `foldcluster`, available at <https://github.com/adombowsky/FOLD>.

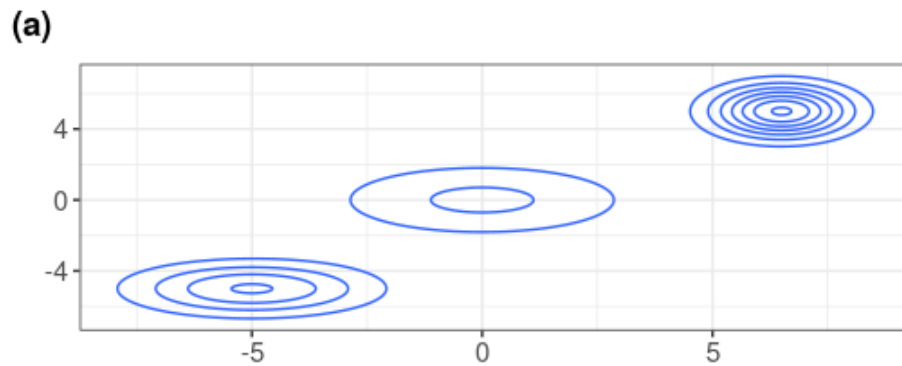
### A POINT ESTIMATION SIMULATION STUDIES

In light of the asymptotic results shown in Section 3, we examine the effect of increasing  $n$  on FOLD and other model-based clustering methods. For a given  $f^0$ , we repeatedly simulate observations with varying  $n \in \{100, 500, 1000, 2500\}$  for 100 replications each. We compare FOLD with  $\omega = \omega^{\text{AVG}}$  to clusterings returned by minimizing Binder’s loss and the VI loss using the packages `mcclust` (Fritsch, 2022) and `mcclust.ext` (Wade, 2015), respectively. Along with these Bayesian approaches, we also cluster the data using `mclust` (Scrucca et al., 2016), which groups observations based on the EM algorithm for a Gaussian mixture.

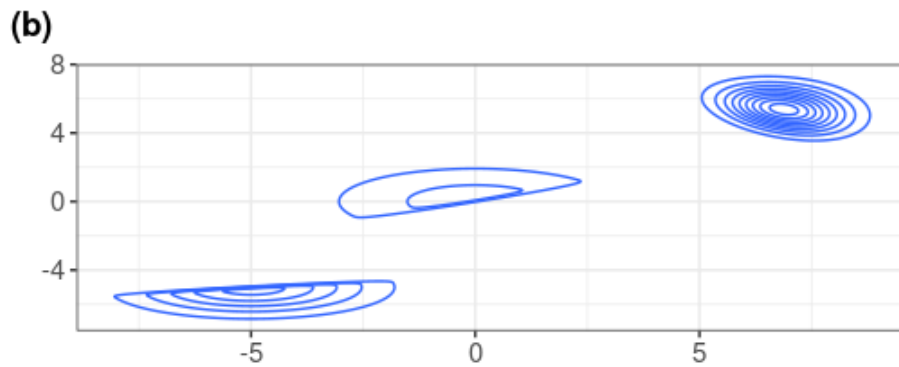
For each replication and  $n$ , we run the EM algorithm and fit a Bayesian location-scale GMM,

$$X_i^0 \mid \mathbf{a}, \boldsymbol{\mu}, \boldsymbol{\Sigma} \sim \sum_{k=1}^K a_k \mathcal{N}_2(\tilde{\boldsymbol{\mu}}_k, \tilde{\boldsymbol{\Sigma}}_k); \quad (\tilde{\boldsymbol{\mu}}_k, \tilde{\boldsymbol{\Sigma}}_k) \sim \mathcal{N}\mathcal{IW}(\boldsymbol{\mu}, \kappa, \nu, \boldsymbol{\Psi}); \quad \mathbf{a} \sim \text{Dir}(\boldsymbol{\alpha}1_K);$$

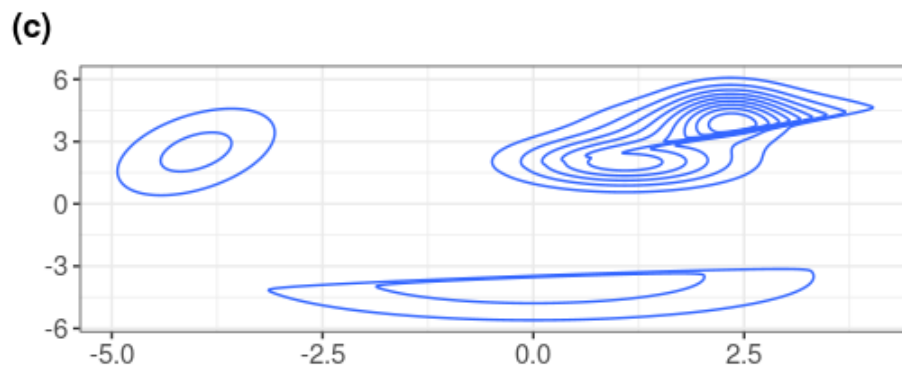
where  $1_K$  is the  $K$ -dimensional vector consisting of ones. We then compute clusterings with FOLD, VI, and Binder’s loss using the posterior samples from the Bayesian model. For each clustering, we save the number of clusters and the adjusted Rand index (Rand, 1971; Hubert and Arabie, 1985) with  $\mathbf{s}^0$ . The hyperparameters are set at  $K = 30$ ,  $\alpha = 1/2$ , and  $\boldsymbol{\mu} = 0_p$ ,  $\kappa = 1$ ,  $\nu = p + 2$ , and  $\boldsymbol{\Psi} = I$ . We run a Gibbs sampler for 9,000 iterations with a burn-in of 1,000, then use every third iteration for computing the Bayesian clusterings. For `mclust`, the number of clusters is automatically selected each replication by minimizing the Bayesian information criterion (BIC).



Contours of the Gaussian mixture.



Contours of the Skew Gaussian mixture.



Contours of the Skew-Symmetric mixture.

Figure 7: Contour plots of the (a) Gaussian mixture, (b) skew Gaussian mixture and (c) skew-symmetric mixture.

	$n$	FOLD	Oracle FOLD	VI	Binder's	Mclust
No. of Clusters	100	2.93 (0.383)	3.00 (0.00)	8.02 (5.714)	19.76 (0.818)	3.10 (0.414)
	500	3.06 (0.278)	3.00 (0.00)	3.53 (0.926)	19.89 (0.852)	3.00 (0.00)
	1000	3.05 (0.219)	3.00 (0.00)	3.30 (0.541)	19.96 (0.400)	3.01 (0.100)
	2500	3.05 (0.219)	3.00 (0.00)	3.08 (0.273)	20.00 (0.00)	3.00 (0.00)
Adj. Rand Index	100	0.903 (0.087)	0.985 (0.021)	0.852 (0.088)	0.822 (0.061)	0.962 (0.052)
	500	0.979 (0.013)	0.998 (0.008)	0.974 (0.014)	0.947 (0.012)	0.987 (0.008)
	1000	0.985 (0.006)	0.987 (0.006)	0.982 (0.007)	0.968 (0.007)	0.985 (0.024)
	2500	0.986 (0.004)	0.987 (0.004)	0.984 (0.004)	0.979 (0.005)	0.987 (0.004)

Table 2: Averages and standard deviations (in parentheses) for the number of clusters and adjusted Rand index with  $\mathbf{s}^0$  on 100 replications from a mixture of bivariate Gaussian kernels.

	$n$	FOLD	VI	Binder's	Mclust
No. of Clusters	100	3.02 (0.141)	3.16 (0.395)	13.84 (6.080)	3.14 (0.377)
	500	3.03 (0.171)	3.42 (0.755)	6.15 (2.258)	3.23 (0.529)
	1000	3.20 (0.449)	3.53 (0.881)	9.32 (3.816)	4.33 (1.429)
	2500	3.19 (0.443)	3.40 (0.682)	8.93 (2.409)	7.99 (0.959)
Adj. Rand Index	100	0.992 (0.016)	0.987 (0.021)	0.915 (0.043)	0.989 (0.030)
	500	0.999 (0.003)	0.998 (0.003)	0.992 (0.006)	0.980 (0.049)
	1000	0.999 (0.002)	0.997 (0.007)	0.990 (0.009)	0.866 (0.149)
	2500	0.999 (0.001)	0.990 (0.020)	0.952 (0.014)	0.576 (0.071)

Table 3: Averages and standard deviations (in parentheses) for the number of clusters and adjusted Rand index with  $\mathbf{s}^0$  on 100 replications from a mixture of bivariate skew Gaussian kernels.

	$n$	FOLD	VI	Binder's	Mclust
No. of Clusters	100	3.25 (0.500)	3.89 (1.014)	12.62 (4.292)	3.56 (0.925)
	500	3.23 (0.601)	3.64 (0.894)	13.94 (4.552)	4.17 (0.779)
	1000	3.10 (0.302)	4.83 (1.025)	15.73 (3.795)	5.08 (0.442)
	2500	3.10 (0.302)	4.58 (0.843)	18.99 (2.634)	6.20 (0.876)
Adj. Rand Index	100	0.982 (0.029)	0.974 (0.026)	0.800 (0.094)	0.884 (0.177)
	500	0.995 (0.032)	0.921 (0.136)	0.799 (0.147)	0.715 (0.159)
	1000	0.975 (0.085)	0.691 (0.057)	0.665 (0.037)	0.574 (0.054)
	2500	0.967 (0.098)	0.679 (0.012)	0.639 (0.027)	0.512 (0.056)

Table 4: Averages and standard deviations (in parentheses) for the number of clusters and adjusted Rand index with  $\mathbf{s}^0$  on 100 replications from the skew-symmetric mixture.

In the first scenario,  $f^0(x) = \sum_{m=1}^3 a_m^0 \mathcal{N}_2(x; \mu_m^0, \Sigma_m^0)$ , with weights  $\mathbf{a}^0 = (0.45, 0.25, 0.3)$  and atoms  $\mu_1^0 = (6.5, 5)$ ,  $\Sigma_1^0 = I$ ,  $\mu_2^0 = (0, 0)$ ,  $\Sigma_2^0 = \text{diag}(5, 2)$ , and  $\mu_3^0 = (-5, -5)$ ,  $\Sigma_3^0 = \text{diag}(3, 1)$ . As shown in Figure 7(a), the three kernels are well separated. The averages and standard deviations for the number of clusters and adjusted Rand index are given in Table 2, with boxplots of these benchmarks displayed in Figure 8. FOLD, oracle FOLD, and mclust achieve high adjusted Rand index with increasing sample size. Oracle FOLD is perfect at computing the true number of clusters, and mclust and FOLD are also excellent. Furthermore, the number of clusters and adjusted Rand index for  $\mathbf{c}_{\text{FOLD}}$  gradually approach the values produced by  $\mathbf{c}_{\text{FOLD}}^*$ . The VI loss improves in the number of clusters as  $n$  increases, but Binder's loss falls short, consistently producing 20 clusters with diminishing variation across replications. VI and Binder's loss produce high adjusted Rand indices that improve with  $n$ .

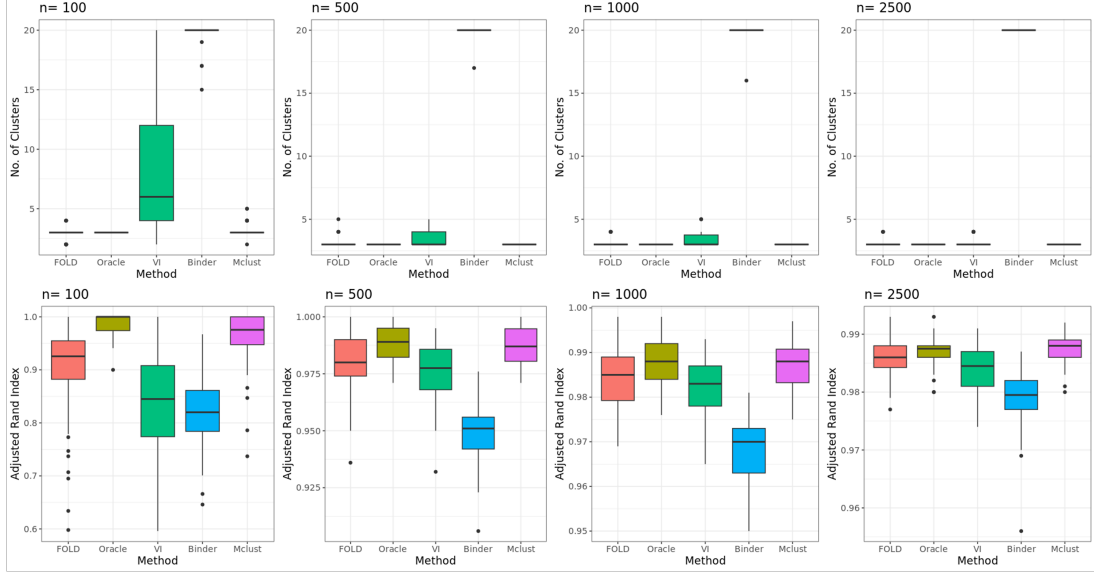


Figure 8: Comparison of the number of clusters and the adjusted Rand index with  $\mathbf{s}^0$  on 100 replications from a mixture of well-separated multivariate Gaussian kernels.

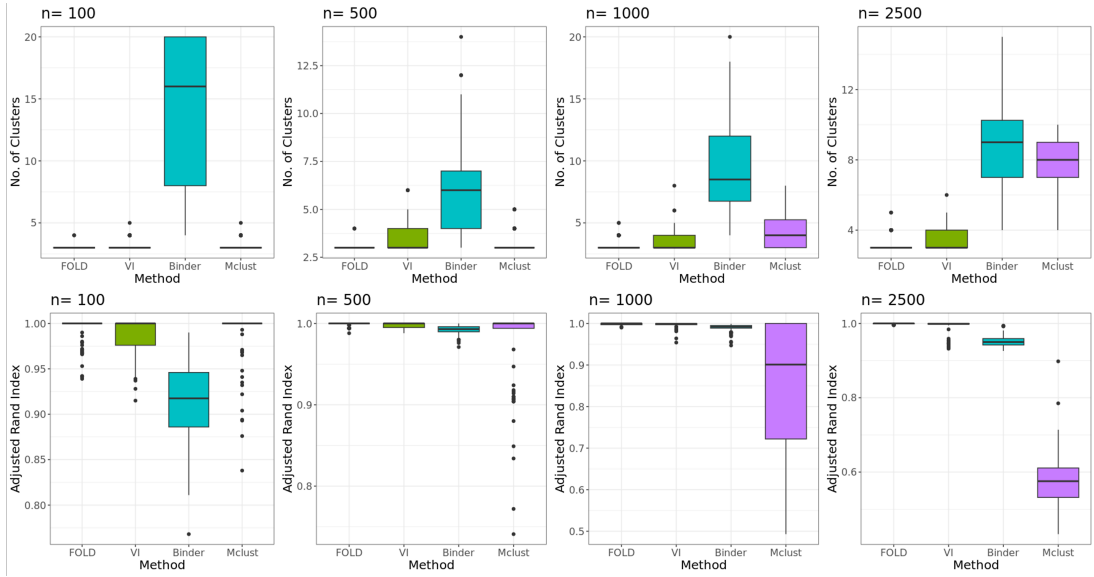


Figure 9: Comparison of the number of clusters and the adjusted Rand index with  $\mathbf{s}^0$  on 100 replications from a mixture of multivariate skew Gaussian distributions.

Next, we let  $f^0(x) = \sum_{m=1}^3 a_m^0 \mathcal{SN}_2(x; \mu_m^0, \Sigma_m^0, \psi_m^0)$ , where  $\mathcal{SN}_2(x; \cdot, \cdot, \cdot)$  denotes the PDF of a bivariate skew Gaussian distribution (Azzalini and Valle, 1996; Azzalini and Capitanio, 1999) and  $\mathbf{a}^0 = (0.45, 0.25, 0.3)$ . These kernels have the same location and scale parameters as the bivariate Gaussian mixture in simulation case 1, and skewness parameters  $\psi_1^0 = (1, 1)$ ,  $\psi_2^0 = (-10, 15)$ , and  $\psi_3^0 = (4, -17)$ . Figure 7(b) shows a contour plot of  $f^0$ . Results across the replications are reported in Figure 9 and Table 3. For all values of  $n$ , FOLD attains high accuracy with a small number of clusters. As  $n$  increases, all four clustering methods achieve high levels of the adjusted Rand index,

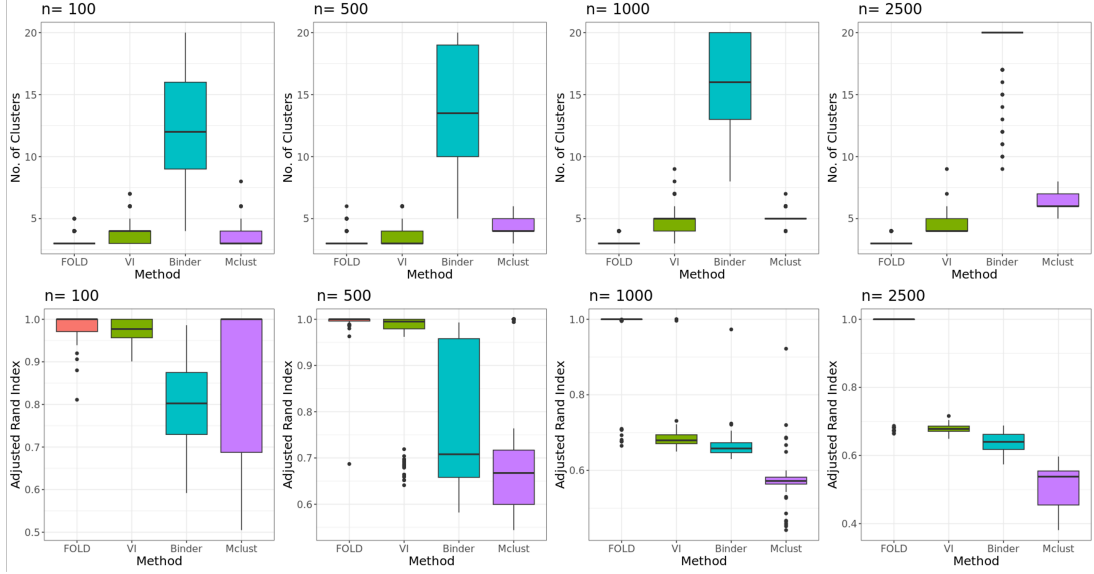


Figure 10: Comparison of the number of clusters and the adjusted Rand index with  $s^0$  on 100 replications from the skew-symmetric mixture.

though FOLD results in values close to 1 while the VI loss and Binder’s loss decline slightly. FOLD tends to produce between 3 and 4 clusters for each  $n$  and reports less than or equal to the number of clusters induced by the VI loss in 94.5% of all instances.

In the final simulation case, we take  $f^0$  to be a bivariate mixture with weights  $\alpha^0 = (0.55, 0.3, 0.15)$ , and kernels

$$\begin{aligned}
g_1^0 &= 0.364 \cdot \mathcal{SN}_p \left( \begin{pmatrix} 2.50 \\ 3.50 \end{pmatrix}, I, \begin{pmatrix} -10 \\ 15 \end{pmatrix} \right) \\
&+ 0.212 \cdot \mathcal{N}_p \left( \begin{pmatrix} 2.325 \\ 4.381 \end{pmatrix}, \text{diag}(0.20, 0.80) \right) \\
&+ 0.424 \cdot \mathcal{N}_p \left( \begin{pmatrix} 1.085 \\ 2.009 \end{pmatrix}, \text{diag}(0.70, 0.60) \right); \\
g_2^0 &= \mathcal{SN}_p \left( \begin{pmatrix} 0 \\ -3.50 \end{pmatrix}, \text{diag}(5, 2), \begin{pmatrix} 4 \\ -17 \end{pmatrix} \right); \\
g_3^0 &= \mathcal{N}_p \left( \begin{pmatrix} -4 \\ -2.50 \end{pmatrix}, \begin{pmatrix} 0.50 & 0.50 \\ 0.50 & 2.50 \end{pmatrix} \right).
\end{aligned}$$

$g_1^0$  is a mixture of one skew Gaussian kernel and two Gaussian kernels,  $g_2^0$  is a skew Gaussian kernel, and  $g_3^0$  is a Gaussian kernel. We refer to  $f^0$  in this case as a skew-symmetric mixture. As can be seen in Figure 7(c),  $g_1^0$  is a non-Gaussian, multimodal density. Similarly, data generated from  $g_2^0$ , the oblong kernel in the lower third of the sample space, will most likely be approximated by multiple

components, despite only constituting one cluster. The results of the simulations are summarized in Table 4 and Figure 10. FOLD generally allocates observations to 3 clusters, but the VI loss favors between 3 and 6 clusters. In 96.5% of the replicates, the number of clusters for FOLD is less than or equal to the number for VI. As in simulation case 2, Binder’s loss and `mclust` frequently return a larger number of clusters than the truth for larger  $n$ . The adjusted Rand index between  $\mathbf{c}_{\text{FOLD}}$  and  $\mathbf{s}^0$  is close to 1 across all sample sizes. In contrast, the three other methods achieve high adjusted Rand index for small  $n$ , but these values sharply drop for  $n \geq 1000$ . This is usually the result of splitting  $g_1^0$  or  $g_2^0$  into multiple clusters.

## B ILLUSTRATION OF THEOREM 1: LOCATION GMMs

We now empirically validate the consistency result in Theorem 1 with a simple example. We set  $M^0 = M^* = 4$  and  $f^0 = f^* = \sum_{m=1}^4 (1/4) \mathcal{N}_2(\mu_m^0, (1/4)I)$ , where  $\mu_1^0 = (1, 1)$ ,  $\mu_2^0 = (1.75, 1.75)$ ,  $\mu_3^0 = (-1.75, -1.75)$ , and  $\mu_4^0 = (-1, -1)$ , then fit the following location Gaussian model with  $K = 4$  components,

$$X_i \sim \mathcal{N}_2(\theta_i, (1/4)I); \quad \tilde{\theta}_k \sim \mathcal{N}_2(0, I); \quad \mathbf{a} \sim \text{Dir}(1/4, \dots, 1/4). \quad (11)$$

We vary  $n \in \{50, 100, 500, 1000\}$ , then fit a Gibbs sampler to extract samples from  $\pi(\boldsymbol{\theta}, \mathbf{s} \mid \mathbf{X})$ . We implement FOLD, oracle FOLD, Binder’s loss, and Binder’s oracle loss using SALS0 to minimize the risk functions, and we set  $d(\cdot, \cdot)$  to be the Hellinger distance. For FOLD, we set  $\omega = \omega^{\text{AVG}}$  and for the FOLD oracle, we take  $\omega = \omega^{*\text{AVG}}$ , which is constructed by setting  $\gamma = \bar{\Delta}^*$  in the oracle risk. For Binder’s loss, we take  $\omega = 1$ , matching the choice used in packages such as `mclust`. Figure 11 shows  $\mathcal{R}(\hat{\mathbf{c}})$  and  $\mathcal{R}^*(\hat{\mathbf{c}})$  for increasing  $n$ , where  $\hat{\mathbf{c}}$  are taken to be clusterings generated by average linkage hierarchical clustering on  $\Delta$ . We can see that as  $n$  grows,  $\mathcal{R}(\hat{\mathbf{c}}) \rightarrow \mathcal{R}^*(\hat{\mathbf{c}})$ . In all plots, the minimum risk over the candidates is attained at 2 clusters, though for larger  $n$  the risk of 3 clusters becomes similar to that of 2 clusters. In addition, the point estimates  $\mathbf{c}_{\text{FOLD}}$  and  $\mathbf{c}_{\text{FOLD}}^*$  are very similar as well even for smaller sample size, with adjusted Rand indices between the two partitions being 0.98 for  $n = 50$ , then 1.0 for  $n = 100, 500, 1000$ . At  $n = 50$ ,  $\mathbf{c}_{\text{FOLD}}$  has 3 clusters, but for  $n > 50$  both  $\mathbf{c}_{\text{FOLD}}$  and  $\mathbf{c}_{\text{FOLD}}^*$  have exactly 2 clusters. Figure 12 shows point estimates for  $\mathbf{c}_{\text{FOLD}}$  and  $\mathbf{c}_{\text{FOLD}}^*$  along with  $\mathbf{c}_{\text{B}}$  and  $\mathbf{c}_{\text{B}}^*$  at the largest sample size. Binder’s loss and its oracle prefer clusterings that approximately correspond to the original 4 Gaussian components, while FOLD and its oracle prefer to merge these. Additionally, several small clusters are present in Binder’s clusterings which seem to exist in the tails of the Gaussian components, leading to 5 clusters in  $\mathbf{c}_{\text{B}}$  and 7 clusters in  $\mathbf{c}_{\text{B}}^*$ .

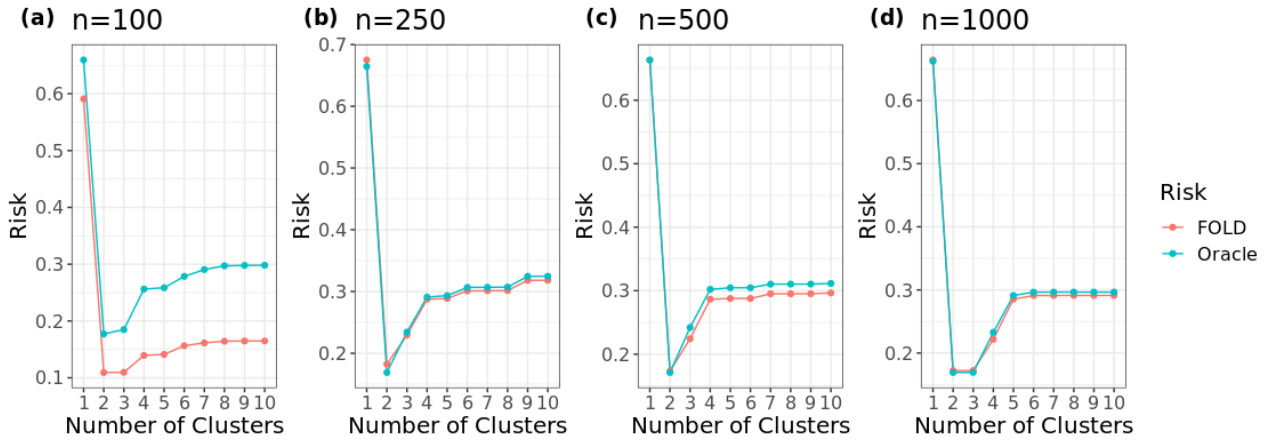


Figure 11:  $\mathcal{R}(\hat{c})$  in red and  $\mathcal{R}^*(\hat{c})$  in green over a set of partitions produced by average linkage hierarchical clustering on  $\Delta$  and ordered by the number of clusters for varying  $n \in \{100, 250, 500, 1000\}$ . As  $n$  grows, the two risk functions and their minimizers begin to closely resemble each other.

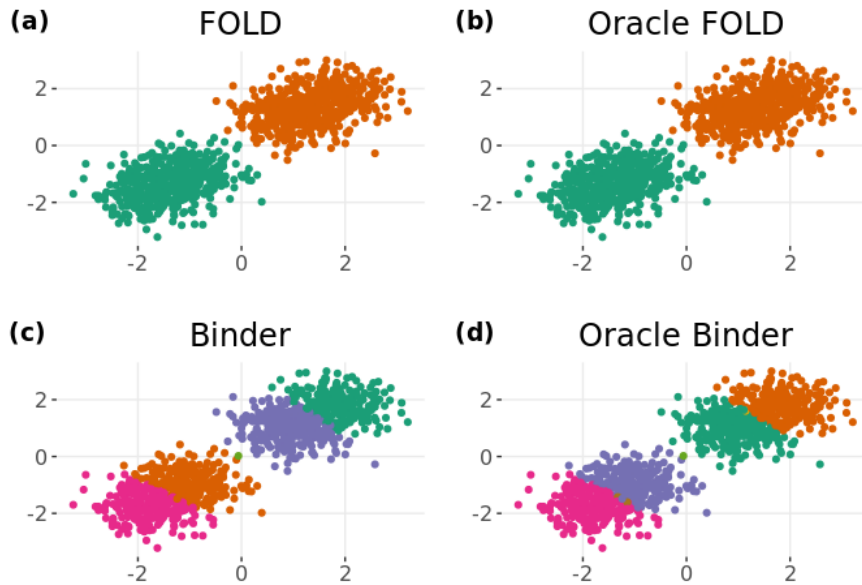


Figure 12:  $c_{\text{FOLD}}$ ,  $c_{\text{FOLD}}^*$ ,  $c_{\text{B}}$ , and  $c_{\text{B}}^*$  for  $n = 1000$  simulated data points from a mixture of 4 Gaussian kernels. The number of clusters for both  $c_{\text{FOLD}}$  and  $c_{\text{FOLD}}^*$  is 2, whereas for  $c_{\text{B}}$  there are 5 clusters and for  $c_{\text{B}}^*$  there are 7 clusters.

To better understand the results in Figure 12, note that the Hellinger distance between the kernels in  $f^*$  is directly related to the Euclidean distance between their centers,

$$1 - d^2 \{ \mathcal{N}_2(\cdot; \theta_m^0, 1/4), \mathcal{N}_2(\cdot; \theta_{m'}^0, 1/4) \} \propto \exp \left\{ -\frac{1}{2} \|\theta_m^0 - \theta_{m'}^0\|^2 \right\}.$$

We have deliberately chosen the true component means so that  $\theta_1^0$  and  $\theta_2^0$  are close, and  $\theta_3^0$  and  $\theta_4^0$  are close. This means that, despite the fact that we originally sampled from 4 mixture components, the scatterplot of the data in Figure 12 resembles 2 ovular clusters rather than 4 spherical ones.  $\mathbf{c}_{\text{FOLD}}^*$  creates ovular clusters because it is less reliant on the fitted model in (11) than Binder’s loss. For example, if  $X_i^0$  is in a high density region of  $\mathcal{N}_2(\cdot; \theta_1^0, 1/4)$  and  $X_j^0$  is in a high density region of  $\mathcal{N}_2(\cdot; \theta_2^0, 1/4)$ , then the Hellinger distance terms in (10) shrink the value of  $\Delta_{ij}^*$  close to 0, ultimately promoting co-clustering of objects  $i$  and  $j$ . In contrast, Binder’s oracle is more reliant on assigning the observations to mixture components and would most likely place  $X_i^0$  and  $X_j^0$  in different clusters.

## C APPLICATION TO BENCHMARK DATASETS

### Galaxy Data

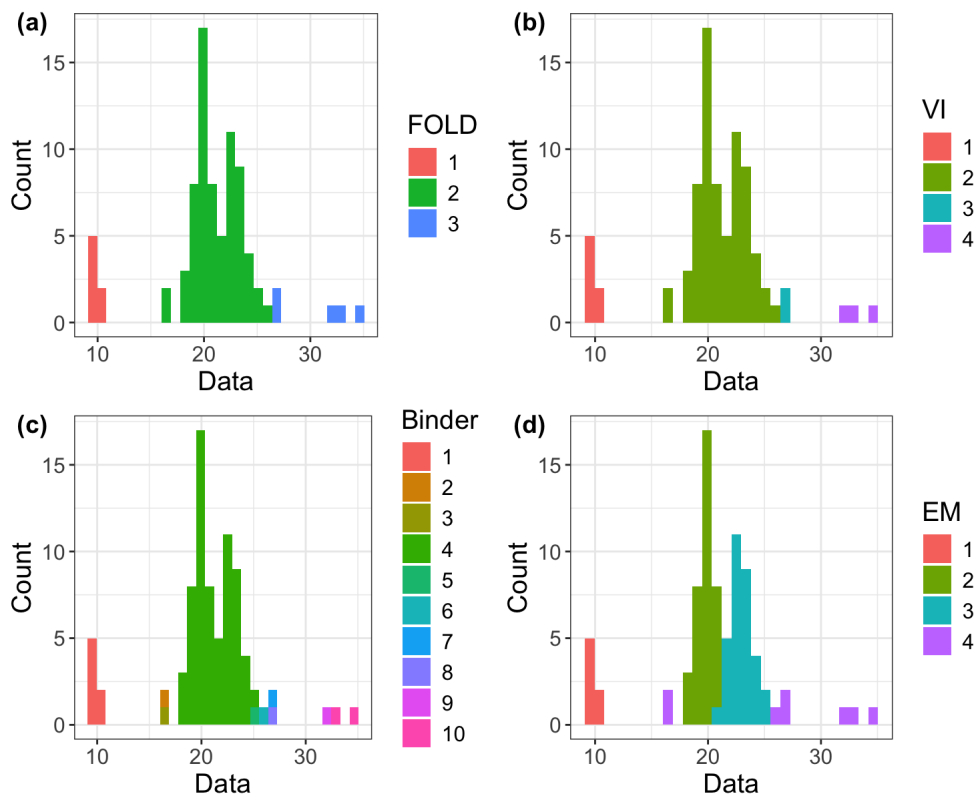


Figure 13: Model-based clusterings of the galaxy dataset.

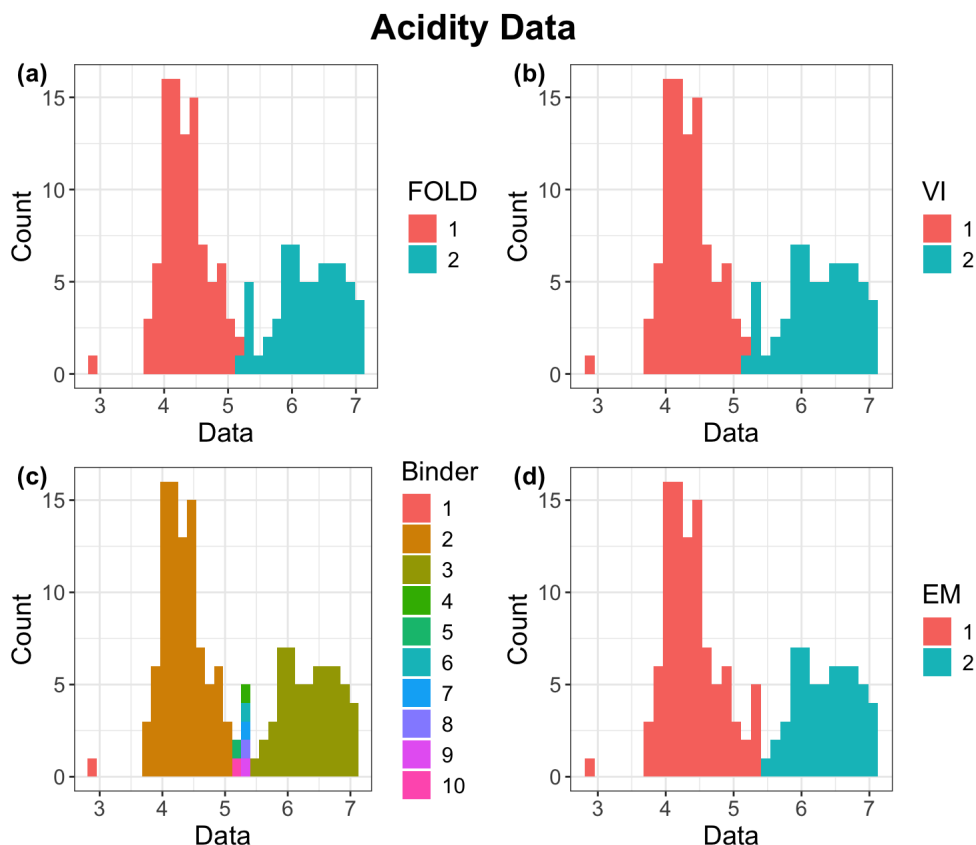


Figure 14: Model-based clusterings of the acidity dataset.

In addition to the cell line application, we apply FOLD and other clustering methods to multiple benchmark datasets. First, we focus on three univariate examples that have been routinely used to evaluate model-based clustering procedures: the galaxy (Roeder, 1990), acidity (Crawford et al., 1992; Crawford, 1994), and enzyme (Bechtel et al., 1993) datasets. For all examples, we fit FOLD, VI, Binder’s loss, and EM, then compute the clustering point estimates. We center and scale the datasets to have mean 0 and unit standard deviation. The three Bayesian methods are implemented with the model  $X_i \sim \mathcal{N}(\mu_i, \sigma_i^2)$ ,  $K = 10$ ,  $(\tilde{\mu}_k, \tilde{\sigma}_k^2) \sim \mathcal{NIG}(0, 1, 1, 1)$ , and  $\mathbf{a} \sim \text{Dir}(1/2, \dots, 1/2)$ . The loss parameter for FOLD is selected with an elbow plot and the number of clusters in the EM algorithm is chosen by minimizing BIC.

Figure 13 displays the point estimates for the galaxy data. FOLD selects 3 clusters, whereas VI prefers 4, Binder’s loss prefers 10, and the EM algorithm prefers 4. FOLD favors coarse, non-Gaussian shaped clusters, while VI, Binder’s loss, and the EM algorithm split the FOLD clusters into multiple sub-clusters. In particular, the EM algorithm divides the multi-modal group of objects in the center of the sample space into two Gaussian clusters. Similarly, VI and Binder’s loss tend to split the clusters in the left and right tails of the data. FOLD, VI, and the EM algorithm perform similarly when applied to the acidity dataset (Figure 14), though there is some disagreement between the methods on how

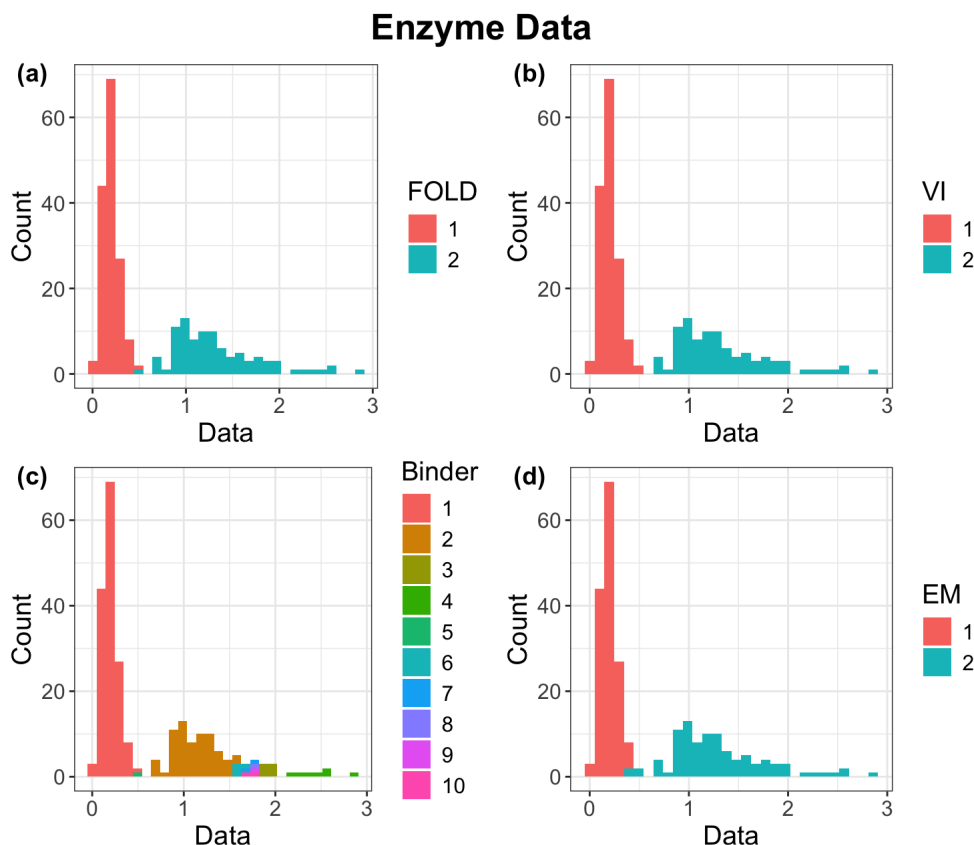


Figure 15: Model-based clusterings of the enzyme dataset.

to allocate objects that are between the two clusters. Binder’s loss is also sensitive to this ambiguity as it splits the data into 10 clusters. Finally, FOLD, VI, and EM result in similar point estimates for the enzyme data (Figure 15), with some disagreement on objects near the boundary of each cluster, whereas Binder’s loss splits the non-Gaussian cluster on the right hand side of the dataset into several sub-clusters.

Next, we compare FOLD to both model-based and algorithmic clustering methods on the iris, flea-beetles (Lubischew, 1962), and wine (Aeberhard and Forina, 1991) datasets. In comparison to the galaxy, acidity, and enzyme data, these examples have ground-truth class labels that correspond to separated clusters in the sample space. Hence, we can evaluate the accuracy of FOLD and other approaches on capturing a well-defined, true grouping of the observations. First, we center and scale the datasets. For the iris dataset, we merge the *Iris virginica* and *Iris versicolor* species into one true cluster, as there is no separation between these species, meaning that  $M^0 = 2$ . The flea-beetles dataset comprises three species (*concinna*, *heikertingeri*, and *heptapotamica*), meaning  $M^0 = 3$ . The wines in the wine dataset are derived from three cultivars, hence  $M^0 = 3$ . Finally, for the wine example, we cluster the projection of the original dataset onto the first two principal components. The Bayesian methods fit the mixture  $X_i \sim \mathcal{N}_2(\mu_i, \Sigma_i)$ ,  $K = 50$ ,  $(\tilde{\mu}_k, \tilde{\Sigma}_k) \sim \mathcal{NTW}(0_2, 1, p + 2, I)$ ,

Dataset	Metric	FOLD	VI	Binder’s	EM	K-Means	HCA	DBSCAN	Spectral
Iris	$\hat{K}$	2	2	2	2	2	2	3	2
	ARI	1.000	1.000	1.000	1.000	0.920	1.000	0.859	1.000
Flea-Beetles	$\hat{K}$	3	10	10	3	3	3	5	5
	ARI	0.917	0.807	0.807	0.958	0.371	0.635	0.069	0.601
Wine	$\hat{K}$	3	5	10	3	3	3	3	4
	ARI	0.912	0.893	0.806	0.829	0.895	0.754	0.439	0.922

Table 5: Comparison of FOLD to competitors on the iris, flea-beetles, and wine datasets based on the number of clusters and ARI.

and  $\mathbf{a} \sim \text{Dir}(1/2, \dots, 1/2)$ . All hyperparameters are chosen in the same manner as the application to the cell line dataset (see Section I.1), with the exception that we set `minPts=5` when implementing DBSCAN.

The number of clusters ( $\hat{K}$ ) and ARI with the true labels are displayed in Table 5. In the iris dataset, all methods except K-means and DBSCAN result in the true partition of the flowers. FOLD and the EM algorithm excel when applied to the flea-beetles data, with both resulting in the true number of species and attaining high ARIs. Finally, FOLD performs particularly well on the wine dataset, scoring the second highest ARI (0.912), while the method with higher ARI (spectral clustering) overestimates the number of cultivars. In both the flea-beetles and wine examples, the FOLD point estimate has fewer clusters than the point estimates of both VI and Binder’s, which are computed using the same MCMC samples as FOLD.

## D BASIC PROPERTIES OF FOLD

### D.1 PROOF OF PROPOSITION 1

*Proof.* We proceed as in Dahl et al. (2022) and decompose the loss function into separate terms that relate to the contingency table between  $\hat{\mathbf{c}}$  and  $\mathbf{s}$ . For any  $k, k' \in [K]$ , let  $\eta_{kk'} = d(g(\cdot; \tilde{\theta}_k), g(\cdot; \tilde{\theta}_{k'}))$ .

For index sets  $\hat{C}_h$  and  $S_k$ , set  $n_{h\cdot} = |\hat{C}_h|$ ,  $n_{\cdot k} = |S_k|$ , and  $n_{hk} = |\hat{C}_h \cap S_k|$ .

$$\begin{aligned}
\mathcal{L}(\hat{\mathbf{c}}, \boldsymbol{\theta}) &= \sum_{i < j} \{ \mathbf{1}_{\hat{c}_i = \hat{c}_j} \mathcal{D}_{ij} + \omega \mathbf{1}_{\hat{c}_i \neq \hat{c}_j} (1 - \mathcal{D}_{ij}) \} \\
&= \sum_{i < j} \{ \mathbf{1}_{\hat{c}_i = \hat{c}_j} (1 - (1 - \mathcal{D}_{ij})) + \omega (1 - \mathbf{1}_{\hat{c}_i = \hat{c}_j}) (1 - \mathcal{D}_{ij}) \} \\
&= \sum_{i < j} \mathbf{1}(\hat{c}_i = \hat{c}_j) + \omega \sum_{i < j} (1 - \mathcal{D}_{ij}) - (1 + \omega) \sum_{i < j} \mathbf{1}_{\hat{c}_i = \hat{c}_j} (1 - \mathcal{D}_{ij}) \\
&= \sum_{h=1}^{\hat{K}_n} \binom{n_{h\cdot}}{2} + \omega \sum_{k=1}^K \binom{n_{\cdot k}}{2} + \omega \sum_{k < k'} n_{\cdot k} n_{\cdot k'} (1 - \eta_{kk'}) \\
&\quad - (1 + \omega) \sum_{h=1}^{\hat{K}_n} \sum_{k=1}^K \binom{n_{hk}}{2} - (1 + \omega) \sum_{h=1}^{\hat{K}_n} \sum_{k < k'} n_{hk} n_{hk'} (1 - \eta_{kk'}).
\end{aligned}$$

Consequently, this shows that the loss is related to the Binder's loss with unit costs  $a = 1$  and  $b = \omega$ ,

$$\mathcal{L}(\hat{\mathbf{c}}, \boldsymbol{\theta}) = \mathcal{L}_B(\hat{\mathbf{c}}, \mathbf{s}) + \mathcal{B}(\hat{\mathbf{c}}, \tilde{\boldsymbol{\theta}})$$

where

$$\begin{aligned}
\mathcal{B}(\hat{\mathbf{c}}, \tilde{\boldsymbol{\theta}}) &= \omega \sum_{k < k'} n_{\cdot k} n_{\cdot k'} (1 - \eta_{kk'}) \\
&\quad - (1 + \omega) \sum_{h=1}^{\hat{K}_n} \sum_{k < k'} n_{hk} n_{hk'} (1 - \eta_{kk'}).
\end{aligned}$$

It is clear that

$$\mathcal{B}(\mathbf{s}, \tilde{\boldsymbol{\theta}}) = \omega \sum_{k < k'} n_{\cdot k} n_{\cdot k'} (1 - \eta_{kk'})$$

which is equal to zero if and only if  $\eta_{kk'} = 1$  for all  $k \neq k'$  pairs.  $\square$

## D.2 PROOF OF PROPOSITION 2

*Proof.* We proceed by showing that the bounded metric properties of the Hellinger distance are preserved by taking the posterior expectation.

1. For each  $i \leq j$ ,  $0 \leq d(g(\cdot; \theta_i), g(\cdot; \theta_j)) \leq 1$  almost surely, and so  $0 \leq \Delta_{ij} \leq 1$ .

2. We next verify the metric axioms on the entries of  $\Delta$ .

(a) For each  $i = 1, \dots, n$ ,  $d(g(\cdot; \theta_i), g(\cdot; \theta_i)) = 0$  almost surely, and so  $\Delta_{ii} = 0$ .

(b)  $\Delta_{ij} = \Delta_{ji}$  since the Hellinger distance is symmetric and  $(\theta_1, \dots, \theta_n)$  are exchangeable conditional on  $\mathbf{X}$ .

- (c)  $\Delta_{il} \leq \Delta_{ij} + \Delta_{jl}$  since the triangle inequality in the Hellinger distance holds almost surely for  $\theta_i, \theta_j, \theta_l$  conditional on  $\mathbf{X}$ .

3. Observe that

$$\begin{aligned}\Delta_{ij} &= \mathbb{E}_\Pi[\mathbb{E}_\Pi[d(g(\cdot; \theta_i), g(\cdot; \theta_j)) \mid \lambda, \mathbf{X}] \mid \mathbf{X}] \\ &= \int_\Lambda \sum_{k < k'} \eta_{kk'} q_{ij}^{kk'} \Pi(d\lambda \mid \mathbf{X}),\end{aligned}$$

where

$$\begin{aligned}q_{ij}^{kk'} &= \Pi(\{s_i = k, s_j = k'\} \cup \{s_i = k', s_j = k\} \mid \lambda, \mathbf{X}), \\ \eta_{kk'} &= d(g(\cdot; \tilde{\theta}_k), g(\cdot; \tilde{\theta}_{k'})),\end{aligned}$$

for all  $1 \leq k < k' \leq K$ . Since  $\eta_{kk'} \leq 1$ ,

$$\Delta_{ij} \leq \int_\Lambda \sum_{k < k'} q_{ij}^{kk'} \Pi(d\lambda \mid \mathbf{X}) = \Pi(s_i \neq s_j \mid \mathbf{X}).$$

□

### D.3 PROOF OF PROPOSITION 3

*Proof.* To see why there is a positive relationship between  $\omega$  and  $r_\omega$ , recall that the candidate clusterings over which we optimize  $\mathcal{R}(\hat{\mathbf{c}})$  are nested. Given a value of  $\omega$  and minimizer  $\mathbf{c}_\omega^*$ , suppose we now increment the tuning parameter from  $\omega$  to  $\omega + \epsilon$  for some  $\epsilon > 0$ . Denote  $\mathbf{c}'$  to be the child clustering of  $\mathbf{c}_\omega^*$  (i.e., it is next in the agglomerative hierarchy), and assume that it results from merging, say,  $C_{\omega_1}^*$  and  $C_{\omega_2}^*$  in  $\mathbf{c}_\omega^*$ . Then  $\mathcal{R}(\mathbf{c}') < \mathcal{R}(\mathbf{c}_\omega^*)$  if  $\sum_{i \in C_{\omega_1}^*, j \in C_{\omega_2}^*} \Delta_{ij} < (\omega + \epsilon)/(1 + \omega + \epsilon)$ . For large enough  $\epsilon$ , this will hold, and so  $\mathbf{c}_{\omega+\epsilon}^*$  will be equal to  $\mathbf{c}'$  (or one of its child clusterings in the hierarchy). Suppose then that  $\epsilon$  is such that  $\mathbf{c}_{\omega+\epsilon}^* = \mathbf{c}'$ . Then clearly,  $r_{\omega+\epsilon} > r_\omega$  because any pairing  $i \in C_{\omega_1}^*$  and  $j \in C_{\omega_2}^*$  will now contribute a non-negative term to  $r_{\omega+\epsilon}$ . Put differently, we have that  $r_{\omega+\epsilon} = r_\omega + (\sum_{i \in C_{\omega_1}^*, j \in C_{\omega_2}^*} \Delta_{ij}) / (\sum_{i < j} \Delta_{ij})$ . □

### D.4 PROOF OF PROPOSITION 4

*Proof.* (a) This oracle rule follows by noting that if  $d\{g(\cdot; \theta_m^*), g(\cdot; \theta_{m'}^*)\} = 1$  for all component pairs, then all components have disjoint support. Hence,  $\mathcal{R}^*(\hat{\mathbf{c}})$  is just Binder's loss of  $\hat{\mathbf{c}}$  to  $\mathbf{s}^*$ , where  $s_i^* = m$  if and only  $X_i^0 \in \text{supp}(g(\cdot; \theta_m^*))$ , which is uniquely minimized at  $\hat{\mathbf{c}} = \mathbf{s}^*$ .

(b) We can verify this by noting that, under the described conditions,  $\mathbf{c}_0$  minimizes  $\mathcal{R}^*(\hat{\mathbf{c}})$  if

$$d\{g(\cdot; \theta_1^*), g(\cdot; \theta_2^*)\} \sum_{i < j} q_{ij}^{12*} \leq \mathcal{R}^*(\hat{\mathbf{c}}).$$

A sufficient condition for this to hold is when  $d\{g(\cdot; \theta_1^*), g(\cdot; \theta_2^*)\} < \gamma/q_{ij}^{12*}$  for all  $i, j$  pairs. Since  $0 \leq q_{ij}^{12*} \leq 1$ , this criteria can be satisfied when  $d\{g(\cdot; \theta_1^*), g(\cdot; \theta_2^*)\} < \gamma$ .

□

## E PRELIMINARIES FOR ASYMPTOTIC ANALYSIS

Recall the assumptions for Theorem 1 that we make in the main article.

**Assumption 2.** Suppose that the following conditions hold.

(A1)  $\Lambda$  consists of measures with uniformly finite support, i.e. there exists an  $L > 0$  so that  $|\text{supp}(\lambda)| \leq L$  for all  $\lambda \in \Lambda$ .

(A2) The KL minimizer  $\lambda^* = \sum_{m=1}^{M^*} a_m^* \delta_{\theta_m^*}$  exists and is unique.

(A3)  $f^*$  and  $f^0$  are such that  $\text{supp}(f^0) \subseteq \text{supp}(f^*)$ .

(A4):  $\mathcal{G} = \{\tilde{g}(x - \theta) : \theta \in \Theta\}$  for some bounded probability density function  $\tilde{g}(\cdot)$ , there exists a  $\zeta > 0$  so that  $\tilde{g}(z)$  is  $\zeta$ -Hölder continuous, and for any fixed  $\theta'$ ,  $D_g(\theta, \theta') = d\{g(\cdot; \theta), g(\cdot; \theta')\}$  is continuous in  $\theta$ .

(A5) The mixing measure of the fitted model contracts to the oracle in the Wasserstein 2-distance, i.e. there exists a non-negative sequence  $\epsilon_n$  so that  $\epsilon_n \rightarrow 0$  and

$$\rho_n(\mathbf{X}) = \Pi \left\{ \lambda \in \Lambda : W_2(\lambda, \lambda^*) \gtrsim \epsilon_n \mid \mathbf{X} \right\} \xrightarrow{\mathbb{P}^0} 0. \quad (12)$$

In this section, we will be primarily concerned with introducing concepts necessary for understanding the proof of Theorem 1. We will also detail conditions under which (A2) and (A5) hold, the latter of which is a statement on the posterior contraction of the mixing measure. The main contribution that (A5) has to the proof of Theorem 1 is that it establishes consistency of the cluster-specific parameters  $\mathbf{a}$  and  $\tilde{\boldsymbol{\theta}}$ . Conditions under which (A5) hold have been extensively explored in [Nguyen \(2013\)](#), [Ho and Nguyen \(2016b\)](#), and [Guha et al. \(2021\)](#).

## E.1 ADDITIONAL NOTATION AND DEFINITIONS

Given  $x = (x_1, \dots, x_p)^T \in \mathbb{R}^p$ , let  $\|x\| = \sqrt{\sum_{s=1}^p x_s^2}$ . For  $q \geq 1$ , the  $q$ -th order Wasserstein distance between the finite measures  $\lambda = \sum_{k=1}^K a_k \delta_{\theta_k}$  and  $\lambda' = \sum_{k'=1}^{K'} a'_{k'} \delta_{\theta'_{k'}}$  is

$$W_q(\lambda, \tilde{\lambda}) = \inf_{\mathbf{b} \in \mathcal{C}(\mathbf{a}, \mathbf{a}')} \left( \sum_{k, k'} b_{kk'} \|\theta_k - \theta'_{k'}\|^q \right)^{1/q},$$

where  $\mathcal{C}(\mathbf{a}, \mathbf{a}')$  is the set of all couplings with marginal probability vectors  $\mathbf{a}$  and  $\mathbf{a}'$ . That is, for all  $k = 1, \dots, K$ ,  $\sum_{k'=1}^{K'} b_{kk'} = a_k$  and for all  $k' = 1, \dots, K'$ ,  $\sum_{k=1}^K b_{kk'} = a'_{k'}$ . The Wasserstein  $q$ -distance is a metric over the space of probability measures on  $\Theta$ , and therefore  $W_q(\lambda, \lambda) = 0$ , if  $\lambda \neq \lambda'$  then  $W_q(\lambda, \lambda') > 0$ ,  $W_q(\lambda, \lambda') = W_q(\lambda', \lambda)$ , and  $W_q$  obeys the triangle inequality. We will only consider mixtures having identifiable mixing measures. That is, if  $\int g(x; \theta) \lambda(d\theta) = \int g(x; \theta) \lambda'(d\theta)$  for all  $x$ , then  $\lambda = \lambda'$ . This identifiability condition is satisfied by Gaussian mixtures, along with several exponential family mixtures (Barndorff-Nielsen, 1965) and location family mixtures (Teicher, 1961).

Recall that  $\mathbb{P}^0$  refers to probability statements with respect to the true data generating process, with  $\mathbb{P}^0(A) = \int_A f^0(x) dx$ . For any sequences  $y_n$  and  $z_n$ ,  $y_n \leq z_n$  if there exists a  $N \in \mathbb{N}$  and constant  $B > 0$  so that  $|y_n| \leq B|z_n|$  for all  $n \geq N$ ;  $y_n \lesssim z_n$  if  $y_n \leq z_n$  and  $z_n \lesssim y_n$ ; and  $y_n \sim z_n$  if  $y_n/z_n \rightarrow 1$ . A random variable  $Z_n = o_{\mathbb{P}^0}(1)$  if  $Z_n \rightarrow 0$  in  $\mathbb{P}^0$ -probability. Finally, we say that an event  $A_n$  holds with high probability if  $\mathbb{P}^0(A_n) \rightarrow 1$  as  $n \rightarrow \infty$ .

## E.2 UNIQUENESS OF $\lambda^*$

While (A2) is trivial in the exact-fitted and well-specified regime, uniqueness of  $\lambda^*$  may not hold in general. Section 4 of Guha et al. (2021) details conditions for uniqueness in the misspecified regime, which we briefly summarize. Let  $\mathcal{M}^* = \{\nu^* \in \Omega : \nu^* \in \arg \min_{\nu \in \Omega} \text{KL}(f^0, f)\}$ , where recall that  $\Omega$  is the space of all probability measures on  $\Theta$ . Additionally, let  $\mathcal{R}^* = \{\lambda^* \in \Lambda : \lambda^* \in \arg \min_{\lambda \in \Lambda} \text{KL}(f^0, f)\}$ , the set of KL-minimizers constrained to be contained within the prior support. By Lemma 4.2 of Guha et al. (2021), the minimizing density  $f^*$  over  $\Omega$  is unique. Hence, under identifiability of the mixing measure, we have that  $\mathcal{M}^* = \{\nu^*\}$  for some unique  $\nu^* \in \Omega$ . Therefore, as long as the KL divergence is minimized over  $\Lambda$ , we have that  $\mathcal{M}^* = \mathcal{R}^*$ , meaning that  $\lambda^* = \nu^*$  and so the oracle is finite and unique.

## E.3 STRONG IDENTIFIABILITY AND LIPSCHITZ CONDITIONS

As stated in Section 3, Wasserstein contraction of  $\lambda$  will generally require that  $\mathcal{G}$  is strongly identifiable, referring to a linear independence condition on the derivatives of  $g(x; \theta)$ . We formally define these

concepts below. Recall that  $\Theta \subset \mathbb{R}^p$  is assumed to be compact and  $f$  to be identifiable in  $\lambda$ . In these definitions,  $\nabla_g(\theta)$  and  $\mathbf{H}_g(\theta)$  denote the gradient and Hessian of  $g(x; \theta)$  with respect to  $\theta$ .

**Definition E.1.** The family  $\mathcal{G} = \{g(\theta) : \theta \in \Theta\}$  is *first order identifiable* if  $g(x; \theta)$  is differentiable in  $\theta$  and, given  $r$  atoms  $\theta_1, \dots, \theta_r \in \Theta$ , if there exists  $\beta_1, \dots, \beta_r \in \mathbb{R}$  and  $\rho_1, \dots, \rho_r \in \mathbb{R}^p$  so that for all  $x$

$$\sum_{s=1}^r \{\beta_s g(x; \theta_s) + \rho_s^T \nabla_g(\theta_s)\} = 0,$$

then  $\beta_s = 0$  and  $\rho_s = \mathbf{0}$  for all  $s = 1, \dots, r$ .

**Definition E.2.** The family  $\mathcal{G} = \{g(\theta) : \theta \in \Theta\}$  is *second order identifiable* if  $g(x; \theta)$  is twice differentiable in  $\theta$  and, given  $r$  atoms  $\theta_1, \dots, \theta_r \in \Theta$ , if there exists  $\beta_1, \dots, \beta_r \in \mathbb{R}$ ,  $\rho_1, \dots, \rho_r \in \mathbb{R}^p$ , and  $\nu_1, \dots, \nu_r \in \mathbb{R}^p$  so that for all  $x$

$$\sum_{s=1}^r \{\beta_s g(x; \theta_s) + \rho_s^T \nabla_g(\theta_s) + \nu_s^T \mathbf{H}_g(\theta_s) \nu_s\} = 0,$$

then  $\beta_s = 0$  and  $\rho_s = \nu_s = \mathbf{0}$  for all  $s = 1, \dots, r$ .

It is clear from the two definitions that second-order identifiability implies first-order identifiability. These notions are commonly used in the literature because they bridge the connection between convergence from  $f$  to  $f^0$  (or  $f^*$ ) in the Hellinger distance and convergence from  $\lambda$  to  $\lambda^0$  (or  $\lambda^*$ ) in Wasserstein distance. This will be useful for showing concentration of the weights and atoms, as this is straightforward to extract from convergence of the mixing measure. A canonical example of a second-order identifiable family is Gaussian location mixtures for a known covariance matrix  $\Sigma$ , i.e.  $\mathcal{G} = \{\mathcal{N}_p(\theta, \Sigma) : \theta \in \Theta\}$ , whereas location-scale Gaussian families  $\mathcal{G} = \{\mathcal{N}_p(\mu, \Sigma) : \mu \in \mathbb{R}^p, \Sigma \in \mathbb{S}^p\}$ , where  $\mathbb{S}^p$  is the set of  $p \times p$  positive semi-definite matrices, are only first-order identifiable.

In addition to strong identifiability, various Lipschitz conditions on the derivatives of  $g(x; \theta)$  are required for contraction of the mixing measure. The strongest condition is the second order integral Lipschitz property, as introduced in [Guha et al. \(2021\)](#).

**Definition E.3.**  $\mathcal{G}$  satisfies the integral Lipschitz property of the second order with respect to the mixing measures  $\lambda^0$  and  $\lambda^*$  if  $g(x; \theta)$  is twice differentiable in  $\theta$  and for all  $x \in \chi$ ,

$$|\zeta^T (\mathbf{H}_g(\theta_1) - \mathbf{H}_g(\theta_2)) \zeta| \leq M(x) \|\theta_1 - \theta_2\|^\xi \|\zeta\|^2 \tag{13}$$

for any  $\zeta \in \mathbb{R}^p$  and for some  $\xi > 0$  that does not depend on  $x$  and  $\theta_1, \theta_2$ , where  $M(x)$  is a function of  $x$  so that  $\mathbb{E}_0[M(X)/f^*(X)] < \infty$ .

Note that this is not only a condition on  $\mathcal{G}$ , but also on  $\lambda^0$  and  $f^0$ . The above inequality is effectively a smoothness condition on the Hessian of  $g(x; \theta)$ , where the Lipschitz constant is a function of  $x$ . [Guha](#)

et al. (2021) invokes the integral Lipschitz property when studying the misspecified regime. Related to the integral Lipschitz property is the uniform Lipschitz property, which was introduced in Ho and Nguyen (2016b).

**Definition E.4.**  $\mathcal{G}$  satisfies the uniform Lipschitz property of the second order if  $g(x; \theta)$  is twice differentiable in  $\theta$  and for all  $x \in \chi$ ,

$$|\zeta^T (\mathbf{H}_g(\theta_1) - \mathbf{H}_g(\theta_2)) \zeta| \leq M \|\theta_1 - \theta_2\|^\xi \|\zeta\|^2$$

for any  $\zeta \in \mathbb{R}^p$  and for some  $\xi, M > 0$  that do not depend on  $x$  and  $\theta_1, \theta_2$ .

The uniform Lipschitz property is generally invoked in well-specified regimes. As in (13), it is also a Lipschitz condition on the Hessian of  $g(x; \theta)$ . The second order Lipschitz property is satisfied by the location-scale Gaussian family and location-scale Student's t family (Ho et al., 2020). A similar notion exists for the gradient, known as the first-order Lipschitz property.

Lipschitz conditions on the derivatives, particularly on the Hessian, of a probability density function are frequently assumed in the literature on mixing measure concentration. See, for example, Lemma 2 in Chen (1995) and Theorem 1 in Nguyen (2013). While it is difficult to characterize what choices of  $f^0$  and  $\mathcal{G}$  can admit the integral Lipschitz property in the misspecified regime, the property will hold if  $\mathcal{G}$  is uniformly Lipschitz of the second order and  $\int_{\mathbb{R}^p} \frac{f^0(x)}{f^*(x)} dx < \infty$ . Hence, for uniformly Lipschitz families, such as location Gaussians, the integral Lipschitz property can be reformulated as a tail condition on  $f^*$  and  $f^0$ .

#### E.4 PROPERTIES OF WASSERSTEIN CONCENTRATION

The proof of Theorem 1 relies on characterizing the mixing measures in the set

$$B_{\epsilon_n}(\lambda^*) = \left\{ \lambda \in \Lambda : W_2(\lambda, \lambda^*) \lesssim \epsilon_n \right\},$$

or the  $\epsilon_n$  ball around  $\lambda^*$ . (A1) becomes a crucial assumption for doing so, as it tells us that each  $\lambda \in \Lambda$  has at most  $L$  support points, where  $L < \infty$ . In the exact fitted case where  $\Pi(K = M^*) = 1$ , Nguyen (2013) shows that for all  $m \in [M^*]$ , there exists a unique  $k \in [K]$  so that  $\|\theta_k - \theta_m^*\| \lesssim \epsilon_n$  and  $|a_k - a_m^*| \lesssim \epsilon_n$ . In this next proposition, we will show that a similar result holds for the overfitted case, i.e., when  $\Pi(K > M^*) > 0$ .

**Proposition 5.** Let  $\lambda = \sum_{k=1}^K a_k \delta_{\theta_k} \in B_{\epsilon_n}(\lambda^*)$ , where  $M^* \leq K \leq L < \infty$  and  $\epsilon_n \rightarrow 0$ , and fix  $0 < \delta < 1$ .

1. For large enough  $n$ , for all  $m \in [M^*]$  there exists an index set  $\mathcal{I}_m^{(\lambda)} \subset [K]$  so that

$$\max_{k \in \mathcal{I}_m^{(\lambda)}} \|\theta_k - \theta_m^*\| \lesssim \epsilon_n, \quad \left| \sum_{k \in \mathcal{I}_m^{(\lambda)}} a_k - a_m^* \right| \lesssim \max(\epsilon_n, \epsilon_n^{2\delta}), \quad (14)$$

and  $\mathcal{I}_m^{(\lambda)} \cap \mathcal{I}_{m'}^{(\lambda)} = \emptyset$  for all  $m \neq m' = 1, \dots, M^*$ .

2. Let  $\mathcal{I}^{(\lambda)} = \bigcup_{m=1}^{M^*} \mathcal{I}_m^{(\lambda)}$ . Then,

$$\sum_{k \notin \mathcal{I}^{(\lambda)}} a_k \lesssim \epsilon_n^{2\delta}. \quad (15)$$

Proposition 5 gives us the necessary tools to establish convergence to the oracle. The statement in (14) tells us that for large enough  $n$ , we can allocate a subset of the components in  $\lambda$  to  $M^*$  groups, given by  $\mathcal{I}_m^{(\lambda)}$  for  $m \in [M^*]$ . In the  $m$ th group, all of the atoms contract to  $\theta_m^*$ , and the total weight of the  $m$ th group contracts to  $a_m^*$ . (15) tells us that any components left over, i.e. any components with atoms that *do not* contract to an atom in  $\lambda^*$ , will have total weight diminishing at an  $\epsilon_n^{2\delta}$  rate. This behavior is comparable to Theorem 1 in [Rousseau and Mengersen \(2011\)](#), which established that under certain settings of overfitted finite mixture models, the total weight of the overfitted components empty at an approximately  $n^{-1/2}$  rate. Under the settings of Theorem 4.3 from [Guha et al. \(2021\)](#), (15) implies that the redundant components empty at an approximately  $(\log n/n)^{1/2}$  rate for misspecified models. We now present the proof of the proposition.

## E.5 PROOF OF PROPOSITION 5

*Proof.* Let  $\lambda \in B_\epsilon(\lambda^*)$ , where  $K \geq M^*$ . We now show concentration of the weights and atoms using techniques from [Nguyen \(2011\)](#) and [Nguyen \(2013\)](#). Let  $0 < \delta < 1$  be a small positive constant. For large enough  $n$ ,  $a_{\min}^* \gtrsim \epsilon_n^{2\delta}$ , implying

$$W_2^{2(1-\delta)}(\lambda, \lambda^*) \geq \min_k \|\theta_k - \theta_m^*\|^2.$$

For any  $m \in [M^*]$  let

$$\mathcal{I}_m^{(\lambda)} = \left\{ k \in [K] : \|\theta_k - \theta_m^*\|^2 \leq W_2^{2(1-\delta)}(\lambda, \lambda^*) \right\}$$

and  $\mathcal{I}^{(\lambda)} = \bigcup_{m=1}^{M^*} \mathcal{I}_m^{(\lambda)}$ . It follows that

$$\begin{aligned} W_2^2(\lambda, \lambda^*) &\geq \sum_{k \notin \mathcal{I}^{(\lambda)}} a_k \min_m \|\theta_k - \theta_m^*\|^2 > W_2^{2(1-\delta)}(\lambda, \lambda^*) \sum_{k \notin \mathcal{I}^{(\lambda)}} a_k \\ &\implies \sum_{k \notin \mathcal{I}^{(\lambda)}} a_k < W_2^{2\delta}(\lambda, \lambda^*) \lesssim \epsilon_n^{2\delta}. \end{aligned} \quad (16)$$

Now, we will show concentration of the weights towards their oracle values. For fixed  $m$ ,

$$\begin{aligned}
\epsilon_n^2 \gtrsim W_2(\lambda, \lambda^*) &\geq \sum_{k \in \mathcal{I}^{(\lambda)} \setminus \mathcal{I}_m^{(\lambda)}} b_{km} \|\theta_k - \theta_m^*\|^2 \geq \min_{k \in \mathcal{I}^{(\lambda)} \setminus \mathcal{I}_m^{(\lambda)}} \|\theta_k - \theta_m^*\|^2 \sum_{k \in \mathcal{I}^{(\lambda)} \setminus \mathcal{I}_m^{(\lambda)}} b_{km} \\
&= \min_{k \in \mathcal{I}^{(\lambda)} \setminus \mathcal{I}_m^{(\lambda)}} \|\theta_k - \theta_m^*\|^2 \left( a_m^* - \sum_{k \in \mathcal{I}_m^{(\lambda)}} b_{km} - \sum_{k \notin \mathcal{I}^{(\lambda)}} b_{km} \right) \\
&= \min_{k \in \mathcal{I}^{(\lambda)} \setminus \mathcal{I}_m^{(\lambda)}} \|\theta_k - \theta_m^*\|^2 \left( a_m^* - \sum_{k \in \mathcal{I}_m^{(\lambda)}} a_k + \sum_{m \in \mathcal{I}_h^{(\lambda)}} \sum_{m' \neq m} b_{km'} - \sum_{k \notin \mathcal{I}^{(\lambda)}} b_{km} \right) \\
&\geq \min_{k \in \mathcal{I}^{(\lambda)} \setminus \mathcal{I}_m^{(\lambda)}} \|\theta_k - \theta_m^*\|^2 \left( a_m^* - \sum_{k \in \mathcal{I}_m^{(\lambda)}} a_k - \sum_{k \notin \mathcal{I}^{(\lambda)}} b_{km} \right) \\
&\geq \min_{k \in \mathcal{I}^{(\lambda)} \setminus \mathcal{I}_m^{(\lambda)}} \|\theta_k - \theta_m^*\|^2 \left( a_m^* - \sum_{k \in \mathcal{I}_m^{(\lambda)}} a_k - \sum_{k \in \mathcal{I}^{(\lambda)} \setminus \mathcal{I}_m^{(\lambda)}} b_{km} - \sum_{k \notin \mathcal{I}^{(\lambda)}} b_{km} \right) \\
&= \min_{k \in \mathcal{I}^{(\lambda)} \setminus \mathcal{I}_m^{(\lambda)}} \|\theta_k - \theta_m^*\|^2 \left( \sum_{k \in \mathcal{I}_m^{(\lambda)}} b_{km} - \sum_{k \in \mathcal{I}_m^{(\lambda)}} a_k \right) \\
&= - \min_{k \in \mathcal{I}^{(\lambda)} \setminus \mathcal{I}_m^{(\lambda)}} \|\theta_k - \theta_m^*\|^2 \sum_{k \in \mathcal{I}_m^{(\lambda)}} \sum_{m' \neq m} b_{km'}.
\end{aligned}$$

For any  $m' \neq m$ ,  $k' \in \mathcal{I}_{m'}^{(\lambda)}$ , and  $k \in \mathcal{I}_m^{(\lambda)}$ ,

$$\begin{aligned}
&\min_{k \in \mathcal{I}^{(\lambda)} \setminus \mathcal{I}_m^{(\lambda)}} \|\theta_k - \theta_m^*\| \leq \|\theta_{k'} - \theta_m^*\| \\
&\leq \|\theta_{k'} - \theta_{m'}^*\| + \|\theta_{k'} - \theta_m^*\| + \|\theta_k - \theta_m^*\| \lesssim \epsilon_n + \|\theta_k - \theta_{m'}^*\|.
\end{aligned}$$

Since  $\Theta$  is compact, this shows that

$$\begin{aligned}
&- \min_{k \in \mathcal{I}^{(\lambda)} \setminus \mathcal{I}_m^{(\lambda)}} \|\theta_k - \theta_m^*\|^2 \sum_{k \in \mathcal{I}_m^{(\lambda)}} \sum_{m' \neq m} b_{km'} \\
&\gtrsim -\epsilon_n - \sum_{k \in \mathcal{I}_m^{(\lambda)}} \sum_{m' \neq m} b_{km'} \|\theta_k - \theta_{m'}^*\|^2 \gtrsim -\epsilon_n - W_2(\lambda, \lambda^*)^2.
\end{aligned}$$

Therefore,

$$\min_{k \in \mathcal{I}^{(\lambda)} \setminus \mathcal{I}_m^{(\lambda)}} \|\theta_k - \theta_m^*\|^2 \left| a_m^* - \sum_{k \in \mathcal{I}_m^{(\lambda)}} a_k - \sum_{k \notin \mathcal{I}^{(\lambda)}} b_{km} \right| \lesssim \epsilon_n.$$

Observe that there exists  $m' \neq m$  so that

$$\min_{k \in \mathcal{I}^{(\lambda)} \setminus \mathcal{I}_m^{(\lambda)}} \|\theta_k - \theta_m^*\|^2 \gtrsim \|\theta_m^* - \theta_{m'}^*\|^2 - \epsilon_n.$$

The above derivation implies that there exists constants  $M, M',$  and  $M'' > 0$  so that

$$\begin{aligned} & \left| a_m^* - \sum_{k \in \mathcal{I}_m^{(\lambda)}} a_k - \sum_{k \notin \mathcal{I}_m^{(\lambda)}} b_{km} \right| \leq \frac{M\epsilon_n}{\|\theta_m^* - \theta_{m'}^*\|^2 - M'\epsilon_n} \\ \implies & \left| a_m^* - \sum_{k \in \mathcal{I}_m^{(\lambda)}} a_k \right| \leq \nu_n := \frac{M\epsilon_n}{\|\theta_m^* - \theta_{m'}^*\|^2 - M'\epsilon_n} + (K - M^*)M''\epsilon_n^{2\delta} \lesssim \max(\epsilon_n, \epsilon_n^{2\delta}). \end{aligned}$$

□

## F PROOF OF THEOREM 1

*Proof.* Recall that  $\lambda^* = \sum_{m=1}^{M^*} a_m^* \delta_{\theta_m^*}$  and that by (A1), if  $\lambda \in \Lambda$  then  $\lambda = \sum_{k=1}^K a_k \delta_{\theta_k}$  for some  $K \leq L$ . Let  $B_{\epsilon_n}(\lambda^*) = \{\lambda \in \Lambda : W_2(\lambda, \lambda^*) \lesssim \epsilon_n\}$  and  $\Lambda_{M^*,L} = \{\lambda \in \Lambda : |\text{supp}(\lambda)| \geq M^*\}$ . We decompose the posterior expectation of  $\mathcal{D}_{ij}$  into

$$\begin{aligned} \Delta_{ij} &= \mathbb{E}[\mathcal{D}_{ij} \mid \mathbf{X}] \\ &= \int_{\Lambda_{M^*,L} \cap B_{\epsilon_n}(\lambda^*)} \mathcal{D}_{ij} \Pi(d\phi_{ij} \mid \mathbf{X}) + \int_{\Lambda_{M^*,L}^c \cap B_{\epsilon_n}(\lambda^*)} \mathcal{D}_{ij} \Pi(d\phi_{ij} \mid \mathbf{X}) + \int_{B_{\epsilon_n}^c(\lambda^*)} \mathcal{D}_{ij} \Pi(d\phi_{ij} \mid \mathbf{X}), \end{aligned}$$

where  $\phi_{ij} = (\theta_i, \theta_j, \lambda)$ . This implies

$$\int_{\Lambda_{M^*,L} \cap B_{\epsilon_n}(\lambda^*)} \mathcal{D}_{ij} \Pi(d\phi_{ij} \mid \mathbf{X}) \leq \Delta_{ij} \leq \int_{\Lambda_{M^*,L} \cap B_{\epsilon_n}(\lambda^*)} \mathcal{D}_{ij} \Pi(d\phi_{ij} \mid \mathbf{X}) + \nu_n(\mathbf{X}) + \rho_n(\mathbf{X}),$$

where  $\nu_n(\mathbf{X}) = \Pi(|\text{supp}(\lambda)| < M^*, W_2(\lambda, \lambda^*) \lesssim \epsilon_n \mid \mathbf{X})$  and  $\rho_n(\mathbf{X}) = \Pi(W_2(\lambda, \lambda^*) \gtrsim \epsilon_n \mid \mathbf{X})$ . By assumption (A5),  $\rho_n(\mathbf{X}) \xrightarrow{\mathbb{P}^0} 0$ . In addition,  $\nu_n(\mathbf{X}) \xrightarrow{\mathbb{P}^0} 0$ , and we can show that  $\mathbb{P}^0 \{\nu_n(\mathbf{X}) = 0\} = 1$  for large enough  $n$ . To see this, note that  $\lambda \in W_2(\lambda, \lambda^*)$  implies that for all  $\theta_m^* \in \text{supp}(\lambda)$ , there exists a  $\theta_k \in \text{supp}(\lambda)$  so that  $\|\theta_m^* - \theta_k\| \lesssim \epsilon_n$ . More formally,

$$\begin{aligned} \epsilon_n^2 &\gtrsim W_2(\lambda, \lambda^*) = \sum_{k,m} b_{km} \|\theta_k - \theta_m^*\|^2 \geq \sum_k b_{km} \|\theta_k - \theta_m^*\|^2 \\ &\geq \min_k \|\theta_k - \theta_m^*\|^2 a_m^* \geq \min_k \|\theta_k - \theta_m^*\|^2 a_{\min}^*, \end{aligned}$$

where  $a_{\min}^* = \min_m a_m^*$ . If we set  $n$  large enough so that  $\min_{m \neq m'} \|\theta_m^* - \theta_{m'}^*\| \gtrsim 2\epsilon_n$ , then we have that there must be at least  $M^*$  support points in  $\lambda$ . Hence, for large enough  $n$ ,  $\Lambda_{M^*,L}^c \cap B_{\epsilon_n}(\lambda^*) = \emptyset$ .

Therefore, we will omit  $\nu_n(\mathbf{X})$  from the remainder of the proof by assuming that  $n$  is large enough so that  $\min_{m \neq m'} \|\theta_m^* - \theta_{m'}^*\| \gtrsim 2\epsilon_n$ . We then formulate the bounds of  $\Delta_{ij}$  via

$$\int_{\Lambda_{M^*,L} \cap B_{\epsilon_n}(\lambda^*)} \mathcal{D}_{ij} \Pi(d\phi_{ij} | \mathbf{X}) \leq \Delta_{ij} \leq \int_{\Lambda_{M^*,L} \cap B_{\epsilon_n}(\lambda^*)} \mathcal{D}_{ij} \Pi(d\phi_{ij} | \mathbf{X}) + \rho_n(\mathbf{X}). \quad (17)$$

Let  $0 < \delta < 1$  and  $\lambda \in \Lambda_{M^*,L} \cap B_{\epsilon_n}(\lambda^*)$ . Proposition 5 states that for any  $m \in [M^*]$  there exists a set of indices  $\mathcal{I}_m^{(\lambda)}$  so that  $\max_{k \in \mathcal{I}_m^{(\lambda)}} \|\theta_k - \theta_m^*\| \lesssim \epsilon_n$  and  $\left| \sum_{k \in \mathcal{I}_m^{(\lambda)}} a_k - a_m^* \right| \lesssim \max(\epsilon_n, \epsilon_n^{2\delta})$ , and in addition that  $\sum_{k \notin \mathcal{I}_m^{(\lambda)}} a_k \lesssim \epsilon_n^{2\delta}$ , where  $\mathcal{I}^{(\lambda)} = \bigcup_{m=1}^{M^*} \mathcal{I}_m^{(\lambda)}$ . We will now translate contraction of the atoms and weights into contraction of the  $\Delta_{ij}$  terms. Recall that we can write

$$\int_{\Lambda_{M^*,L} \cap B_{\epsilon_n}(\lambda^*)} \mathcal{D}_{ij} \Pi(d\phi_{ij} | \mathbf{X}) = \int_{\Lambda_{M^*,L} \cap B_{\epsilon_n}(\lambda^*)} \sum_{k < k'} \eta_{kk'} q_{ij}^{kk'} \Pi(d\lambda | \mathbf{X}), \quad (18)$$

We then decompose the integrand in (18):

$$\begin{aligned} & \sum_{k < k'} \eta_{kk'} q_{ij}^{kk'} \\ &= \sum_{k < k' \in \mathcal{I}^{(\lambda)}} \eta_{kk'} q_{ij}^{kk'} + \sum_{(k \notin \mathcal{I}^{(\lambda)}) \text{ or } (k' \notin \mathcal{I}^{(\lambda)})} \eta_{kk'} q_{ij}^{kk'} \\ &= \sum_{m=1}^{M^*} \sum_{k < k' \in \mathcal{I}_m^{(\lambda)}} \eta_{kk'} q_{ij}^{kk'} + \sum_{m < m'} \sum_{\substack{k \in \mathcal{I}_m^{(\lambda)} \\ k' \in \mathcal{I}_{m'}^{(\lambda)}}} \eta_{kk'} q_{ij}^{kk'} + \sum_{(k \notin \mathcal{I}^{(\lambda)}) \text{ or } (k' \notin \mathcal{I}^{(\lambda)})} \eta_{kk'} q_{ij}^{kk'}. \end{aligned} \quad (19)$$

Let  $\psi_m^*(\theta) = D(\theta, \theta_m^*)$ . By (A4), Lemma 1, and Remark 1, for any  $1 \leq m \leq M^*$ ,

$$\max_{k \in \mathcal{I}_m^{(\lambda)}} D(\theta_k, \theta_m^*) \leq \kappa_{nm} = \max_{\theta: \|\theta - \theta_m^*\| \lesssim \epsilon_n} \varphi_m^*(\theta)$$

and  $\kappa_{nm} \rightarrow 0$ . Let  $\kappa_n := \max_{m=1, \dots, M^*} \kappa_{nm}$ . Then, for any  $k, k' \in \mathcal{I}_h^{(\lambda)}$ ,

$$D(\theta_k, \theta_{k'}) \leq 2\kappa_n, \quad (20)$$

and for any  $k \in \mathcal{I}_m^{(\lambda)}, k' \in \mathcal{I}_{m'}^{(\lambda)}$ ,

$$D(\theta_m^*, \theta_{m'}^*) - 2\kappa_n \leq D(\theta_m, \theta_{k'}) \leq D(\theta_m^*, \theta_{m'}^*) + 2\kappa_n.$$

(A4) implies similar concentration for the densities at  $X_i^0$  and  $X_j^0$ . For  $X \sim f^0$ ,

$$\begin{aligned} |g(X; \theta_k) - g(X; \theta_m^*)| &= |\tilde{g}(X - \theta_k) - \tilde{g}(X - \theta_m^*)| \\ &\lesssim \|X - \theta_k - \theta_m^* - X\|^\zeta = M \|\theta_k - \theta_m^*\|^\zeta \lesssim \epsilon_n^\zeta. \end{aligned}$$

It follows that,

$$\left| \sum_{m=1}^{M^*} \sum_{k \in \mathcal{I}_m^{(\lambda)}} a_k g(X_i^0; \theta_k) - f^*(X_i^0) \right| \lesssim \max(\epsilon_n^\zeta, \nu_n)$$

where  $\nu_n$  is defined in (E.5). Condition (A3) and the dominated convergence theorem implies that for large  $n$ , the following holds with  $\mathbb{P}^0$ -probability tending to 1 (see Remark 2),

$$0 \leq f_-^{(n)}(X_i^0) \lesssim f(X_i^0) \lesssim f_+^{(n)}(X_i^0) + \epsilon_n^{2\delta}, \quad (21)$$

where

$$\begin{aligned} f_-^{(n)}(X_i^0) &= f^*(X_i^0) - M \max(\epsilon_n^\zeta, \nu_n); \\ f_+^{(n)}(X_i^0) &= f^*(X_i^0) + M \max(\epsilon_n^\zeta, \nu_n), \end{aligned}$$

for some constant  $M > 0$ . We can now begin to bound some of the terms in (19). For any  $k, k' \notin \mathcal{I}^{(\lambda)}$ ,

$$0 \leq q_{ij}^{kk'} = a_k a_{k'} \frac{g(X_i^0; \theta_k) g(X_j^0; \theta_{k'}) + g(X_i^0; \theta_{k'}) g(X_j^0; \theta_k)}{f(X_i^0) f(X_j^0)} \lesssim \frac{\epsilon_n^{4\delta}}{f_-^{(n)}(X_i^0) f_-^{(n)}(X_j^0)}.$$

Similarly, for any  $k \notin \mathcal{I}^{(\lambda)}$  and  $k' \in \mathcal{I}^{(\lambda)}$ ,

$$0 \leq q_{ij}^{kk'} \lesssim \frac{\epsilon_n^{2\delta}}{f_-^{(n)}(X_i^0) f_-^{(n)}(X_j^0)}.$$

Next, if  $k, k' \in \mathcal{I}_m^{(\lambda)}$ , by (20),

$$0 \leq \eta_{kk'} q_{kk'}^{kk'} \leq 2\kappa_n.$$

Additionally,

$$\left| \sum_{\substack{k \in \mathcal{I}_m^{(\lambda)} \\ k' \in \mathcal{I}_{m'}^{(\lambda)}}} a_k a_{k'} g(X_i^0; \theta_k) g(X_j^0; \theta_{k'}) - a_m^* a_{m'}^* g(X_i^0; \theta_m^*) g(X_j^0; \theta_{m'}^*) \right| \lesssim \max(\epsilon_n^\zeta, \nu_n).$$

Therefore,

$$\begin{aligned}
(\eta_{mm'}^* - 2\kappa_n)R_{ij}^{mm'} &\leq \sum_{\substack{k \in \mathcal{I}_m^{(\lambda)} \\ k' \in \mathcal{I}_{m'}^{(\lambda)}}} \eta_{kk'} q_{ij}^{kk'} \leq (\eta_{mm'}^* + 2\kappa_n)S_{ij}^{mm'}; \\
R_{ij}^{mm'} &= \frac{a_m^* a_{m'}^* \left\{ g(X_i^0; \theta_m^*) g(X_j^0; \theta_{m'}^*) + g(X_j^0; \theta_m^*) g(X_i^0; \theta_{m'}^*) \right\} - M \max(\epsilon_n^\zeta, \nu_n)}{(f_+^{(n)}(X_i^0) + M' \epsilon_n^{2\delta})(f_+^{(n)}(X_j^0) + M' \epsilon_n^{2\delta})}; \\
S_{ij}^{mm'} &= \frac{a_m^* a_{m'}^* \left\{ g(X_i^0; \theta_m^*) g(X_j^0; \theta_{m'}^*) + g(X_j^0; \theta_m^*) g(X_i^0; \theta_{m'}^*) \right\} + M \max(\epsilon_n^\zeta, \nu_n)}{f_-^{(n)}(X_i^0) f_-^{(n)}(X_j^0)},
\end{aligned}$$

where  $M, M' > 0$  are constants. Finally, this gives us the following bound on (19) for all  $\lambda \in \Lambda_{M^*, L} \cap B_{\epsilon_n}(\lambda^*)$ ,

$$\Delta_{ij}^{*-} \leq \sum_{m < l} \eta_{ml}^{(\lambda)} q_{ij}^{ml(\lambda)} \leq \Delta_{ij}^{*+},$$

where

$$\Delta_{ij}^{*-} := \sum_{m < m'} (\eta_{mm'} - 2\kappa_n) R_{ij}^{mm'}; \quad (22)$$

$$\Delta_{ij}^{*+} := M^*(R^* + 1)R^* \kappa_n + \sum_{m < m'} (\eta_{mm'}^* + 2\kappa_n) S_{ij}^{mm'} + \frac{M \left\{ \binom{L}{2} - \binom{M^*}{2} \right\} \epsilon_n^{2\delta}}{f_-^{(n)}(X_i^0) f_-^{(n)}(X_j^0)}, \quad (23)$$

where  $R^* = (L - M^*)$ . By working through the multiplication above, we can write  $\Delta_{ij}^{*-} = \Delta_{ij}^* + \delta_{ij}^-$  and  $\Delta_{ij}^{*+} = \Delta_{ij}^* + \delta_{ij}^+$ , where  $\delta_{ij}^-, \delta_{ij}^+ \rightarrow 0$  almost surely and depend on  $\lambda^*, R^*, \delta$ , and  $\zeta$ .

Returning to the bounds established in (17), we can see that with probability tending to 1,

$$(\Delta_{ij}^* + \delta_{ij}^-) \{1 - \rho_n(\mathbf{X})\} \leq \Delta_{ij} \leq (\Delta_{ij}^* + \delta_{ij}^+) \{1 - \rho_n(\mathbf{X})\} + \rho_n(\mathbf{X}). \quad (24)$$

Define

$$\mathcal{S}(\hat{\mathbf{c}}, \mathbf{X}) = \sum_{i < j} \left\{ \mathbf{1}_{\hat{c}_i = \hat{c}_j} \Delta_{ij}^* (1 - \rho_n(\mathbf{X})) + \omega \mathbf{1}_{\hat{c}_i \neq \hat{c}_j} (1 - \Delta_{ij}^* (1 - \rho_n(\mathbf{X}))) \right\},$$

and note that

$$|\mathcal{R}^*(\hat{\mathbf{c}}) - \mathcal{S}(\hat{\mathbf{c}}, \mathbf{X})| \leq \binom{n}{2} \rho_n(\mathbf{X}) \max(\omega, 1) \bar{\Delta}^*,$$

where  $\bar{\Delta}^* = \binom{n}{2}^{-1} \sum_{i < j} \Delta_{ij}^*$ . Using (24), it follows that

$$|\mathcal{R}(\hat{\mathbf{c}}) - \mathcal{S}(\hat{\mathbf{c}}, \mathbf{X})| \leq \max(\omega, 1) \binom{n}{2} \mathcal{Q}(\mathbf{X});$$

$$\mathcal{Q}(\mathbf{X}) = \binom{n}{2}^{-1} \sum_{i < j} \max \left\{ \delta_{ij}^+ (1 - \rho_n(\mathbf{X})) + \rho_n(\mathbf{X}), -\delta_{ij}^- (1 - \rho_n(\mathbf{X})) \right\}.$$

Therefore, we have that

$$\binom{n}{2}^{-1} |\mathcal{R}(\hat{\mathbf{c}}) - \mathcal{R}^*(\hat{\mathbf{c}})| \leq \max(\omega, 1) \{ \rho_n(\mathbf{X}) \bar{\Delta}^* + \mathcal{Q}(\mathbf{X}) \}.$$

Observe that  $\mathcal{Q}(\mathbf{X})$ ,  $\rho_n(\mathbf{X})$ , and  $\bar{\Delta}^*$  do *not* depend on  $\hat{\mathbf{c}}$ . Hence, we can think of the above result as a notion of uniform convergence towards the KL-oracle risk. An important consequence is convergence of the optimal values of  $\mathcal{R}$  and  $\mathcal{R}^*$ . Let  $\mathbf{c}_{\text{FOLD}}$  be a minimizer of  $\mathcal{R}(\hat{\mathbf{c}})$  and  $\mathbf{c}_{\text{FOLD}}^*$  be a minimizer of  $\mathcal{R}^*(\hat{\mathbf{c}})$  over the space of partitions of  $[n]$ . Then observe that

$$\begin{aligned} & \binom{n}{2}^{-1} \{ \mathcal{R}(\mathbf{c}_{\text{FOLD}}) - \mathcal{R}^*(\mathbf{c}_{\text{FOLD}}^*) \} \\ &= \binom{n}{2}^{-1} \{ \mathcal{R}(\mathbf{c}_{\text{FOLD}}) - \mathcal{R}(\mathbf{c}_{\text{FOLD}}^*) + \mathcal{R}(\mathbf{c}_{\text{FOLD}}^*) - \mathcal{R}^*(\mathbf{c}_{\text{FOLD}}^*) \} \\ & \lesssim 0 + \max(\omega, 1) \{ \rho_n(\mathbf{X}) \bar{\Delta}^* + \mathcal{Q}(\mathbf{X}) \}, \end{aligned}$$

and, similarly,

$$\begin{aligned} & \binom{n}{2}^{-1} \{ \mathcal{R}(\mathbf{c}_{\text{FOLD}}) - \mathcal{R}^*(\mathbf{c}_{\text{FOLD}}^*) \} \\ &= \binom{n}{2}^{-1} \{ \mathcal{R}(\mathbf{c}_{\text{FOLD}}) - \mathcal{R}^*(\mathbf{c}_{\text{FOLD}}) + \mathcal{R}^*(\mathbf{c}_{\text{FOLD}}) - \mathcal{R}^*(\mathbf{c}_{\text{FOLD}}^*) \} \\ & \gtrsim -\max(\omega, 1) \{ \rho_n(\mathbf{X}) \bar{\Delta}^* + \mathcal{Q}(\mathbf{X}) \} + 0, \end{aligned}$$

ultimately showing that

$$\binom{n}{2}^{-1} |\mathcal{R}(\mathbf{c}_{\text{FOLD}}) - \mathcal{R}^*(\mathbf{c}_{\text{FOLD}}^*)| \lesssim \max(\omega, 1) \{ \rho_n(\mathbf{X}) \bar{\Delta}^* + \mathcal{Q}(\mathbf{X}) \}.$$

□

**Lemma 1.** Let  $\chi \subset \mathbb{R}^p$  be compact and  $f : \chi \rightarrow \mathbb{R}$ , where  $f$  is bounded on  $\chi$  and continuous at a point  $y \in \chi$ . Let  $\delta_n$  be a sequence with  $\lim_{n \rightarrow \infty} \delta_n = 0$  and  $B_{\delta_n}(y) = \{x \in \chi : \|x - y\| \leq \delta_n\}$ . Then,

there exists a sequence  $\epsilon_n$  that only depends only  $y$  and with  $\lim_{n \rightarrow \infty} \epsilon_n = 0$  so that for all  $x \in B_{\delta_n}(y)$ ,

$$|f(x) - f(y)| \leq \epsilon_n.$$

*Proof.* Consider sequences of within-neighborhood maximizers and minimizers of  $f$ ,

$$x_n = \operatorname{argmax}_{x \in B_{\delta_n}(y)} f(x); \quad z_n = \operatorname{argmin}_{x \in B_{\delta_n}(y)} f(x).$$

In the case where there are multiple minimizers or maximizers, simply choose one of these points as  $x_n$  or  $z_n$ . Since  $f$  is continuous and bounded and  $B_{\delta_n}(y)$  is a compact set,  $x_n, z_n \in B_{\delta_n}(y)$ . This means that  $x_n \rightarrow y$  and  $z_n \rightarrow y$ , which implies  $f(x_n) \rightarrow f(y)$  and  $f(z_n) \rightarrow f(y)$  by continuity. Therefore, for any  $x \in B_{\delta_n}(y)$ ,

$$|f(x) - f(y)| \leq \epsilon_n := |f(x_n) - f(z_n)| \rightarrow 0.$$

□

**Remark 1.** Observe that if  $y = \operatorname{argmin}_{x \in \mathcal{X}} f(x)$ , the proof of Lemma 1 implies that we can instead set  $\epsilon_n = |f(x_n) - f(y)|$ .

## F.1 FURTHER REMARKS ON THEOREM 1

**Remark 2.** Note that we state Theorem 1 as a high probability statement, not an almost everywhere statement. Pragmatically, this is because of (21), as we will need to show

$$\mathbb{P}^0 \left\{ f^*(X_i^0) \gtrsim \max(\epsilon_n, \nu_n) \quad \forall i \in [n] \right\} \rightarrow 1 \quad (25)$$

in order for us to construct  $\Delta_{ij}^{*-}$  and  $\Delta_{ij}^{*+}$  without dealing with negative numbers that could change the direction of the inequalities. It is simple to verify that the probability of (25) goes to 1 for any probability density functions  $f^*$  and  $f^0$  by the dominated convergence theorem. Alternatively, one can make the assumption that there exists an  $\epsilon^0 > 0$  so that  $\mathbb{P}^0(f^*(X) > \epsilon^0) = 1$ , but this would not apply for well-specified regimes.

**Remark 3.** A special case for the well-specified kernel regime is the location mixture of Gaussians. Here, we have that for any constant  $M > 0$ ,

$$\begin{aligned} & \mathbb{P}^0 \{ \mathcal{N}_d(X; \theta_h^0; \Sigma) \geq M \max(\epsilon_n, \nu_n) \mid s_0 = h \} \\ = & \mathbb{P}^0 \left[ \left\| \Sigma^{-1/2}(X - \theta_h^0) \right\|^2 \leq -2 \log \left\{ (2\pi)^{d/2} \det(\Sigma)^{1/2} M \max(\epsilon_n, \nu_n) \right\} \mid s_0 = h \right] \\ & \geq 1 + \frac{d}{2 \log \left\{ (2\pi)^{d/2} \det(\Sigma)^{1/2} M \max(\epsilon_n, \nu_n) \right\}} \end{aligned}$$

by Markov's inequality as  $\left\| \Sigma^{-1/2}(X - \theta_h^0) \right\|^2 \sim \chi_d^2$ . If we set  $a_{\min}^0 = \min_h a_h^0$ , we then have that for any  $M > 0$ ,

$$\begin{aligned} \mathbb{P}^0 \{ f^0(X) \geq M \max(\epsilon_n, \nu_n) \} &= \sum_{h=1}^{M^0} a_h^0 \mathbb{P}^0 \{ f^0(X) \geq M \max(\epsilon_n, \nu_n) \mid s_0 = h \} \\ &\geq \sum_{h=1}^{M^0} a_h^0 \mathbb{P}^0 \left\{ \mathcal{N}_d(X; \theta_h^0; \Sigma) \geq \frac{M}{a_h^0} \max(\epsilon_n, \nu_n) \mid s_0 = h \right\} \\ &\geq \sum_{h=1}^{M^0} a_h^0 \mathbb{P}^0 \left\{ \mathcal{N}_d(X; \theta_h^0; \Sigma) \geq \frac{M}{a_{\min}^0} \max(\epsilon_n, \nu_n) \mid s_0 = h \right\} \\ &= \mathbb{P}^0 \left\{ \mathcal{N}_d(X; \theta_h^0; \Sigma) \geq \frac{M}{a_{\min}^0} \max(\epsilon_n, \nu_n) \mid s_0 = h \right\}, \end{aligned}$$

because (3) does not depend on  $h$ . This tells us that (25) goes to 1 at an approximately  $\log(\log n/n)$  rate.

## G COMPARISON TO EXISTING METHODS

The general idea of merging mixture components to improve clustering results has been implemented in a variety of other methods. For example, [Chan et al. \(2008\)](#) merged mixture components to infer asymmetric cell subsets in an application to flow cytometry using numerical optimization of the probability density function. Also motivated by flow cytometry, [Baudry et al. \(2010\)](#) proposed first selecting the number of clusters using BIC, then successively merging components by minimizing the entropy of the clustering. [Hennig \(2010\)](#) showcases multiple methods for merging mixture components, including methods that preserve unimodality in the clustering, a method that successively merges clusters based on the Bhattacharyya distance, and methods based off diagnostic graphs. An algorithm that combines components sharing significant overlap was proposed in [Melnykov \(2016\)](#), where they also explored the misspecified kernel regime. More recently, the problem has attracted theoretical attention, with [Aragam et al. \(2020\)](#) showing explicitly that merging mixture components in a GMM via single link-

age clustering can identify a variety of clustering structures. They provide a Bayes optimal clustering algorithm known as NPMIX that implements their approach.

Similar to our approach, these methods are post-processing procedures motivated by improving the results of the GMM, particularly in the regime of kernel misspecification. However, there are multiple key differences between FOLD and other density merging methods. First, FOLD implements component merging from a Bayesian perspective, whereas existing methods tend to expand on maximum likelihood estimation. Next, with the exception of the NPMIX algorithm, most of the existing density merging algorithms make locally-optimal moves in order to improve the result of the EM algorithm, then terminate after a stopping criterion. NPMIX terminates when the desired number of clusters is reached, which is assumed to be either known or estimated in advance. In contrast, the minimization of the FOLD loss is based off a decision theoretic formulation that concretely quantifies the loss of co-clustering two objects. Furthermore, using the credible ball and posterior similarity matrix, we can coherently express uncertainty about the clustering estimate itself, whereas NPMIX and the other procedures characterize uncertainty in individual cluster allocation via misclassification probabilities.

NPMIX and the other existing algorithms often rely on a two step procedure: first, they estimate and merge the mixture components, and then they assign observations to the merged components (typically using MAP estimation), ultimately creating clusters. In FOLD, we completely bypass the first step by associating each object with a component via their localized density  $g(\cdot; \theta_i)$ , then group the localized densities in a one-step procedure (i.e, when we minimize the risk). The main idea here is to use  $\boldsymbol{\theta} = (\theta_1, \dots, \theta_n)$  as the parameter of interest for merging the components, rather than the unique values  $\tilde{\boldsymbol{\theta}} = (\tilde{\theta}_1, \dots, \tilde{\theta}_K)$ . While these paradigms may seem equivalent at first since  $\theta_i = \tilde{\theta}_k$  for some  $k$  almost surely, focusing on  $\boldsymbol{\theta}$  results in formulating the merging problem in terms of partitioning  $[n]$  rather than partitioning  $[K]$ . In addition, the two step procedure greatly reduces the partition space. If, say, a merging procedure takes  $L$  components and combines these into  $M < L$  merged components, then the resulting clustering must have at most  $M$  clusters. Conversely,  $\mathcal{R}(\hat{\mathbf{c}})$  is minimized over the space of *all* partitions of  $[n]$ . Finally, a drawback of using a two-step procedure is sensitivity to the point estimates for  $\mathbf{a}$  and  $\tilde{\boldsymbol{\theta}}$  when constructing the clustering. FOLD, on the other hand, does not need to estimate the components in order to derive clusters.

Recently, the Variation of Information (VI) (Meilă, 2007) has attracted attention in the literature for use as a clustering loss function for Bayesian mixture models (Wade and Ghahramani, 2018; De Iorio et al., 2023; Denti et al., 2023; Wade, 2023). The VI loss between  $\hat{\mathbf{c}}$  and  $\mathbf{s}$  is defined as

$$\mathcal{L}_{\text{VI}}(\hat{\mathbf{c}}, \mathbf{s}) = - \sum_{h=1}^{\hat{K}} \frac{n_{h\cdot}}{n} \log_2 \left( \frac{n_{h\cdot}}{n} \right) - \omega \sum_{k=1}^K \frac{n_{\cdot k}}{n} \log_2 \left( \frac{n_{\cdot k}}{n} \right) - (1 + \omega) \sum_{h=1}^{\hat{K}} \sum_{k=1}^K \frac{n_{hk}}{n} \log_2 \left( \frac{n_{hk}n}{n_{h\cdot}n_{\cdot k}} \right),$$

where  $n_h = |\hat{C}_h|$ ,  $n_k = |S_k|$ , and  $n_{hk} = |\hat{C}_h \cap S_k|$ . The first term gives the entropy of a random assignment of an observation to a cluster, where the probability of an assignment is given by  $n_h/n$ . The second term is analogous but for the task of randomly assigning an object to a component with weights  $n_k/n$ . The third term is the mutual information of the two random allocation tasks, in which the joint probabilities of assigning the object to cluster  $h$  and component  $k$  are given by  $n_{hk}/n$ . The VI shares multiple key properties with Binder’s loss, including that it is a metric when  $\omega = 1$  and a quasimetric otherwise (Meilă, 2007; Wade and Ghahramani, 2018; Dahl et al., 2022).

Unlike FOLD, the VI was not motivated as a loss function in Bayes estimation, but was instead originally proposed by Meilă (2007) as a metric over the partition space. The VI only takes into account information from the component labels rather than the other parameters in the mixture model, as in Binder’s loss. Hence, in the context of kernel misspecification, minimizing the VI may not be reasonable due to the inherent brittleness of  $\mathbf{s}$ . In addition, the VI is not a pair-counting loss, i.e. it cannot be expressed as a sum over all object pairs  $i < j$ , and therefore does not admit an interpretation in terms of quantifying the loss of co-clustering two objects. This also makes the role of  $\omega$  in  $\mathcal{L}_{\text{VI}}(\hat{\mathbf{c}}, \mathbf{s})$  less interpretable than for both Binder’s loss and FOLD, despite its influence on the resulting point estimate  $\mathbf{c}_{\text{VI}} = \operatorname{argmin}_{\hat{\mathbf{c}}} \mathbb{E}_{\Pi} \{\mathcal{L}_{\text{VI}}(\hat{\mathbf{c}}, \mathbf{s}) \mid \mathbf{X}\}$  in practice (Dahl et al., 2022). Finally, while the VI has been observed to yield fewer clusters than Binder’s loss empirically when  $\omega = 1$  on synthetic and real data (Wade and Ghahramani, 2018), we show in a simulation study in the Section A and an application in Section 4 of the main article that  $\mathbf{c}_{\text{VI}}$  is still vulnerable to the over-clustering problem, albeit usually to a lesser degree than  $\mathbf{c}_{\text{B}}$ .

## H ADDITIONAL DETAILS ON CREDIBLE BALLS

We express uncertainty in  $\mathbf{c}_{\text{FOLD}}$  using a 95% credible ball. For visualizations, we rely on the notions of horizontal and vertical bounds, as introduced in Wade and Ghahramani (2018). For completeness, we include the formal definitions of these bounds below. The horizontal bounds are given by the clusterings in  $B(\mathbf{c}_{\text{FOLD}})$  furthest from  $\mathbf{c}_{\text{FOLD}}$  by  $\mathbb{D}(\cdot, \cdot)$ .

**Definition H.1.** The horizontal bound(s) of  $B(\mathbf{c}_{\text{FOLD}})$  are

$$H(\mathbf{c}_{\text{FOLD}}) = \{\mathbf{c} \in B(\mathbf{c}_{\text{FOLD}}) : \mathbb{D}(\mathbf{c}, \mathbf{c}_{\text{FOLD}}) \geq \mathbb{D}(\mathbf{c}', \mathbf{c}_{\text{FOLD}}) \forall \mathbf{c}' \in B(\mathbf{c}_{\text{FOLD}})\}.$$

For any clustering  $\mathbf{c}$ , let  $K_{\mathbf{c}}$  be the number of clusters. The vertical bounds also consider clusterings in  $B(\mathbf{c}_{\text{FOLD}})$  that are far from  $\mathbf{c}_{\text{FOLD}}$ , but impose additional constraints on the number of clusters.

**Definition H.2.** The vertical upper bound(s) of  $B(\mathbf{c}_{\text{FOLD}})$  are

$$\begin{aligned} \text{VU}(\mathbf{c}_{\text{FOLD}}) &= \{\mathbf{c} \in B(\mathbf{c}_{\text{FOLD}}) : K_{\mathbf{c}} \leq K_{\mathbf{c}'} \forall \mathbf{c}' \in B(\mathbf{c}_{\text{FOLD}}), \\ \mathbb{D}(\mathbf{c}, \mathbf{c}_{\text{FOLD}}) &\geq \mathbb{D}(\mathbf{c}', \mathbf{c}_{\text{FOLD}}) \forall \mathbf{c}' \in B(\mathbf{c}_{\text{FOLD}}) \text{ with } K_{\mathbf{c}} = K_{\mathbf{c}'}\}. \end{aligned}$$

**Definition H.3.** The vertical lower bound(s) of  $B(\mathbf{c}_{\text{FOLD}})$  are

$$\begin{aligned} \text{VL}(\mathbf{c}_{\text{FOLD}}) &= \{\mathbf{c} \in B(\mathbf{c}_{\text{FOLD}}) : K_{\mathbf{c}} \geq K_{\mathbf{c}'} \forall \mathbf{c}' \in B(\mathbf{c}_{\text{FOLD}}), \\ \mathbb{D}(\mathbf{c}, \mathbf{c}_{\text{FOLD}}) &\geq \mathbb{D}(\mathbf{c}', \mathbf{c}_{\text{FOLD}}) \forall \mathbf{c}' \in B(\mathbf{c}_{\text{FOLD}}) \text{ with } K_{\mathbf{c}} = K_{\mathbf{c}'}\}. \end{aligned}$$

In practice, we compute the credible balls using the R function `credibleball()` in the `mcclust.ext` package (Wade, 2015).  $\mathbb{D}(\cdot, \cdot)$  can be either the Variation of Information distance or Binder’s loss. The bounds may not be unique in general.

## I EXTENDED IMPLEMENTATION DETAILS

### I.1 GSE81861 CELL LINE DATASET APPLICATION

We use the following priors for the Bayesian GMM:

$$(\tilde{\mu}_k, \tilde{\Sigma}_k) \sim \mathcal{NTW}(0_p, 1, p + 2, I); \quad \mathbf{a} \sim \text{Dir}((1/2)\mathbf{1}_K).$$

Recall that along with model-based clustering methods, we implement average linkage hierarchical clustering (HCA), k-means, DBSCAN, and spectral clustering. All methods were applied to the projection of the original cell line data onto the first  $p = 5$  principal components. For HCA, we set the number of clusters to be equal to 7, corresponding to the correct number of types. In k-means, we select the number of clusters with an elbow plot. We use the R package `dbscan` (Hahsler et al., 2019) to implement the DBSCAN algorithm. Following the documentation, we set `minPts = p + 1 = 6`, then use an elbow plot to choose the `eps` parameter, which comes out to `eps = 1.0`. For spectral clustering, we first compute a Gaussian kernel affinity matrix  $A = (A_{ij})_{i \in [n], j \in [n]}$ , where  $A_{ij} = \exp\left\{-\left\|X_i^0 - X_j^0\right\|^2\right\}$ . We compute the Laplacian matrix and plot the eigenvalues in ascending order to determine the number of clusters  $\hat{K}_n$ , then create a matrix  $V$  consisting of the first  $\hat{K}_n$  eigenvectors. Finally, we apply k-means to  $V$  with  $k = \hat{K}_n$ . UMAP plots of the clusterings given by the algorithmic methods are displayed in Figure 16.

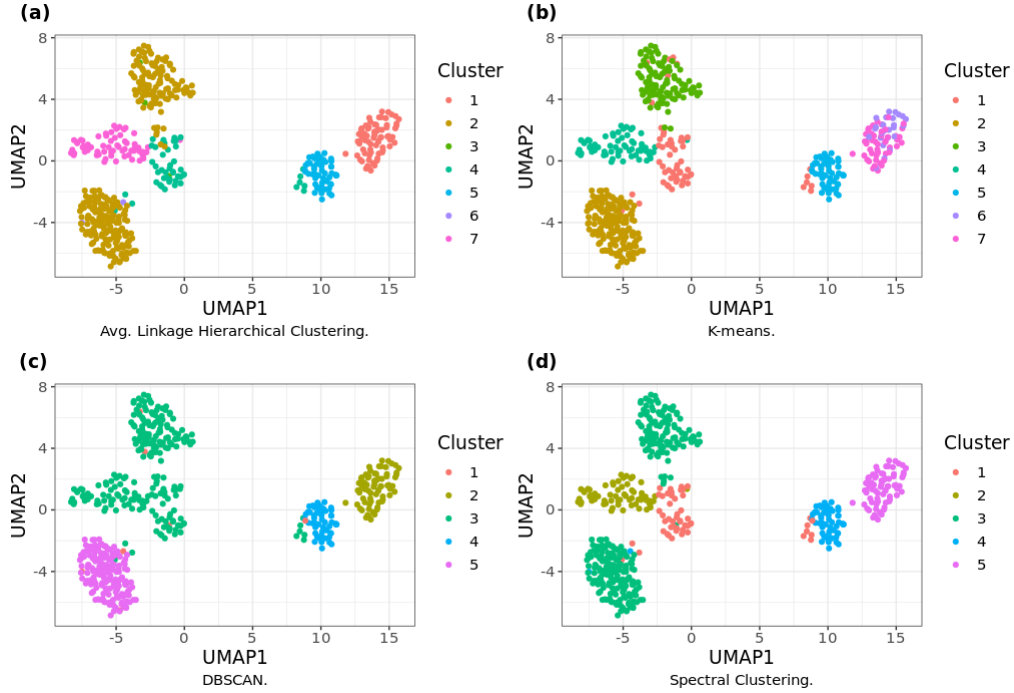


Figure 16: UMAP plots for the algorithmic clustering methods fit to the cell line dataset.

## I.2 MOONS EXAMPLE

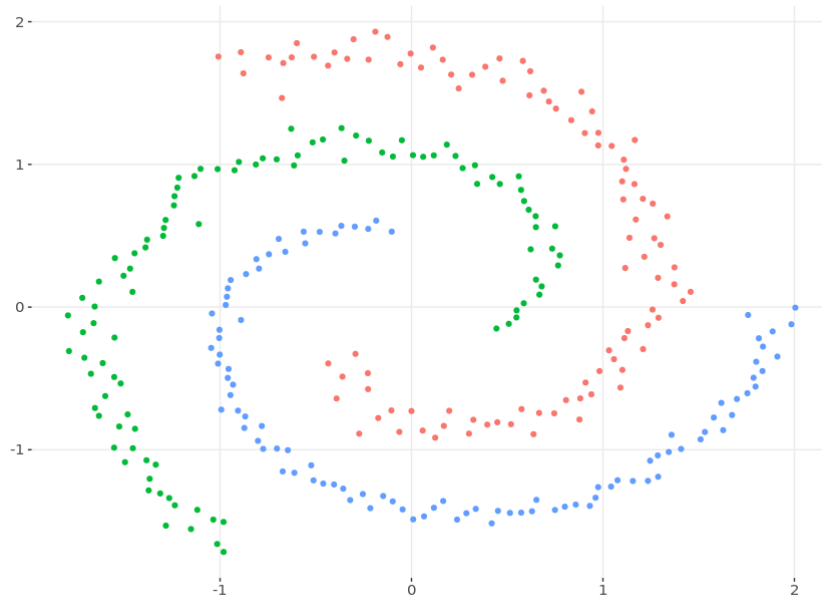
The `moons` dataset is simulated using the `RSSL` package (Krijthe and Loog, 2015; Krijthe, 2016) with  $n = 500$ . We fit a Bayesian location GMM with  $K = 30$  components, i.e.,  $X_i \sim \mathcal{N}(\theta_i, 0.02I)$ ,  $\tilde{\theta}_k \sim \mathcal{N}(0, 2I)$ ,  $\Pi(s_i = k | a_k) = a_k$ , and  $\mathbf{a} \sim \text{Dir}(1/K, \dots, 1/K)$ . We run a Gibbs sampler for  $T = 35,000$  iterations, remove the first 10,000 as burn-in, and take every fourth iteration to compute  $\Delta$ .

## I.3 APPLICATION TO BENCHMARK CLUSTERING DATASETS

For all datasets, the Gibbs sampler is run for  $T = 50,000$  iterations, the first 1,000 are treated as burn-in, and we take every fourth iteration to compute  $\Delta$ . The FOLD loss parameter  $\omega$  is chosen with an elbow plot, and the other clustering methods are tuned using the same workflow as in the cell line dataset application, with the exception that we fix `minPts=5` when running DBSCAN.

## J UNCERTAINTY QUANTIFICATION SIMULATION STUDY

In this section, we focus on the 95% credible ball around  $\mathbf{c}_{\text{FOLD}}$ . We simulate from a notably difficult scenario for clustering, the `spirals` dataset, as generated from the `KODAMA` package (Cacciatore and Tenori, 2022). Figure 17 shows a scatterplot of one example of the `spirals` data. The data are partitioned into  $M^0 = 3$  groups, each represented as interlocked spirals. Clustering these data is very



Example of the spirals data.

Figure 17: A sample of  $n = 300$  observations with the `spirals()` function, with colors corresponding to  $\mathbf{s}^0$ . The thin, interlocking nature of the spirals make this dataset a difficult problem for clustering algorithms.

difficult because the true clusters have long, thin, non-elliptical shapes, and are quite close to each other in the sample space. Our main interest here is whether  $B(\mathbf{c}_{\text{FOLD}})$  includes the true grouping of the data, analogous to coverage of a true real parameter by a credible interval.

For each replication, we sample  $n = 300$  observations using the `spirals()` function, where each spiral comprises 100 observations. We fit a Bayesian location-scale Gaussian mixture, with  $K = 30$ ,  $\mu = 0_p$ ,  $\kappa = 0.5/2$ ,  $\nu = p + 2$ , and  $\Psi = 0.5I$ . The Dirichlet concentration parameter for  $\mathbf{a}$  is  $\alpha = 1/2$  and we use  $\omega = \omega^{\text{AVG}}$  to compute  $\mathbf{c}_{\text{FOLD}}$  and generate samples from  $\Pi(\mathbf{c}_\theta | \mathbf{X})$ . In total, we simulate  $R = 100$  replications. In each replication, we run a Gibbs sampler for 15,000 MCMC iterations, discard 1,000 burn-in iterations, and keep every fourth MCMC draw. We compute the credible ball by setting  $\mathbb{D}(\cdot, \cdot)$  to be the VI.

For these simulations, our main area of interest is whether  $\mathbf{s}^0 \in B(\mathbf{c}_{\text{FOLD}})$ . To do this, we simply evaluate if the horizontal bounds cover  $\mathbf{s}^0$ , that is, if  $\text{VI}(\mathbf{s}^0, \mathbf{c}_{\text{FOLD}}) \leq \text{VI}(\mathbf{c}_H, \mathbf{c}_{\text{FOLD}})$ , where  $\mathbf{c}_H$  is any clustering in  $H(\mathbf{c}_{\text{FOLD}})$ . We also saved the number of clusters in  $\mathbf{c}_{\text{FOLD}}$  and the adjusted Rand index between  $\mathbf{c}_{\text{FOLD}}$  and  $\mathbf{s}^0$ .

The results are given in Table 6. In 89 of the replications,  $\mathbf{s}^0$  is contained in  $B(\mathbf{c}_{\text{FOLD}})$ , despite  $\mathbf{c}_{\text{FOLD}}$  consistently underscoring in the adjusted Rand index. This latter phenomena comes about because  $E_{\Pi}(\tilde{\Sigma}_k) = 0.5I$ , which means that the model is likely to fit Gaussian kernels that span multiple spirals, rather than approximating each spiral with multiple Gaussian kernels. Interestingly,

Avg. $VI(\mathbf{s}^0, \mathbf{c}_{\text{FOLD}}) \leq VI(\mathbf{c}_H, \mathbf{c}_{\text{FOLD}})$	Avg. No. of Clusters (SD)	Avg. ARI (SD)
0.890	3.120 (0.327)	0.223 (0.046)

Table 6: Results from the credible ball simulation study.  $\mathbf{s}^0$  is covered by the horizontal bounds of  $B(\mathbf{c}_{\text{FOLD}})$  in 89% of replications, despite the point estimator consistently scoring low adjusted Rand index with  $\mathbf{s}^0$ .

the average number of clusters achieved by  $\mathbf{c}_{\text{FOLD}}$  is 3.120, which is very close to the truth. We can then conclude that, even when the fitted model makes accurately clustering the data difficult,  $\Pi(\mathbf{c}_\theta | \mathbf{X})$  can still achieve high coverage rates of the truth. However, note that FOLD could be applied with recent approaches for density estimation of manifold data (e.g. the GMM in [Berenfeld et al. \(2022\)](#)), which would likely improve results for the `spirals` data.